NOV 20 1946

THE JOURNAL OF CHEMICAL PHYSICS

VOLUME 14 NUMBER 11

NOVEMBER, 1946

Published by the
AMERICAN INSTITUTE OF PHYSICS
Incorporated
Lancaster Press, Inc. New York, N. Y.

CHEMICA

EDITORS

Editor

Editors

Term ending December 31, 1947

[illegible] Cross

[illegible] Fuoss

[illegible] Kirkwood

[illegible]

[illegible] Oppenberg

[illegible] Oscar K. Rice

Term ending December 31, 1948

Charles D. Coryell

F. [illegible]

L. H. Thomas

C. W. Wieland

E. Bright Wilson, Jr.

---

cated exponents. The solidus (/) should be used wherever possible for fractions.

All illustrations should accompany manuscript and should always be referred to in the text. Line drawings should be made with India ink on glazed white paper or on tracing cloth. Coordinate paper is not desirable, but if used must be blue-lined and all coordinates to be reproduced drawn with India ink. Lettering should be of sufficient size to be legible after reduction.

Proof and all correspondence concerning papers in the process of publication should be addressed to the Publications Manager, American Institute of Physics, 57 East 55 Street, New York 22, New York.

Subscription Price

In United States and Possessions, Canada and Mexico $10.00

Elsewhere 11.00

Back Numbers

Complete set: Vol. 1, 1933—Vol. 13, 1945 ..... $130.00

Yearly rate: $11.00.

Single copies: $1.00 each.

Subscriptions and orders for back issues should be addressed to Prince and Lemon Streets, Lancaster, Pennsylvania, or to the American Institute of Physics, 57 East 55 Street, New York 22, New York.

Changes of address should be sent to the Business Manager, American Institute of Physics.

[illegible] Prince and Lemon Streets, Lancaster, Pennsylvania.

[illegible] at Lancaster, Pa., under the Act [illegible] 24, 1912. Acceptance for [illegible] 1918, embodied in paragraph 4, [illegible] P. L. & R., authorized

THE JOURNAL
OF
CHEMICAL PHYSICS

VOLUME 14, NUMBER 11 NOVEMBER, 1946

Some Thermodynamic Constants for the Solution Processes of Atoms in Metallic Solvents

SHENG-NIEN WANG
2051 W. Grand Boulevard, Detroit 8, Michigan

(Received August 7, 1946)

By combining the gas-metal equilibrium data available in literature and the thermodynamic quantities of gaseous molecules and atoms from the method of statistical mechanics, thermodynamic constants for the solution processes of some atoms in some metallic solvents have been obtained.

I. INTRODUCTION

THE nature of solution in metallic solvents has been little understood. For instance, consider the case of carbon in iron. It would be of interest to know the nature of the interaction between the single carbon atom and its closest neighbors of iron atoms. It would be also of interest to inquire how much the presence of the carbon atom affects the electronic structure of the region around it. The solution of such problems must await the efforts of many investigators. In the present paper the author has endeavored to derive from the few available equilibrium studies between gas and metal a few thermodynamic constants of the solution processes by which an atom is transferred from the gaseous phase to the interior of metallic solvent.

II. METHOD OF EVALUATION

The equilibria considered here are those for which the quantitative relationship indicates that the solute exists inside the metallic solvent in atomic form.

The method used may be illustrated by the cases of the solution of nitrogen atom in iron and the solution of carbon atom in iron.

In the case of the nitrogen atom in iron, it is only necessary to combine the thermodynamic constants of the processes

$$\tfrac{1}{2}N_2(g)=N(Fe)$$

and

$$\tfrac{1}{2}N_2(g)=N(g)$$

in order to obtain the thermodynamic constants of the process

$$N(g)=N(Fe).$$

In the case of carbon in iron, a round-about way has to be used. To illustrate, the free energy change of the process

$$CO(g)=C(Fe)+O(Fe)$$

around 1600°C is known. The free energy change of the process

$$CO(g)=C(g)+O(g)$$

is obtained from the free energy values of the individual gases as obtained by the method of statistical mechanics as well as the energy change at absolute zero. In addition, free energy changes at 1600°C of both processes, namely,

$$\tfrac{1}{2}O_2(g)=O(Fe)$$

and

$$\tfrac{1}{2}O_2(g)=O(g)$$

TABLE I. Equilibrium studies used in this paper.

Nature of equilibrium	Temperature range	Reference
$\frac{1}{2}H_2(g)=H(Fe)$	500°C–1650°C	a
$\frac{1}{2}N_2(g)=N(Fe)$	800°C–1540°C	a
$\frac{1}{2}N_2(g)=N(Fe)$	1600°C	b
$2CO(g)=CO_2(g)+C(\gamma Fe)$	750°C–1150°C	c
$H_2O(g)=H_2(g)+O(Fe)$	1600°C	d
$H_2S(g)=H_2(g)+S(Fe)$	1600°C	e
$CO(g)=O(Fe)+C(Fe)$	1540°C–1700°C	f
$\frac{1}{2}H_2(g)=H(Cu)$	530°C–1450°C	g
$H_2O(g)=H_2(g)+O(Cu)$	1090°C–1350°C	h
$SO_2(g)=2O(Cu)+S(Cu)$	1100°C–1300°C	i

[a] A. Sieverts, G. Zaff, and H. Moritz, Zeits. f. physik. Chemie **A183** 19–37 (1938).
[b] J. Chipman and D. Murphy, Trans. A.I.M.E. **116**, 179 (1935).
[c] A. Bramley and H. D. Lord, J. Chem. Soc. p. 1641 (1932).
[d] M. G. Fontana and J. Chipman, Trans. Am. Soc. Metals **24**, 329 (1936).
[e] J. Chipman and Ta Li, Trans. Am. Soc. Metals **25**, 435 (1937).
[f] S. Marshall and J. Chipman, Trans. Am. Soc. Metals **30**, 695 (1942).
[g] P. Rontgen and F. Moller, Metallwirtschaft **13**, 81 (1934).
[h] N. P. Allen and T. Hewitt, J. Inst. Metals **51**, 257 (1933).
[i] C. F. Floe and J. Chipman, Trans. A.I.M.E. **147**, 28 (1942).

are known. By combining all these values the free energy change of the process $C(g)=C(Fe)$ at 1600°C can be obtained.

III. LISTS OF EQUILIBRIA EXPERIMENTALLY STUDIED AND THERMODYNAMIC CONSTANTS THEORETICALLY EVALUATED USED IN THIS PAPER

The equilibrium studies used in this paper are listed in Table I.

The calculated values of free energies of the following gases are used in the calculations: C, H, O, S, CO, N_2, O_2, CO_2, H_2O, H_2S, and SO_2. Their origins are stated in the footnote.[1]

The values of reaction energies at absolute zero of the reactions involved in the calculation are presented in Table II.

IV. RESULTS

The results of calculations will be presented in the form of tables in three categories, namely, molten iron as solvent, γ iron as solvent, and copper as solvent. For the first group only the free energy change at one single temperature (1600°C) will be given. For the latter two groups the free energy change can be obtained for a series of temperatures. Thus it is possible to calculate both the energy change and entropy change accompanying the solution process.

As usual, the state of fugacity equal to 1 atmos. is chosen as the standard state of the gaseous phase. For the solute, the solute concentration of 1 atom of solute in 100 atoms of solvent, otherwise with the properties of a solute in an infinitely dilute solution, is chosen as the standard state.

A. Molten iron as solvent—At 1600°C

1. Hydrogen

$\frac{1}{2}H_2$ (1 atmos.) = H (1 in 100 Fe)
$-\Delta F^\circ = -7.14$ kcal.

$\frac{1}{2}H_2$ (1 atmos.) = H (1 atmos.)
$-\Delta F^\circ = -27.1$ kcal.

H (1 atmos.) = H (1 in 100 Fe)
$-\Delta F^\circ = 20$ kcal.

2. Carbon

CO (1 atmos.) = C (1 in 100 Fe) + O (1 in 100 Fe)
$-\Delta F^\circ = -12.3$ kcal.

CO (1 atmos.) = C (1 atmos.) + O (1 atmos.)
$-\Delta F^\circ = -152.7$ kcal.

O (1 atmos.) = O (1 in 100 Fe)
$-\Delta F^\circ = 64.7$ kcal.

Thus C (1 atmos.) = C (1 in 100 Fe)
$-\Delta F^\circ = 75.7$ kcal.

3. Nitrogen

$\frac{1}{2}N_2$ (1 atmos.) = N (1 atmos.)
$-\Delta F^\circ = -57.4$ kcal.

$\frac{1}{2}N_2$ (1 atmos.) = N (1 in 100 Fe)
$-\Delta F^\circ = -6.8$ kcal.

Thus N (1 atmos.) = N (1 in 100 Fe)
$-\Delta F^\circ = 50.6$ kcal.

4. Oxygen

H_2 (1 atmos.) + O (1 in 100 Fe) = H_2O (1 atmos.)
$-\Delta F^\circ = 0.4$ kcal.

H_2 (1 atmos.) + $\frac{1}{2}O_2$ (1 atmos.) = H_2O (1 atmos.)
$-\Delta F^\circ = 34.3$ kcal.

$\frac{1}{2}O_2$ (1 atmos.) = O (1 atmos.)
$-\Delta F^\circ = -30.8$ kcal.

Thus O (1 atmos.) = O (1 in 100 Fe)
$-\Delta F^\circ = 64.7$ kcal.

5. Sulfur

H_2S (1 atmos.) = S (1 atmos.) + H_2 (1 atmos.)
$-\Delta F^\circ = -15.1$ kcal.

H_2S (1 atmos.) = S (1 in 100 Fe) + H_2 (1 atmos.)
$-\Delta F^\circ = -22.1$ kcal.

Thus S (1 atmos.) = S (1 in 100 Fe)
$-\Delta F^\circ = 7.0$ kcal.

[1] C: Calculated by the author based upon the energy values given by Goudsmit and Bacher in *Atomic Energy States* (1932). The values at 2000°K, 3000°K, and 4000°K check with the values given by A. R. Gordon (J. Chem. Phys. **5**, 352 (1937)) within 0.002 in terms of $(F^\circ - E_0^\circ)/T$. S: C. W. Montgomery and L. S. Kassel, J. Chem. Phys. **2**, 417 (1934). H and H_2: W. F. Giauque, J. Am. Chem. Soc. **52**, 4816 (1930). N and N_2: W. F. Giauque and J. C. Clayton, J. Am. Chem. Soc. **55**, 4875 (1933). O and O_2: H. L. Johnson and M. K. Walkers, J. Am. Chem. Soc. **55**, 187 (1933). CO: J. O. Clayton and W. F. Giauque, J. Am. Chem. Soc. **54**, 2622 (1932). CO_2: L. S. Kassel, J. Am. Chem. Soc. **56**, 1838 (1934). H_2O: A. R. Gordon, J. Chem. Phys. **2**, 65 (1934). H_2S: P. C. Cross, J. Chem. Phys. **3**, 168 (1935). SO_2: A. R. Gordon, J. Chem. Phys. **3**, 336 (1935). In cases, Murphy's formulae have been used (J. Chem. Phys. **5**, 637 (1937)).

B. γ iron as solvent

(1) Hydrogen—γ iron

T°C	T°K	$-\Delta F^\circ_1/T$	$-\Delta F^\circ_2/T$	$-\Delta F^\circ/T$
1100	1373	−6.66	−26.44	19.78
1200	1473	−6.35	−23.79	17.44
1250	1523	−6.21	−22.59	16.38
1350	1623	−5.94	−20.42	14.48
1400	1673	−5.86	−19.42	13.56

$\frac{1}{2}H_2$ (1 atmos.) = H (1 in 100 Fe) ΔF°_1
$\frac{1}{2}H_2$ (1 atmos.) = H (1 atmos.) ΔF°_2
H (1 atmos.) = H (1 in 100 Fe) ΔF°

$-\Delta E^\circ$ is equal to 44 kcal. for the reaction

$$H(g) = H(\gamma Fe).$$

$-\Delta S^\circ$ is equal to 14.4 cal. per mole per degree for the reaction

H (1 atmos.) = H (1 in 100 Fe) around 1200°C.

(2) Carbon—γ iron

T°C	T°K	$-\Delta F^\circ_1/T$	$-\Delta F^\circ_2/T$	$-\Delta F^\circ/T$
827	1100*	2.66	82.48	79.82
877	1150*	3.83	79.06	75.23
927	1200	4.97	75.92	70.96
977	1250	5.99	73.03	67.05
1027	1300	6.82	70.36	63.54
1077	1350	7.59	67.84	60.26

C (1 in 100 Fe) + CO_2 (1 atmos.) = 2CO (1 atmos.) ΔF°_1
C (1 atmos.) + CO_2 (1 atmos.) = 2CO (1 atmos.) ΔF°_2
C (1 atmos.) = C (1 in 100 Fe) ΔF°

$-\Delta E^\circ$ is equal to 113 kcal. for the reaction

$$C(g) = C(\gamma Fe).$$

$-\Delta S^\circ$ is equal to 25.2 cal. per mole per degree for the reaction

C (1 atmos.) = C (1 in 100 Fe) around 1350°C.

(3) Nitrogen—γ iron

T°C	T°K	$-\Delta F^\circ_1/T$	$-\Delta F^\circ_2/T$	$-\Delta F^\circ/T$
1400	1673	−5.30	−36.21	30.91
1390	1663	−4.93	−36.52	31.59
1380	1653	−4.89	−36.84	31.95
1310	1583	−4.86	−39.16	34.30
1300	1573	−4.77	−39.51	34.74
1200	1473	−4.66	−43.27	38.61

$\frac{1}{2}N_2$ (1 atmos.) = N (1 in 100 Fe) ΔF°_1
$\frac{1}{2}N_2$ (1 atmos.) = N (1 atmos.) ΔF°_2
N (1 atmos.) = N (1 in 100 Fe) ΔF°

$-\Delta E^\circ$ is equal to 90 kcal. for the reaction

$$N(g) = N(\gamma Fe).$$

$-\Delta S^\circ$ is equal to 24.5 cal. per mole per degree for the reaction

N (1 atmos.) = N (1 in 100 Fe) around 1200°C.

* For the temperatures 1100°K and 1150°K, γ iron phase is stable only when the carbon concentrations are above certain values.

TABLE II. Energies of reactions at absolute zero.[a]

Reaction	Increase in energy content at absolute zero in kcal. ΔE_0°
$H_2(g) = 2H(g)$	103.2
$O_2(g) = 2O(g)$	117.2
$N_2(g) = 2N(g)$	170.2
$CO(g) = C(g) + O(g)$	210.8
$H_2S(g) = H_2(g) + \frac{1}{2}S_2(g)$	19.6
$\frac{1}{2}S_2(g) = S(g)$	42
$H_2S(g) = H_2(g) + S(g)$	61.6
$SO_2(g) = \frac{1}{2}S_2(g) + O_2(g)$	85.9
$H_2O(g) = H_2(g) + \frac{1}{2}O_2(g)$	57.8
$2CO_2(g) = 2CO(g) + O_2(g)$	133.5

[a] The references to these values in Table II are the same as those in the previous footnote (reference 1) except that $\frac{1}{2}S_2(g) = S(g)$ and $N_2(g) = 2N(g)$ are from *Molecular Spectra and Molecular Structure* by Herzberg and that $CO(g) = C(g) + O(g)$ is also due to Herzberg (J. Chem. Phys. **10**, 306 (1942)).

C. Copper as solvent

(1) Hydrogen—solid copper

T°C	T°K	$-\Delta F^\circ_1/T$	$-\Delta F^\circ_2/T$	$-\Delta F^\circ/T$
843	1116	−11.04	−35.40	24.36
995	1268	− 9.72	−29.67	19.95
1074	1347	− 9.02	−27.19	18.18

$\frac{1}{2}H_2$ (1 atmos.) = H (1 in 100 Cu) ΔF°_1
$\frac{1}{2}H_2$ (1 atmos.) = H (1 atmos.) ΔF°_2
H (1 atmos.) = H (1 in 100 Cu) ΔF°

$-\Delta E^\circ$ is equal to 37.5 kcal. for the reaction

$$H(g) = H \text{ (Cu, solid)}.$$

$-\Delta S^\circ$ is equal to 11.5 cal. per mole per degree for the reaction

H (1 atmos.) = H (1 in 100 Cu) around 1000°C.

(2) Hydrogen—liquid copper

T°C	T°K	$-\Delta F^\circ_1/T$	$-\Delta F^\circ_2/T$	$-\Delta F^\circ/T$
1106	1379	−6.86	−26.27	19.42
1128	1401	−6.72	−25.66	18.94
1180	1453	−6.43	−24.29	17.86
1312	1585	−5.82	−21.21	15.40
1450	1723	−5.11	−18.49	13.38

$-\Delta E^\circ$ is equal to 39 kcal. for the reaction

$$H(g) = H \text{ (Cu, liq.)}.$$

$-\Delta S^\circ$ is equal to 9 cal. per mole per degree for the reaction

H (1 atmos.) = H (1 in 100 Cu, liq.) around 1200°C.

(3) Oxygen—copper (liq.)

T°C	T°K	$-\Delta F^\circ_1/T$	$-\Delta F^\circ_2/T$	$-\Delta^\circ F/T$
1127	1400	56.29	13.00	43.29
1177	1450	53.33	12.39	40.94
1227	1500	50.57	11.80	38.77
1277	1550	47.98	11.27	36.71
1327	1600	45.56	10.75	34.81

H_2 (1 atmos.) + O (1 atmos.) = H_2O (1 atmos.) ΔF°_1
H_2 (1 atmos.) + O (1 in 100 Cu) = H_2O (1 atmos.) ΔF°_2
O (1 atmos.) = O (1 in 100 Cu) ΔF°

$-\Delta E^\circ$ is equal to 92 kcal. for the reaction

$$O(g) = O \text{ (Cu, liq.)}.$$

$-\Delta S^\circ$ is equal to 24.5 cal. per mole per degree for the reaction

O (1 atmos.)=O (1 in 100 Cu) around 1200°C.

(4) Sulfur—copper (liq.)

T°C	T°K	$-\Delta F^\circ_1/T$	$-\Delta F^\circ_2/T$	$2.-\Delta F^\circ_3/T$	$-\Delta F^\circ/T$
1127	1400	−2.23	−114.94	86.58	26.13
1177	1450	−1.47	−108.78	81.88	25.43
1227	1500	−0.77	−103.02	77.54	24.72
1277	1550	−0.11	− 97.64	73.42	24.11
1327	1600	+0.51	− 92.59	69.60	23.51

SO_2 (1 atmos.)=S (1 in 100 Cu)+2O (1 in 100 Cu) ΔF°_1

SO_2 (1 atmos.)=S (1 atmos.)+2O (1 atmos.) ΔF°_2

O (1 atmos.)=O (1 in 100 Cu) ΔF°_3

S (1 atmos.)=S (1 in 100 Cu) ΔF°

$-\Delta E^\circ$ is equal to 26 kcal. for the reaction

S(g)=S (Cu, liq.).

$-\Delta S^\circ$ is equal to 5.5 cal. per mole per degree for the reaction

S (1 atmos.)=S (1 in 100 Cu) around 1200°C.

V. DISCUSSION

In view of the present inadequacy of our knowledge about the metallic state the discussion offered here will be brief and qualitative.

The case of hydrogen atom as solute is different from those of other atoms, inasmuch as the hydrogen atom (or rather the proton) is essentially free to roam all over the free volume of the metal while the other atoms as solute are restricted by surrounding solvent atoms. Therefore in a general treatment of solutions of hydrogen in metals where the solvent lattice is preserved (such as hydrogen in copper, iron, nickel, cobalt, etc.), Fowler and Smithells[2] used a picture of protons as a gas enclosed inside the free volume of the metallic solvent. The solutions of carbon and nitrogen in metals perhaps could be pictured as the random distribution of the atoms (in dilute solution, at least) among the interstices (slightly enlarged), with the atoms behaving as three-dimensional oscillators inside the interstices. It is to be noted that the entropy changes attending the solution processes of carbon and nitrogen atoms in γ-iron are nearly equal.

The energy changes attending the solution processes are summarized below:

Process	$-\Delta E^\circ$	Process	$-\Delta E^\circ$
H(g)=H(γFe)	44 kcal.	H(g)=H(Cu, liq.)	39 kcal.
C(g)=C(γFe)	113 kcal.	O(g)=O(Cu, liq.)	92 kcal.
N(g)=N(γFe)	90 kcal.	S(g)=S(Cu, liq.)	26 kcal.

[2] R. H. Fowler and C. J. Smithells, Proc. Roy. Soc. **160**, 37 (1937).

Consider the cases of carbon and nitrogen in austenite. The metallic radius of the iron atom in γ iron (f. c. c.) is 1.26A.[3] The carbon atoms, and the nitrogen atoms presumably, are distributed in the octahedral interstices.[4] A sphere of diameter 1.04A can be inscribed in the octahedral interstices of pure γ-iron. Thus even carbon and nitrogen with single covalent radii of 0.77 and 0.70A,[5] respectively, have to push out the surrounding iron atoms to certain extent in order to accommodate themselves. A crude estimate of the lattice expansion due to the addition of carbon atom is as follows: G. Hagg[6] mentioned that the axial length of austenite containing 0.9 percent carbon is 3.58_6A while that of pure γ iron is 3.56_4A. The expression $(3.58_6)^3-(3.56_4)^3$ thus denotes the average increase in size of the unit cell as the result of the addition of carbon for the amount of 0.9 weight percent. The composition of 0.9 percent carbon corresponds to an iron and carbon number ratio of 24 to 1. If all octahedral interstices were filled with carbon atoms and the contribution towards volume increase for each carbon atom were still equal to the amount when the solution is dilute, the size of a unit cell of such a hypothetical crystal, of equal numbers of iron and carbon atoms and of a structure like NaCl, would be $[(3.58_6)^3-(3.56_4)^3]\times 24+(3.56_4)^3$, i.e., 65.7A^3. The axial length for such a unit cell is $(65.7)^{\frac{1}{3}}$, i.e., 4.0_3A. It would be equal to two times the radius of the iron atom plus two times the radius of the carbon atom, the value of the radii being those in the state of chemical combination between carbon and iron as in the dilute austenite. Using the covalent radius of 0.77A for carbon and the metallic radius of 1.26A for iron, we get the value of 4.06A. The agreement is good, indicating that the assignment of covalent radius to carbon and metallic radius to iron is a rather fair approximation.

The energy decrease accompanying the solution of a carbon atom into the γ iron lattice, i.e., 113 kcal., is the resultant of the energy increase in the expansion of the lattice and the energy decrease in the filling of the cavity with carbon

[3] L. Pauling, *Nature of the Chemical Bond* (Cornell University Press, New York, 1940), p. 390.

[4] N. J. Petch, J. Iron and Steel Inst. **145**, No. I, 111 (1942).

[5] L. Pauling, reference 3, p. 154.

[6] G. Hagg, J. Iron and Steel Inst. **130**, No. II, 439 (1934).

atom. The same type of consideration should also be true of the solution of nitrogen in γ iron lattice.

The cases of oxygen and sulfur in copper are similar. Although we are dealing with the liquid phase of copper, we may still consider the arrangement of copper atoms as close packed inasmuch as only the short range order is important. According to Fowler and Guggenheim,[7] "a recent experimental study by Lark-Horowitz of the scattering of x-rays by liquids has shown that the average value of the number of closest neighbors for normal liquids is close to eleven."

Consider the copper atoms in the close packed structure as spheres having a radius of 1.28A.[3] The radius of an oxygen atom in the metal should be somewhere between the single covalent radius of 0.66A[5] and the bivalent ionic radius of 1.40A.[8] The radius of a sulfur atom similarly is somewhere between the covalent radius of 1.04A[5] and the bivalent ionic radius of 1.84A.[8] Because of the strong electronegative character of oxygen and sulfur, unlike carbon, the covalent radius cannot be taken as an approximation. It can only be said that the work spent on the creating of the cavity for the oxygen atom and also for the sulfur atom to be accommodated would be considerable.

[7] R. H. Fowler and E. A. Guggenheim, *Statistical Thermodynamics* (Cambridge University Press, New York, 1939), p. 345.

[8] L. Pauling, reference 3, p. 330.

Although our results in regard to the processes with molten iron as solvent are restricted to a single temperature, namely 1600°C, and to one kind of thermodynamic constant, namely free energy change, a short remark may be made about the solutions of carbon and nitrogen in molten iron.

As noted before, the entropy changes attending the solution processes of carbon and nitrogen atoms in γ iron are nearly equal. It is probable that the entropy changes of the similar processes in molten iron are also nearly equal. The difference in free energy change would then be equal to the difference in energy change. The difference between the free energies of solution of carbon and nitrogen in molten iron is nearly equal to the difference between the energies of solution of carbon and nitrogen atoms in γ iron as is shown in the summary below:

Process	$-\Delta F^\circ$ in kcal.	Process	$-\Delta E^\circ$ in kcal.
C(1 atmos.) = C(1 in 100 Fe, liq.)	75.7	C(g) = C(γFe)	113
N(1 atmos.) = N(1 in 100 Fe, liq.)	50.6	N(g) = N(γFe)	90
Difference	25.1		23

Thus the supposition of the equivalence in entropy change is tantamount to saying that the difference in the energies of solution of carbon and nitrogen atoms in iron would be only minorly affected by the phase change and the temperature difference of few hundred degrees.

THE JOURNAL OF CHEMICAL PHYSICS VOLUME 14, NUMBER 11 NOVEMBER, 1946

The Use of Punched Cards in Molecular Structure Determinations

I. Crystal Structure Calculations

P. A. SHAFFER, JR., VERNER SCHOMAKER, AND LINUS PAULING
Gates and Crellin Laboratories, California Institute of Technology, Pasadena, California*

(Received July 22, 1946)

The application of punched cards and electrical accounting machines (of the International Business Machines Corporation) to crystal structure calculations is described. The machines may be used to evaluate Fourier series with greater accuracy, greater speed, and greater density of calculated points than is possible by the methods used heretofore. A method for the punched-card calculation of structure factors is also set forth, and the use of the machines for the reduction of observational equations to normal equations in least squares is discussed.

INTRODUCTION

THE extensive applications of Fourier methods of crystal structure analysis in recent years, including the representation both of electron-distribution functions[1] and of vector-distribution functions,[2] has emphasized the need of rapid and accurate means of making Fourier projections and carrying out related calculations. The increased complexity of structures now being investigated requires that many calculations of the Fourier type and many structure factor computations be made during a single structure determination. These two types of calculation are the most laborious ones in this field of work, and the time which they require largely determines the period of an investigation. The efficiency and precision with which such calculations may be made is, therefore, a factor of considerable importance in determining the success of a structural investigation. We have found that these calculations and other calculations involved in the processes of determining the structure of molecules and crystals can be carried out very easily and effectively by the use of punched-card methods, with the machines of the International Business Machine Corporation.

EVALUATION OF FOURIER SERIES

The Fourier calculations made in this work are the evaluation of one, two, or three-dimensional Fourier series; the one-dimensional case is represented by

$$f(x)=\sum_{h=0}^{\infty}(A_h\cos 2\pi hx+B_h\sin 2\pi hx). \quad (1)$$

The series is evaluated at the points $x=n\Delta x$, where Δx is small enough to give the desired detail in the complete curve of the function. Before the application of punched-card electrical accounting machines to these problems, series were most easily evaluated by use of an adding machine and the Beevers-Lipson Strips.[3] These are cardboard strips on which are printed values of $A\sin 2\pi hx$ and $A\cos 2\pi hx$ with $A=\pm 1, 2, 3, 4, \cdots, 100$, $h=0, 1, 2, 3, \cdots, 20$, and $x=0$ to $\frac{1}{4}$, $\Delta x=1/60$. The numerical values are given to $\pm\frac{1}{2}$ in the unit position. The strip corresponding to each term of the series is taken from a file and the strips are then arranged to permit the convenient addition of terms for constant x from all strips.

The use of the Beevers-Lipson strips greatly facilitates the evaluation of Fourier series, but the method has several unsatisfactory features. First, there is no check on the terms used or on the operations performed; the wrong strips may be drawn or errors may be made in summing them. Second, the method requires for long

* Contribution No. 1019 from Gates and Crellin Laboratories.

[1] W. H. Bragg, Trans. Roy. Soc. (London) **215**, 253 (1915); W. Duane, Proc. Nat. Acad. Sci. **11**, 489 (1925); R. J. Havinghurst, Proc. Nat. Acad. Sci. **11**, 502, 507 (1925); A. H. Compton, *X-rays and Electrons* (Van Nostrand Company, Inc., New York, 1926); W. L. Bragg, Proc. Roy. Soc. (London) **A123**, 537 (1929).

[2] A. L. Patterson, Phys. Rev. **46**, 372 (1934), Zeits. f. Krist. **90**, 517, 543 (1935); D. Harker, J. Chem. Phys. **4**, 381 (1934).

[3] H. Lipson and C. A. Beevers, Proc. Phys. Soc. (London) **48**, 772 (1936). An electrical machine for the summation of Fourier series has been described by C. A. Beevers, Proc. Phys. Soc. (London) **51**, 660 (1939), and D. Macewan and C. A. Beevers, J. Sci. Inst. **19**, 150 (1942).

periods of time the constant attention of the operator putting numbers into the adding machine and recording the results; the fatigue due to these operations contributes greatly to the probability of error. Third, the tabulated functions are not given to a number of places sufficient for all present-day needs. Fourth, the interval Δx is too large and the range of h too small for the resolution of structural features in large unit cells. Further, the extension of the computed range 0 to $\frac{1}{4}$ of the argument x to a larger one can be made only by summing the odd and even sines and cosines separately and combining the four terms with proper changes of sign; the method of doubling or quadrupling the frequencies of the terms cannot be used because the multiplied frequencies soon exceed the range of the tables. Because of these difficulties we have sought during the last few years to devise a mechanical means of carrying out Fourier calculations in a precise and efficient manner.

A machine for making the calculations for crystal structure work was first designed. While the construction of this machine was under consideration, Dr. W. J. Eckert suggested that the punched-card machines of the International Business Machines Corporation might be used for evaluating Fourier series, and proposed a method of using these machines. We then worked out somewhat different methods of using the IBM machines for evaluating not only the Fourier series required for crystal structure investigations but also the Fourier sums and integrals occurring in electron diffraction work; the latter calculations are discussed in the following paper. Other important uses of the machines in molecular structure work have also been found.

The Machines Used in the Calculations

The machines used in punched-card calculations have been described in detail elsewhere.[4] Specially prepared cards of insulating paper are passed under several sets of reading brushes in the machine. When holes punched in a card come into position, the brushes are permitted to touch an electrified roller beneath the card. The card feed is synchronized with the other operating units of the machine and the timing of the impulses picked up by the reading brushes is thus given numerical significance. The brushes are connected to plug positions in a removable plugboard. Almost all of the electrical circuits of the tabulating machine have terminals in the plugboard, and these circuits may be plugged together to cause the machine to perform in a variety of ways. For instance, number impulses read by the card brushes can be transmitted to counters, through the counter entrance hubs, and the counter exit hubs can be plugged to print bar hubs in order to print totals of numbers represented by the punches in the cards. In this way holes punched in the cards activate sorting, printing, and accumulating mechanisms as desired. In the calculations at hand only three pieces of machine equipment are used. These are an electric key punch (type 11), an electric sorting machine (type 80), and an alphabetic direct-subtraction tabulating machine (type 405). The punch is used to replace damaged cards and to punch special cards used in the arrangement of the printed result of the calculation. The sorter is used for arranging the cards in order before filing or machine tabulation. The tabulator accumulates totals of numbers punched on the cards, prints the results, and then continues with the next step of the calculation, thus performing the duties of an adding machine and its operator at the same time.

The alphabetic tabulator used is a standard machine except for the addition of seven relays, besides the five which are standard equipment, for the switching of counters from addition to subtraction; twelve of these relays, called "X-distributors," are needed for the controlled addition and subtraction of numbers in twelve independent six-place counters. With modification of the card files to permit addition of complements rather than direct subtraction, the standard machine could be used to give identical results; but the standard machine without modification cannot be used with our present card files.

The character of the calculations requires that essentially all of the circuits of the machine be

[4] W. J. Eckert, *Punched Card Methods in Scientific Computation* (Thomas J. Watson Astronomical Computing Bureau, January 1940); *Practical Applications of the Punched Card Method in Colleges and Universities* edited by G. W. Baehne (Columbia University Press, New York, 1935); *Machine Methods of Accounting* (International Business Machines Corporation, 1936); Harry P. Hartkemeier, *Principles of Punched Card Machine Operation* (Thomas Y. Cromwell Company, New York, 1942).

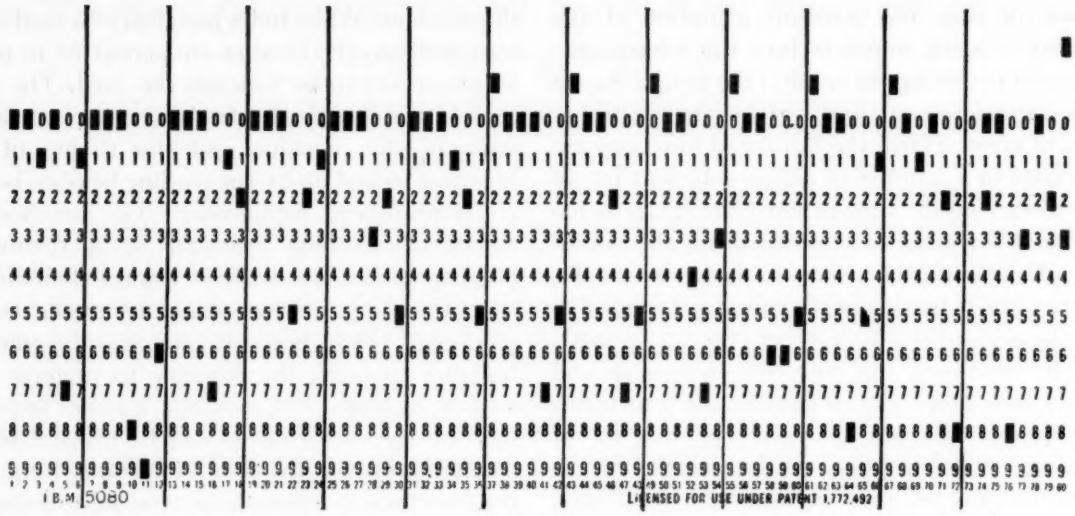

FIG. 1. A typical punched card. The vertical lines indicate the twelve function fields and the classification field for the card design described in the text.

used. The "automatic plugboard," a board which may be removed, completely wired, from the machine and replaced by another, is almost completely plugged, and several toggle switches have been attached to the cover of the board to increase the flexibility of the wiring arrangement. All of the problems to be discussed in the papers of this series with the exception of the least-squares calculations and tabulation of "reflection cards" are performed with use of one plugboard. The external toggle switches permit also the running of electron-diffraction calculations and verification of the files with the same board. A second board is kept wired for least-squares use, and a third is used for the tabulation of "reflection cards" and for incidental calculations of a temporary or experimental nature. The wiring of the plugboard and extra toggle switches for the electron diffraction and crystal structure calculations is described in a set of supplementary notes which may be obtained from the Gates and Crellin Laboratories on request. Additional details of card design and procedure are also described in these notes.

Arrangement of the Punched-Card Tables

Four equivalent files, each of about 20,000 cards, have been prepared to represent the functions $A \sin 2\pi hx$ and $A \cos 2\pi hx$. The argument x runs from 0.000 to 0.250 cycle with a tabular interval of 0.002, the frequency h has the values 0, 1, 2, $\cdots$, 30, and the amplitude values A are $\pm 1, 2, 3, 4, 5, 10, 20, 30, 40, 50, 100, 200, 500$.

The eighty-column tabulating card (see Fig. 1) is divided for this use into twelve six-column fields for punches which represent the numerical values of the tabulated functions for twelve values of the argument, and an eight-column field for punches which identify the card and control the sorting and tabulating. Eleven of these cards, which we call "function cards," are required for the representation of the 126 tabulated values of the function from zero to one-quarter cycle. The six empty fields are symmetrically placed—two on the left of the first card, two in the middle of the sixth card, and two at the end of the eleventh card.

As an example, the values of the function punched in successive cards of the packet $100 \cos 2\pi x$ are shown in the upper half of Fig. 2. The corresponding values of the argument are listed in a similar array at the bottom of the figure. The number 100 listed at (A) indicates that the amplitude of the function represented is 100; the (C) on the extreme left of the same row shows that the function is a cosine. The frequency of the function is determined by the position of the amplitude entry in the table. The serial order of the cards is printed in the column indicated by (B). The numbers printed in row 5 are the figures

contained in the card of serial number 5, etc. The card-count indicates how many cards have been summed to give the printed totals; the count is printed in the column marked by (C). Since only a single packet has been tabulated in this example, the card count is 1 throughout the table.

In addition to the eleven function cards there is an index card for each packet. The index cards have a filing tab on the upper left-hand corner on which are printed the amplitude, frequency, and phase of the function represented by the packet. The amplitude of the packet is also punched in a numerical field of the index card which corresponds to the units digit of the frequency. The purpose of the index cards is to permit easy identification and separation of the packets in the files and to print, during tabulation, a record of the amplitudes and frequencies of the terms. Index cards are recognized by an "x-punch" in card-column 72. This punch activates relays during the tabulation of the index cards and brings about the changes of wiring necessary for the special tabulation of the data punched in them.

The packet labeled 20 cos $16\pi x$, for example, thus consists of twelve cards: the index card (serial number 00) and eleven function cards (serial numbers 01 through 11); x runs across the cards, 0.000 through 0.018 on the first function card, 0.020 through 0.042 on the second, and so on up to 0.250. When negative values of the function occur, they are indicated by an x-punch in the first column of the field in which the value is punched. Examples of this punching appear in the seventh and following fields in Fig. 1. The eight-place classification field of the cards of the packet are the same except for the serial number (columns 78, 79). The remaining six columns of this field give the sign (74), frequency (75, 76), amplitude code (77), phase (80), and file number (74). The filing arrangement in order of decreasing detail is amplitude, sign, frequency, and phase (sine and cosine).

Calculation Procedure

In carrying out a calculation the operator first pulls from the files the packets corresponding to the terms of the series; a term $+26C12$ $(+26\cos 2\pi 12x)$ would require the packets $+30C12$ and $-4C12$, or $+20C12$ and $+5C12$ and $+1C12$. The drawing of the required amplitudes is facilitated by the amplitude color-coding of the cards; all the functions of a given amplitude are punched into cards of the same color. The cards drawn from the file are then sorted on the columns containing the serial punches. Special cards for controlling the form of the report are introduced automatically during the sorting operation, and title cards are placed on the top of the sorted stack. The entire set of cards, sometimes as many as 8000, is fed continuously into the hopper of the tabulator. The series is summed and the results, together with all data necessary for assuring the correctness of the calculation, are printed by the tabulator in a continuous and automatic operation, at a rate of about 140 cards per minute for typical summations. Several calculations may be tabulated in a single running of the machine, since the card-activated control mechanisms of the tabulator permit spacing, printing, and clearing of totals, or listing of numerical or alphabetic information upon the occurrence of punches or changes in the sequence of punches specified by the wiring of the tabulator plugboard. After a calculation or group of calculations has been tabulated, the cards are

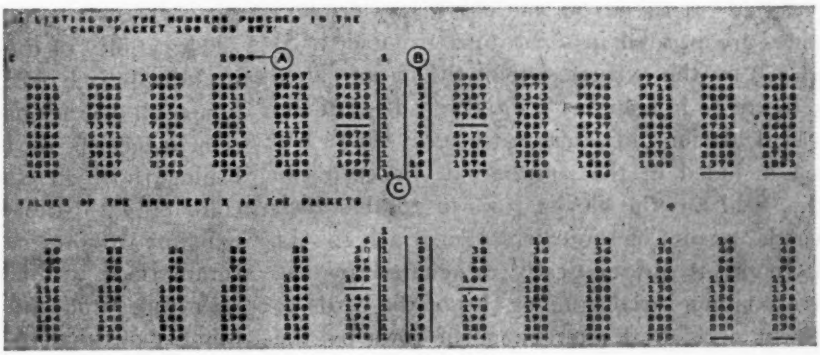

FIG. 2. Tabulator records illustrating the card design.

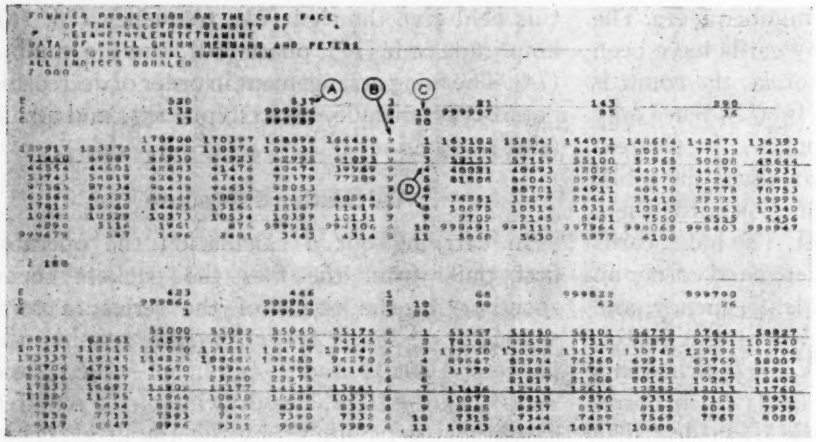

FIG. 3. Two-dimensional Fourier series. Sample second-step summations for two values of the parameter z.

gathered into the original packets by machine sorting on the columns containing the amplitude, sign, frequency, phase, and file number. The operator then restores the cards to their proper places in the files.

One-Dimensional Series

The printed results of two one-dimensional series calculations are shown in Fig. 3. At the top of the form are the title of the calculation and a description of special aspects of the problem. Following the title field is the index field (printed from the punches contained in index cards), which contains the amplitudes and frequencies of the terms summed. The amplitudes are printed explicitly (for example the number 537 indicated by the arrow at (A) represents the term $537 \cos 2\pi 2x$) and the frequencies are indicated by the position of the numbers in the field. The unit of frequency is given by the number of the column in which the amplitude is printed (numbering column 3 "0," column 12 "9") and the ten of frequency by the number of the row ("00," "10," "20" at the arrow marked (C)); sines and cosines are printed in separate rows labeled (S) and (C) on the extreme left of the figure. Thus the figure 85 in column "6" and row 10-C of the first calculation indicates that a term 85C16 has been included in the summation. Beneath the index field are the eleven rows of totals which give the results of the calculation. Each row of the report is automatically designated by the corresponding serial number (D) of the cards to prevent accidental interchange of rows by the operator. A card-count (B) which gives the units place of the number of cards tabulated in each row is printed also; the card-count is essential for the detection of extra or missing cards. (The card-count is one less than the true count when the sixth counter contains a negative total because the card count is accumulated in the extreme left-hand position of the eight-place counter used for the sixth field.)

When the calculation has been completed the index field is checked against the original data sheet and the card count is examined for deviations. If there is no indication of error the calculation is presumed to be correct. The only possible errors not checked in this manner are those arising from extreme coincidence or machine error. Machine errors may be brought to negligible incidence by running test cards prior to the calculation. The index-field tabulation and the card count make it possible for the calculation to be carried out by a person not acquainted with the significance of the calculation; the crystal structure investigator can check the correctness of the results in a few minutes at any time thereafter.

The ability of the tabulator to detect changes in the sequence of cards and to perform a variety of special operations when activated by specially punched cards is the principal factor in establishing the high efficiency of the method; this coupled with the high running speed of the machine and its capacity to carry out twelve summations at once permits the reduction of operating time and the great extension of the number of calculated points.

Two-Dimensional Series

The automatic control feature of the tabulator is of great convenience in extended calculations; as an example two-dimensional summations will now be considered. It is possible to reduce a two-dimensional Fourier series to a product of one-dimensional series.[5] For example the function

$$f(x, y) = \sum_{k=0}^{\infty} \left(\sum_{h=0}^{\infty} A_{hk} \cos 2\pi hx\right) \cos 2\pi ky - \sum_{k=0}^{\infty} \left(\sum_{h=0}^{\infty} B_{hk} \sin 2\pi hx\right) \sin 2\pi ky, \quad (2)$$

which is symmetric about the origin, may be rewritten as

$$f(x, y) = \sum_{k'=0}^{\infty} C(k', x) \cos 2\pi k'y - \sum_{k'=0}^{\infty} S(k', x) \sin 2\pi k'y, \quad (3)$$

with

$$C(k', x) = \sum_{h=0}^{\infty} A_{hk'} \cos 2\pi hx$$

and

$$S(k', x) = \sum_{h=0}^{\infty} B_{hk'} \sin 2\pi hx. \quad (4)$$

The first step in the calculation is to determine $C(k', x)$ and $S(k', x)$ for $k' = 0, 1, 2, \cdots$. To determine $f(x', y)$ one carries out the summation indicated above for $x = x'$. The result is a Fourier function of y only, for given x'; this summation is then carried out, giving the function $f(x', y)$, which is a section across the function $f(x, y)$. The contour map for $f(x, y)$ is developed from several sections (up to as many as 500 per cycle in an extreme case) calculated in this manner.

The first step of the machine calculation might be the tabulation of the many one-dimensional series separately, as it is carried out by other methods; the values of the C's and S's would then be picked out of the individual series. The tabulator is able to carry out the first step in one operation, however, and to arrange the C's and S's of given x in a column, listing with each item the frequency to be associated with it in subsequent summations. Thus to obtain the slice

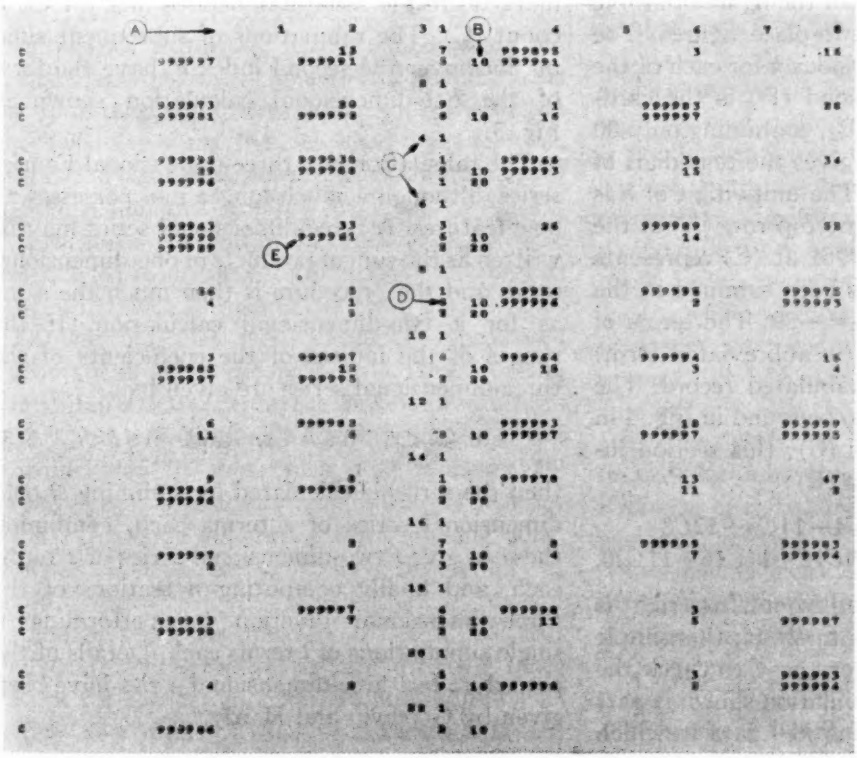

FIG. 4. Two-dimensional Fourier series. Sample tabulation of index cards for part of a first-step summation. (Column 9 is not included in this figure because it contains no entries. This column did appear in the original report, however.)

[5] C. A. Beevers and H. Lipson, Phil. Mag. 17, 855 (1934).

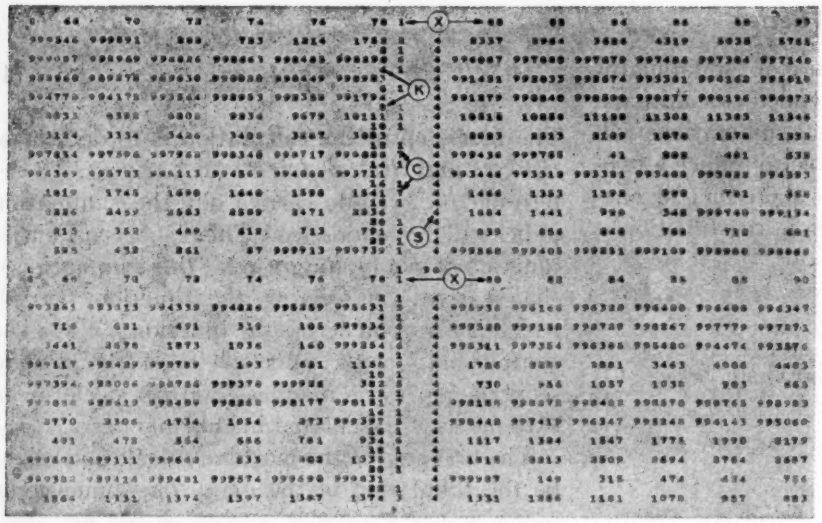

FIG. 5. Two-dimensiona Fourier series. Sample first-step summation giving the coefficients of the sine and cosine terms of the second summation for $z=0.068, 0.070, \cdots, 0.090$.

$f(0.120, y)$, the operator uses the terms listed in order in a single column labeled 0.120.

Portions of a first-dimensional step of a two-dimensional Fourier projection are shown in Figs. 4 and 5. Figure 4 is a reproduction of a part of the index field tabulation. The C's at the extreme left indicate that the terms listed are cosine terms. In the center of the figure are three columns of one-place or two-place figures. The first of these (C) gives the index k for each of the tabulated groups. The second (D) is the card-count column. The third (B), containing only 00 (not printed), 10, and 20, gives the tens digit of the index of frequency h. The units digit of h is given by the numbers in the top row (A) of the figure. Thus the entry 999961 at (E) represents a term $-39C12$ which has been summed in the $k=6$ group; in short $A_{12,6}=-39$. The terms of the group $k=6$ are given (in abbreviated form) for comparison with the tabulated record. The corresponding figures are to be found in Fig. 4 in the section headed "6" at (C); this section includes the term marked by (E):

$$C(6, x) = -37+33C2+26C4-11C6+52C8 \\ -10C10-39C12+14C16-11C20.$$

The order of the entries read from left to right is the order of the original data sheet; this simple correspondence makes it very easy to check the terms of the series. The tabulation shown is part of a Fourier projection using $hk0$ data in which both h and k are even; thus every other column is vacant.

Figure 5 is a copy of a portion of the tabulation record of function cards, both cosine and sine, for values of the argument from 0.068 to 0.090 cycle. The cards tabulated in this section have the serial number 4. The rows marked (X) give the values of x in thousandths. Some of the listed values of k are indicated by (K); other items marked are the serial number (S) and the card-count (C). The tabulations of subsequent summations over the second index k' have the form of the one-dimensional calculation shown in Fig. 3.

The calculation of a three-dimensional Fourier series, although a much longer job, possesses no new features. A three-dimensional series may be written as the sum of products of one-dimensional series and the procedure is then much the same as for a two-dimensional calculation. If the ranges of the indices of the coefficients of the three-dimensional series are given by

$$0 \leqslant h < r, \quad 0 \leqslant k < s, \quad \text{and} \quad 0 \leqslant l < t, \qquad (5)$$

then the series is calculated by summing st one-dimensional series of r terms each, combining these to give t two-dimensional series of s terms each, and finally computing n sections of the three-dimensional function by performing n single summations of t terms each. Details of the procedure for three-dimensional series have been given by Goodwin and Hardy.[6]

[6] T. H. Goodwin and R. Hardy, Phil. Mag. **25**, 1096 (1938).

Preparation of the Master Fourier-Series File and Duplicate Files

The master Fourier-series file of 21,960 cards was prepared in the following way. A four-place table of values of cos $2\pi x$ for $x=0$, 0.002, 0.004, $\cdots$, 1.000 was taken from standard trigonometric tables. The first 126 of these numbers are those punched on the set of cards 1*C*1. The numbers for other frequencies were obtained by suitable selection from these numbers; thus for cos $2\pi 2x$ the values for $x=0$, 0.002, 0.004, etc., are the first, third, fifth, etc., numbers in the original sequence. In this way tables were prepared for $100 \cos 2\pi hx$, $-100 \cos 2\pi hx$, $100 \sin 2\pi hx$, and $-100 \sin 2\pi hx$, $h=0$ to 30. These were then transferred to punched cards by an experienced operator, using a motor-driven key punch. They were checked by sorting into alternate sequence the complete set for amplitude +100 and that for amplitude −100 and adding in pairs on the tabulator; each non-zero sum tabulated indicated an error.

The complete set of cards in alternate sequence was then tabulated in pairs by subtraction of the second card of each pair from the first, to give the numbers for amplitude +200, which were then transferred to cards by a summary punch. Cards for amplitude −200 were similarly prepared, and the two sets were then checked by the same method. The process was repeated for amplitudes ±300, ±400, and ±500.

The cards for amplitudes ±1 to ±50 were reproduced from these automatically by the Los Angeles Service Bureau of the IBM Corporation. The working files were similarly reproduced automatically from the master file. Each working file contains 19,032 cards; the cards for amplitudes ±300 and ±400, which are not of great use, are not included in these files. One working file permits the satisfactory evaluation of Fourier series. If a large amount of work is being done, however, it is convenient to have several files at hand.

The values of the function entries in the cards are accurate to ±1 in the last (hundredth's) place except for the cards of amplitude 200 and 500, which, as a result of their preparation from the cards of amplitude 100, are accurate only to within ±2 and ±5 hundredths, respectively. In consequence of the method of generation of the lower amplitudes (1, $\cdots$, 50) by diagonal reproduction, proper rounding could not be accomplished, and the entries on these cards have an average error of −0.005 in the *magnitude* of the function superimposed on the random error (which does not exceed ±0.005). This degree of non-randomness of the errors will significantly increase the resulting average error of the sums for values of the argument at which most of the Fourier terms happen to be in phase.

From time to time the files are checked for errors caused by card damage or incorrect replacement of damaged cards by tabulating the cards in their file order with control on frequency using a special control circuit which is set up by a toggle switch mounted on the tabulator plugboard. If a non-zero total appears, indicating an error, the frequency group in which the error exists is sorted into groups of corresponding cards of the same amplitude (positive or negative), and the cards are tabulated again with control on column 77 using a second special wiring. The error is located as to amplitude by a non-vanishing total in the printed record. The faulty amplitude pack is now sorted according to serial number and tabulated in the normal way. The error is thus limited to one of two cards—the positive and negative pair of the last non-zero total—where it is finally located by direct inspection and comparison with the corresponding cards of the master file. It is important that this procedure of verification also serves to reveal by non-zero totals and an incorrect card count when, through sorting or filing error, cards are missing from a frequency group or misplaced or extra cards are present. The identification of missing or extra cards can readily be completed by inspection, after the tabulation by amplitude groups, with much less trouble than is the lot of the operator if a missing or extra card error turns up in a lengthy normal calculation.

Our master file is available for the production of working files for use by investigators in universities and research laboratories.

REFLECTION CARDS AND THEIR USE

It has been found convenient to punch a card for each x-ray reflection obtained in a given investigation; a reflection card may contain the

indices, the interplanar distance, the observed intensity, the product of the Lorentz and polarization factors, the observed and calculated structure amplitudes, the multiplicity factor, and other information which it may be desired to list, tabulate, or sort in any order. Such cards are of use particularly in the tabulation of data sheets for the calculation of two- or three-dimensional series. For example, the Fourier series representing the electron density distribution in the plane $z=\frac{1}{2}$ of a crystal cell is

$$\rho(x, y, \tfrac{1}{2})=\frac{1}{VN}\sum_{h=-\infty}^{\infty}\sum_{k=-\infty}^{\infty}\sum_{l=-\infty}^{\infty}F_{hkl} \times\cos 2\pi(hx+ky+l/2), \quad (6)$$

where V is the volume of the cell, F_{hkl} is the amplitude of the reflection hkl, and N is the total number of electrons in one unit cell. This may be written

$$\rho(x, y, \tfrac{1}{2})=\frac{1}{VN}\sum_{h=-\infty}^{\infty}\sum_{k=-\infty}^{\infty} \times\{\sum_{l=-\infty}^{\infty}F_{hkl}(-1)^{|l|}\}\cos 2\pi(hx+ky). \quad (7)$$

With use of the control facilities of the tabulator the summation over l can be made in a few minutes. In a problem requiring extensive use of Fourier methods the time saved in the arrangement of data prior to calculation may greatly exceed the few hours required for the punching of the reflection cards.

STRUCTURE-FACTOR CALCULATIONS

The evaluation of structure factors generally consists in forming the quantities $a=(hx+ky+lz)$, looking up in tables the atomic scattering factors for the reflections and the values of the trigonometric functions of $(hx+ky+lz)$ for each atomic term, multiplying these in pairs, and summing these products over all atoms in the unit.

Parameter Cards

A considerable fraction of the time used in calculating structure factors is consumed in computing quantities of the type $(hx+ky+lz)=a$ for each of the several atoms in the unit of structure. The calculation of these quantities is greatly facilitated by the use of parameter cards; the parameters $x_1, x_2, \cdots$ of the atoms are punched into the successive fields of a card, and the y and z parameters in the same fields of other cards, one field being used for each independent atom in the unit. Several copies of each of the cards are made; differently colored cards are used for x, y, and z so that they may be distinguished visually. The evaluation of $(5x+3y+7z)$, for example, is then accomplished by tabulating together 5 x-cards, 3 y-cards, and 7 z-cards. The result is printed together with the indices of the reflection.

Atomic Scattering Cards

Most of the schemes for the computation of structure factors which we have considered require either the preparation of very extensive card files or the use of machines in existence but not available in these Laboratories at present. A relatively simple application of the machines to this problem is described below. The values of $f_j\cos 2\pi a$ are tabulated in card files, f_j being the scattering factor of the atom of kind j. There is one card for each value of a from 0.000 to 0.500 in steps of 0.002. The twelve numerical function-fields of each card contain $f_j\cos 2\pi a$ for $\sin\vartheta/\lambda=0.05$, 0.10, $\cdots$, 0.60. The values of a and $1-a$ are stamped on the face of each card. Thus far files for carbon, nitrogen, and oxygen have been prepared using Pauling-Sherman[7] and Hartree[8] scattering factors; each file contains only 250 cards. If these files are used in conjunction with parameter cards only the cosines are needed, since sines are obtained by summing $(hx+ky+lz-0.250)$, and negatives of either function by adding 0.500 during the parameter summation.

The complete procedure for structure-factor calculation is as follows. Parameter cards for x, y, and z are punched and tabulated, as described in the preceding section, in small hand-picked groups to give a quadruple-spaced tabular report of the required parameter sums a. This report sheet, generally 6 to 12 feet long, is run

[7] Linus Pauling and J. Sherman, Zeits. f. Krist. **81**, 1 (1932).

[8] The "Hartree scattering factors" have been calculated by R. W. James and G. W. Brindley, Phil. Mag. **12**, 81 (1932), using electron density functions computed by D. R. Hartree, Proc. Cambridge Phil. Soc. **24**, 89, 111 (1928).

back to its starting position on the platen of the machine. Reading from the parameter-sum list on this report sheet, the operator draws from the small $f_j \cos 2\pi a$ files the terms indicated on the report sheet and tabulates them on the report sheet just under the appropriate parameter sums. The used cards are allowed to collect until the files have been so depleted as to be no longer usable; then the files are refreshed by sorting in the used cards by machine. For continued use several copies of each file could be prepared, their size and cost being very small. When the desired set of structure factors has been tabulated the investigator interpolates the true structure factor from those given over the range of $\sin \vartheta/\lambda$, with use of the value of $\sin \vartheta/\lambda$ for the reflection. For crystals of small scattering power, such as those containing only carbon, nitrogen, and oxygen, visual interpolation or simple proportion is sufficient for most needs, errors running well under 5 percent in all the calculations which have been made. This method of calculation seems to be sufficiently accurate for all but the most exacting investigations, and it is certainly of great use in the calculation of structure factors for many preliminary models.

LEAST-SQUARES CALCULATIONS

The evaluation of crystal parameter values by the least-squares method as applied by Hughes[9] has been greatly expedited by the use of the punched-card machines. The numerical factors of the observational equations are punched into cards, one card being used for each observational equation containing not more than 23 parameters. It is convenient to punch in an additional field of each card the sum of all of the elements of the observational equation. The pack of cards is then sorted on the units-digit of the first field; the cards punched "9" in this column are passed through the tabulator, then the "8" and "9" packs are put through, etc., until all the cards except the "0" pack have been added the indicated number of times. The complete pack is then sorted on the tens-digit column of the first field, and the small packs added as before with a one-place displacement of the counter wiring. If only two-place figures have been used, the operations mentioned suffice to compute the numerical factors of the first normal equation. The results are printed by pressing the hand total key of the machine. Continued sorting and totaling of the rest of the fields result in the printing of the complete matrix representing the set of normal equations. The symmetry of the matrix of the set provides a check of the correctness of the calculation except for the diagonal terms, which may be checked by forming the sum of the elements in each row or column of the matrix and comparing it with the corresponding values which the machine computes from the sums of the elements of the observational equations. The solution of the set of normal equations is then carried out by any of the various methods for the solution of simultaneous equations. In the reduction of 80 observational equations to 12 normal equations in 12 variables the following times were required in the computational steps:

Punching of observational equations into cards	1½ hours
Verification and correction of cards	½ hour
Tabulation of cards to give normal equations	3 hours

The normal equations were solved by methods not using punched cards in about one and one-half days. The total time required was thus about two days. The same calculation made with an adding machine would have taken about five days. The time reduction in the step carried out with the IBM machines is from 3½ days to 5 hours. The procedure just described is longer than the progressive digiting method described by A. E. Brandt of Iowa State College in "Practical Applications of the Punched Card Method in Colleges and Universities."[4] This method, however, requires the use of a summary punch, which is not available to us at the present time. Although the saving in time is great in the longer method just described, still greater efficiency may be attained with the progressive digiting method.

THE SAVING OF TIME

The time factor is in all cases greatly in favor of the punched-card method relative to summation procedures used in the past. Fourier projections which by the Beevers-Lipson method required several days of calculation can now be made in 5 to 7 hours. At the same time the density of calculated points is much greater and the accuracy of the computation is assured. The machine steps in the least-squares calculations require

[9] E. W. Hughes, J. Am. Chem. Soc. **63**, 1737 (1941).

only a few hours, as compared to one or two days with use of an adding machine, and again the accuracy of the work is assured. With the use of parameter cards and the structure-factor files the calculation of structure factors can be accomplished in about one-eighth of the time previously required.

During the past five years the punched-card files and machines have been used by a dozen different investigators in the study of the structures of more than a score of crystals. Among the crystals whose investigation has been facilitated by this method of calculation are melamine,[9] the addition compound of urea and hydrogen peroxide,[10] dl-alanine,[11] biphenylene,[12] hexamethylenetetramine,[13] and nickel glycine dihydrate.[14]

[10] Chia-Si Lu, E. W. Hughes, and Paul A. Giguère, J. Am. Chem. Soc. **63**, 1507 (1941).
[11] Henri A. Lévy and Robert B. Corey, J. Am. Chem. Soc. **63**, 2095 (1941).

ACKNOWLEDGMENTS

We wish to express our gratitude to the International Business Machines Corporation, which has made available the machines for this work, and to the Committee on Scientific Aids to Learning, which made the California Institute of Technology a grant for the preparation of sets of punched cards and for incidental expenses. We are also grateful to Dr. W. J. Eckert for suggesting the use of the IBM machines, and to Mr. A. A. Burgoyne, Jr., of the Los Angeles Office of the IBM Corporation, Dr. A. J. Stosick, Dr. H. Lévy, Dr. S. Weinbaum, and Dr. J. H. Sturdivant for their assistance in the development of the methods which have been described.

[12] Jürg Waser and Chia-Si Lu, J. Am. Chem. Soc. **66** 2035 (1944).
[13] Philip A. Shaffer (to be published).
[14] A. J. Stosick, J. Am. Chem. Soc. **67**, 365 (1945).

THE JOURNAL OF CHEMICAL PHYSICS VOLUME 14, NUMBER 11 NOVEMBER, 1946

The Use of Punched Cards in Molecular Structure Determinations

II. Electron Diffraction Calculations*

P. A. SHAFFER, JR., VERNER SCHOMAKER, AND LINUS PAULING
Gates and Crellin Laboratories, California Institute of Technology, Pasadena, California

(Received July 22, 1946)

Special files of punched cards for use with the electrical accounting machines of the International Business Machines Corporation in evaluating the Fourier sums and integrals used in the determination of the structure of gas molecules from electron diffraction photographs are described.

INTRODUCTION

IN this article we discuss briefly the evaluation of the intensity and radial distribution functions which are involved in the determination of the structures of gas molecules by the electron diffraction method.[1] Heretofore, these calculations were by far the most time-consuming part of the entire investigation; however, with International Business Machines Corporation equipment and the punched card files described here the calculations typically require about the same amount of time as the preparation and visual examination of the diffraction photographs. In addition to speeding up the ordinary course of the work, the rapid punched card methods make feasible the use of certain powerful and generally useful numerical methods which would have proved too time-consuming to be practical with the earlier computational procedures. These new methods may be expected to facilitate the study of relatively complicated molecules.

THE THEORETICAL INTENSITY FUNCTIONS

The intensity functions and radial distribution functions which are utilized in the interpretation of the observed diffraction pattern are related to the theoretical expression

$$I(s)=K\sum_{i,j}\psi_i(s)\psi_j(s)\frac{\sin sl_{ij}}{sl_{ij}}, \qquad (1)$$

for the intensity of coherent scattering of a beam of electrons at angles ϕ by randomly oriented molecules. In this expression K is a constant, ψ_i is the scattering factor (for electrons) of the ith atom, l_{ij} is the distance between the ith and jth atoms in the molecule, and

$$s=\frac{4\pi\sin\phi/2}{\lambda}, \qquad (2)$$

λ being the wave-length of the electrons. The summation is extended over all the atoms in the molecule. The factor ψ_i is related to the x-ray form factor $f_i(s)$:

$$\psi_i=(Z_i-f_i(s))/s^2, \qquad (3)$$

where Z_i is the atomic number of atom i.

Because of the contrast-sensitive properties of the eye the appearance of the electron diffraction photographs is more closely related to some derived expression in which the very rapid decline of $I(s)$ with increasing s is suppressed. Graphs of what we call the simplified intensity function

$$\frac{1}{\sum_i\psi_i^2}\{I(s)-I_{at}(s)\}=\frac{K}{\sum_i(Z-f)_i^2}\sum_{\substack{i,j\\ i\neq j}}(Z-f)_i(Z-f)_j\frac{\sin l_{ij}s}{l_{ij}s} \qquad (4)$$

and the reduced intensity function

$$I^0(s)=\frac{s[I(s)-I_{at}(s)]}{\sum\psi_i^2}=\frac{K}{\sum_i(Z-f)_i^2}\sum_{\substack{i,j\\ i\neq j}}\frac{(Z-f)_i(Z-f)_j}{l_{ij}}\sin l_{ij}s, \qquad (5)$$

* Contribution No. 1020 from Gates and Crellin Laboratories.

[1] Comprehensive discussions of the methods of interpretation of electron diffraction photographs of gas molecules are contained in the following papers: L. Pauling and L. O. Brockway, J. Chem. Phys. 2, 867 (1934); L. Pauling and L. O. Brockway, J. Am. Chem. Soc. 57, 2684 (1935); L. O. Brockway, Rev. Mod. Phys. 8, 231 (1936); V. Schomaker, Thesis, California Institute of Technology, 1938.

both represent the appearance of the photographs well enough for our purposes. In both functions the atomic scattering, I_{at} (given by the terms of (1) for $i=j$, which are independent of the molecular structure), has been omitted. Equations (4) and (5) represent the diffraction pattern for essentially rigid molecules, such as carbon dioxide or carbon tetrachloride, in which the relative displacements of the atoms caused by intramolecular vibration are negligibly small. For non-rigid molecules Eqs. (1), (4), and (5) must be suitably modified[1] to represent, essentially, the appropriate average over all the instantaneous configurations assumed by the molecules in the course of their vibrations. Each term in the intensity function must accordingly be replaced by an integral over all values of the interatomic distance l, with a radial distribution function $l^2D_{ij}(l)$ which gives the probability of finding a molecule with the atoms i and j separated by a distance l:

$$I^0(s)=\frac{K}{\sum_i (Z-f)_i^2}\sum_{\substack{i,j\\ i\neq j}}(Z-f)_i(Z-f)_j \times\int_0^\infty l_{ij}D(l_{ij})\sin l_{ij}s\,dl_{ij}. \quad (6)$$

It usually happens that the molecule is significantly non-rigid with respect to only a few of the interatomic distances.

It is possible to write Eq. (6) in a formally simpler fashion as

$$I^0(s)=K\int_0^\infty lD(l)\sin ls\,dl, \quad (7)$$

in which $D(l)$ is a radial distribution function. If all the atoms of the molecule are of the same kind, $l^2D(l)$ gives the relative probability of finding two of them a distance l apart and peaks of $l^2D(l)$ obviously correspond to interatomic distances, but if the atoms are not all of the same kind, the precise meaning of $D(l)$ may become rather abstruse, and will not be discussed here. For any assumed molecular model, however, $D(l)$ can readily be found; moreover, the interpretation of a known $D(l)$ in terms of interatomic distances is usually not difficult.

THE RADIAL DISTRIBUTION INTEGRAL

Equation (7) is a Fourier integral, which, like the Fourier series discussed in Part I, can be inverted. The resulting expression

$$lD(l)=K'\int_0^\infty I^0(s)\sin ls\,ds \quad (8)$$

is called the radial distribution integral. It does not matter that s^2 is not defined for values greater than $4\pi/\lambda$ because with the usual values of λ the amplitude of variation $I^0(s)$ always decreases essentially to zero at a value of s smaller than $4\pi/\lambda$, but it is important when $lD(l)$ is to be evaluated that $I^0(s)$ cannot be determined throughout the range in which it is supposed to have an appreciable amplitude. The devices mentioned in this connection in the next paragraph constitute only one of the possible ways of making use of the radial distribution integral in spite of our incomplete knowledge of $I^0(s)$.

---

[2] Three items concerning this calculation need mention here: (1) Because the first maximum of $I^0(s)$ (corresponding to the central maximum of the simplified intensity function) is essentially unobservable, it is either estimated entirely from past experience or is taken from a theoretical intensity curve, and suitable (but altogether minor) allowances for error and arbitrariness ultimately have to be made. (2) $I^0_{visual}(s)$ is multiplied by an attenuation or convergence factor in order that the requirements of Eq. (8) may practically be satisfied by an integration extending only to the largest angle s_{max} for which the diffraction pattern is observed. We use the factor $\exp(-as^2)$ (generally with a chosen so that $\exp(-as^2_{max})=0.1$), which has the effect of transforming any potentially sharp peak of $lD(l)$ into a normal error curve distribution function with $\langle\delta l^2\rangle_{Av}=2a$. Since this is just the distribution function which is ordinarily assumed (reference 1), for example in Eq. (6), to represent the distributions of interatomic distances which arise from the thermal and zero-point vibrations of molecules, $\exp(-as^2)$ is sometimes called the artificial temperature factor. (3) It is necessary to approximate the integration in Eq. (8) by a summation over selected values of s. Heretofore (reference 1), the summation has been restricted to a set of terms in $I(s_i)\sin(ls_i)$ corresponding to the apparent maxima, or to the apparent maxima and minima, of the diffraction pattern. This summation is neither very satisfactory nor easy to comprehend, although it does give fairly useful results; yet for even a simple molecule it may be rather time consuming, by the usual methods, involving the accumulation of twenty or thirty products for each calculated point. With the help of punched cards, however, it is not difficult to sum a series of even a hundred terms. Accordingly, we now usually evaluate a sum over evenly spaced s values (reference 3) that is loosely called the radial distribution integral, the spacing being chosen so small that the summation is a fully satisfactory approximation to the integration for the range of l which is of interest. Ordinarily we take a spacing $\Delta s=(\pi/10)\text{A}^{-1}(\Delta q=1$, see below) that in practice is satisfactory even for $l=7$A.

The Interpretation of the Electron Diffraction Pattern

The interatomic distances that occur in a molecule, and determine its structure, can be deduced from the diffraction photograph in two different ways. In the correlation procedure theoretical intensity curves (computed according to Eqs. (4), (5), or (6)) are drawn for all the likely molecular models. Any model whose curve adequately represents the details of the appearance of the photographs is compatible with the electron diffraction experiment; if satisfactory models of only one distinct type can be found, the structure determination is unique, at least within the realm of what have been considered likely models, and the parameters of the structure are determined with a precision that depends on how widely they may be varied without destroying the agreement between calculated curves and photographs. In the radial distribution method an approximation to the radial distribution function (Eq. (8)) is calculated with the use of a curve, representing a reduced intensity function, $I^0_{\text{visual}}(s)$, which has been drawn in accordance with the appearance of the diffraction photographs and the expected general behavior of $I^0(s)$ for the type of molecule being investigated.[2,3] The plotted radial distribution function shows immediately what interatomic distances occur in the molecule, and from these the molecular structure can usually be deduced. Mathematically the two methods are almost strictly equivalent, but in practice the two procedures are almost always used together in order to take advantage of the greater directness of the radial distribution method and the greater speciality and somewhat greater sensitivity of the correlation method.

The Calculations

The general form of the calculations described in the foregoing sections is seen to be the evaluation of

$$F(x) = \sum_i G_i(x) \sin y_i x. \qquad (9)$$

For the simplest intensity functions there may be only two sine terms with constant coefficients; for more complicated molecules there may be ten or twenty or more terms in the intensity function and many of the $G_i(x)$ may be variable. For non-rigid molecules even more terms are required to approximate adequately the integrals which appear in Eq. (6). The adequate representation of the radial distribution integral[2] typically requires 75 to 100 terms with constant coefficients, while the older type of radial distribution summation involves from 10 to 30 or more terms. In all cases it is necessary to evaluate Eq. (1) for about 100 values of x.

In the beginning these calculations were made with the aid of only the usual trigonometric tables and an adding machine, so that only the simplest types could be carried out in a reasonable time. Later, with the Sherman-Cross strips described below and a motor-driven adding-calculator, a ten-term intensity function with constant coefficients could be evaluated by a skilled operator in two to four hours, but longer calculations such as the radial distribution integrals were too difficult to be used at all. With our present punched-card equipment the filing, sorting, and tabulating operations for a ten-term intensity calculation with constant coefficients require only ten to fifteen minutes while a hundred-term approximation to a radial distribution integral can be evaluated in an hour and a half or two hours. For the longer calculations the work can be so arranged as to provide useful subtotal tabulations without appreciably increasing the time required. Although the transition to variable coefficients is relatively very much more troublesome and time-consuming for the punched-card methods than with the Sherman-Cross strips, in our work a considerable advantage for the punched-cards remains. Fortunately, however, most of the calculations can be carried out with constant coefficients by means of a suitable device.

The Sherman-Cross Tables

The Sherman-Cross tables consist of a set of paper strips, each an inch wide and two feet long, on which are printed the values of $\sin y_i x/y_i x$ for values of y_i at intervals of 0.01 from 0.80 to 4.00 for values of x up to 40, and for values of y_i from 4.02 to 8.00 at intervals of 0.02 for values of x up to 20. The tabular interval in x is 0.2 throughout. Each strip corresponds to a given

[3] R. Spurr and V. Schomaker, J. Am. Chem. Soc. 64, 2693 (1942).

value of y_i (indicated at the top of the strip) and a range of x values, the values of $(\sin y_i x/y_i x)$ being arranged along the length of the strip in correspondence to the successive values of x. For computation with these strips Eq. (9) is written in the form

$$\frac{F(x)}{x}=\sum_i y_i G_i(x)\frac{\sin y_i x}{y_i x} \qquad (10)$$

and the required strips are arranged side by side on a suitable holder so that entries corresponding to the same value of x lie in the same horizontal row. Then for each value of x, the sum of the products of the entries read from the strips by the corresponding coefficients $(y_i G_i(x))$ is accumulated on an adding-calculator and recorded.

THE PUNCHED-CARD FILES AND THEIR USE IN MAKING ELECTRON DIFFRACTION CALCULATIONS

In design, preparation, and use the punched-cards for electron diffraction calculations are so similar to those already described in the preceding paper that only the important differences need be given here.

For all the cards, which happen to be designated by three different file numbers, the tabulated function is $A \sin yx$. In file No. 1, the amplitudes A (indicated by the same color and punch codes as for the crystal structure cards) are $+1$, -1, $+2$, -2, $+3$, -3, $+4$, -4, $+5$, -5, $+10$, -10, $+20$, -20, $+30$, -30, $+40$, -40, $+50$, -50, $+100$, -100, $+200$, -200, $+500$, and -500; and in file No. 3 they are $+300$, -300, $+400$, -400; file No. 2 contains the same amplitudes as file No. 1 up to and including -100. The cards of file No. 1 of amplitudes $+100$, -100, $+200$, -200, $+500$, -500 and the cards of file No. 3 are regarded as constituting a master set which is never used in routine work, but is held in reserve for use in preparing further working sets by high speed machine reproduction. The "frequency" y, which in intensity calculations is identified with l and in radial distribution calculations with s, ranges from 0.01 to 5.00 in steps of 0.01.[4] Each amplitude-frequency pack contains, besides the index card, 12 function cards which give $(A \sin yx)$ for 144 values of x ranging from 0.0 to 143 $(\pi/10)$ in steps of $(\pi/10)$.[5] In our electron diffraction files there are accordingly altogether 312,000 function cards and 26,000 index cards.

The classification field of the electron diffraction cards consists of columns 73–80, just as for the Fourier cards, and the same plugboard is used for both. In column 73 is punched the file number and an x or a 0 to indicate, respectively, whether the amplitude is negative or positive. The frequency y is punched in columns 74, 75, and 76, the amplitude code in column 77, the serial number in columns 78 and 79 (the serial number ranges from 20 to 32), and E (12–5) is punched in column 80. The transition from crystal structure to electron diffraction cards thus requires that the wirings to columns 73 and 74 on the tabulator be interchanged; this is done by means of a toggle switch mounted on the plugboard cover. The index cards are similar to those of the crystal-structure set with the addition of a second punching of the amplitude in columns 66 (sign), 67, 68, and 69. A second toggle switch controlling a class selector which is activated by the X-72 punch of the index cards makes it possible to list and tabulate the index cards either after the crystal structure fashion or in another way, with a control on all digits of the frequency, such that the amplitude, the frequency, and an "E" are printed (the card count is suppressed) at the extreme left-hand side of the record for each term of the summation. A sample calculation, a radial distribution function for hexamethylenetetramine, in which this second method of listing and tabulating the index

[4] In the radial distribution integral calculation the interval in s is usually identified with an interval of 0.05 in y, and only moderate amplitudes are required for suitable accuracy in the representation of $I^0_{\text{vib}}(s) \exp(-as^2)$. It has been convenient, therefore, to keep separately for this calculation the cards of file No. 1 with amplitudes $+1$, -1, $\cdots$, $+20$, -20 and frequencies 0.05, 0.10, $\cdots$, 5.00.

[5] There are somewhat fewer entries (72,000 $x-y$ combinations) in the punched card tables than in the Sherman-Cross tables (84,200 $x-y$ combinations); we find that the arrangement of our tables makes them more convenient to use in electron diffraction work while their content ($\sin z$, instead of $\sin z/z$) often makes them useful for problems outside the field of electron diffraction. The inconvenience of the odd tabular interval in x, which becomes s in making intensity calculations, is entirely eliminated by dealing always with the new quantity

$$q=\frac{10}{\pi}s=\frac{40}{\lambda}\sin\phi/2. \qquad (11)$$

In terms of q the tabular interval becomes unity.

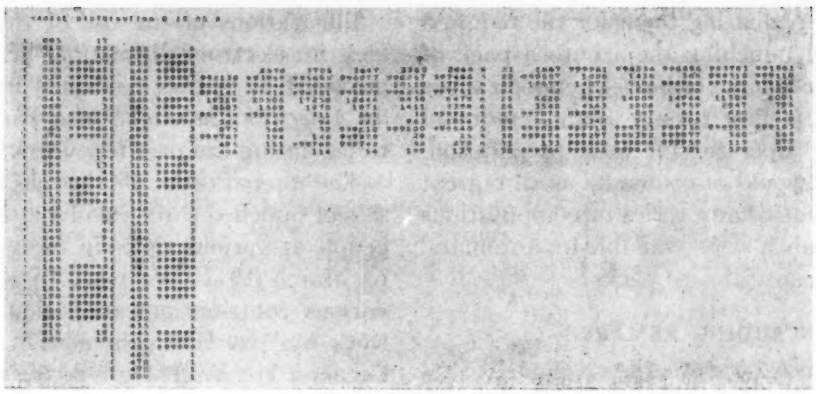

FIG. 1. Sample tabulation of electron diffraction cards. A radial distribution function for hexamethylenetetramine.

cards has been used, is shown in Fig. 1. For electron diffraction calculations this special treatment of the index cards is usually to be preferred to the normal one because it gives a much more compact and legible record—only rarely does an electron diffraction calculation involve frequencies which are spaced closely enough to favor the normal treatment.

The function to be evaluated by use of the punched cards is written in the form of Eq. (9). If the coefficients $G_i(x)$ are constants, the appropriate packs of cards are then withdrawn from the files, sorted, tabulated, resorted into filing order, and returned to the files in essentially the manner described in the preceding paper for the crystal structure calculations. The printed report is like that obtained in the crystal structure work except (usually) for the tabulation of the index cards. The only significant difference in procedure is in the resorting for filing where the sequence of operations is to sort on columns 77, 73 (zone), 76, 75, 74, and 73 (normal). Very frequently, however, some of these sorting operations can be omitted or performed manually, or the order may be changed to advantage, as, for example, in the evaluation of a series of intensity functions which have one or several terms in common. It is then useful to take the common packs from one file, and the rest from the other, so that the cards used in one calculation which are required also for the next may be recovered after one sorting, that on column 73 (normal).

If the coefficients $G_i(x)$ of the summation as first written down are not constants it is possible to carry out a mathematical transformation which makes them so, as is suggested by Eq. (7) which can indeed be approximated by a sum of sine terms with constant coefficients. Sometimes this is the expeditious thing to do, but often it is better to adopt some other procedure. Because our practical methods of handling variable coefficients are still being developed, it seems best not to give them in detail here, although two devices which are well established may be mentioned. The most common distribution of interatomic distances $l^2D_{ij}(l)$ which occurs as a result of the vibrations of molecules is a normal error curve distribution about l_0, the equilibrium value of $l_{ij}(l^2D_{ij}(l) = \text{Const. exp}\,[-\alpha(l_{ij}-l_0)^2])$. In our present work this distribution is best represented directly by the use of Eq. (6) (in the actual calculation the integration is adequately approximated by a summation over three to seven terms for values of l_{ij} spaced at intervals of about 0.05A in the neighborhood of l_0); heretofore, it was customary to make use of the mathematical transformation according to which the integral over l_{ij} is replaced by the single, approximately equivalent term $\exp(-as^2)\sin l_0 s$, with $a = 1/4\alpha$.

The second device is useful whenever a group of terms of the summation appear unchanged in a series of calculations. These terms are tabulated separately and the results are transferred to a special pack of cards which is then used for each calculation of the series. In particular, terms with variable coefficients may be handled

in this way by evaluating them for the required values of x and punching them onto a pack of cards. These cards have to be used enough times to justify the fifteen or twenty minutes required by an unskilled operator for their preparation. This procedure would of course be used to great advantage in almost any series of computations if a summary punch were available for automatic punching of the special card packs.

CONCLUDING REMARKS

A typical electron diffraction study involves the calculation of one or more radial distribution summations or integrals and five to thirty or more theoretical intensity functions, depending on the complexity of the molecule and the thoroughness of the investigation. By affording a threefold to tenfold reduction of the time required for these calculations the punched card procedure makes feasible the study of more complicated molecules for which the labor of making intensity calculations would otherwise be too great and makes practical the use of more powerful methods than could heretofore be used (e.g., the radial distribution integral). It reduces fatigue, for the operations of filing, sorting, and tabulating make less exacting demands on the operator than those of multiplication and adding involved with the Sherman-Cross strips. Finally, it is easier to check the correctness of all parts of the calculations, and the incidence of errors is decreased.

Illustrations of the use of the punched card files in electron diffraction investigations are provided by papers published in the *Journal of the American Chemical Society* from these Laboratories during the past few years.[6]

The preparation of the electron diffraction sets of punched cards involved the help of many people at various times in the period June 1940 to March 1941. We wish to acknowledge the various contributions to various phases of the work by Mr. H. Feldman, Dr. and Mrs. Paul Giguère, Mr. W. J. Howell, Jr., Dr. H. A. Lévy, Dr. R. E. Rundle, Dr. M. T. Rogers, Dr. W. Shand, Jr., Dr. R. A. Spurr, Dr. S. M. Swingle, Dr. A. L. Wahrhaftig, Dr. J. Waser, Dr. S. Weinbaum, and Dr. W. West. We are also greatly indebted to the International Business Machines Corporation, which made available the machines for this work, and to the Committee on Scientific Aids to Learning, which made the California Institute of Technology a grant for the preparation of sets of punched cards and for incidental expenses.

[6] The propargyl halides: L. Pauling, W. Gordy, and J. H. Saylor, J. Am. Chem. Soc. **64**, 1753 (1942); pirylene: reference 3; spiropentane: J. Donohue, G. L. Humphrey, and V. Schomaker, *ibid.* **67**, 332 (1945); methylisocyanide, W. Gordy and L. Pauling, *ibid.* **64**, 2952 (1942); ozone, W. Shand, Jr., and R. Spurr, *ibid.* **65**, 179 (1943); biphenylene, J. Waser and V. Schomaker, *ibid.* **65**, 1451 (1943); methylenecyclobutane and 1-methylcyclobutene, W. Shand, Jr., V. Schomaker and J. R. Fischer, *ibid.* **66**, 636 (1944); sulfur nitride, arsenic disulfide, arsenic trisulfide, and sulfur, Chia-Si Lu and J. Donohue, *ibid.* **66**, 818 (1944); hexamethylenetetramine, V. Schomaker and P. A. Shaffer, Jr. (to be published).

THE JOURNAL OF CHEMICAL PHYSICS VOLUME 14, NUMBER 11 NOVEMBER, 1946

Rotational Structure of Some Electronic Bands of Chlorine Dioxide

JESSE B. COON
Department of Physics, A. and M. College of Texas, College Station, Texas
(Received August 12, 1946)

The rotational structure of several violet absorption bands of ClO_2 has been studied. The bands considered correspond to the vibration transitions $(v_1'\ 0\ 0)\leftarrow(0\ 0\ 0)$ where $v_1'=1$, 2, 3, 4, and 5. The most prominent identifiable feature of the rotational structure is a doublet qQ branch resolved in the tail of each band. For $v_1'=1$, 2, and 3, the rotational wave numbers of these branches are given by

$$\nu_{1,2}{}^r=-\tfrac{1}{2}(0.0615+0.0042v_1')L(L+1)-\tfrac{1}{2}(1.188+0.008v_1')K^2+0.13L+0.174(v_1'-0.4)K\mp\tfrac{1}{2}[0.109(2K-L)-0.045(v_1'-1)].$$

This fits the spectrum in the observed range of quantum numbers, $K=11$ to 20 and $L=K$ to $K+8$. The first two terms are associated with that prolate symmetrical top which comes closest to the actual ClO_2 molecule. Hence, neglecting the effect of asymmetry on the spectrum,

$$2\Delta\bar{B}=-(0.0615+0.0042v_1')\ \text{cm}^{-1}$$

and

$$2(\Delta A-\Delta\bar{B})=-(1.188+0.008v_1')\ \text{cm}^{-1}.$$

The last term is associated with spin doubling. The coupling is shown to be close to Hund's "case b." The linear terms in L and K may be a consequence of the doubling. The term in $v_1'K$ describes an outstanding feature of the spectrum but is not interpreted. The bands are shown to be of the parallel type. A few qP and qR branches have also been identified and Δ_1F values have been found. Assuming the spectrum to be that of a prolate symmetrical top, the resulting values of $2\bar{B}$ for the vibrationless states are $2\bar{B}''=0.612$ cm^{-1} and $2\bar{B}'=0.550$ cm^{-1}. The value of $2\bar{B}''$ with the Cl—O distance $s''=1.53$A from electron diffraction is sufficient to determine the lower electronic state. The upper state is then determined from the values of $2\Delta\bar{B}$ and $2(\Delta A-\Delta\bar{B})$ for the vibrationless states. The resulting model of both states is designated as model (2). Error in this model, because of the fact that the effect of asymmetry was neglected, is found to be small. Asymmetry correction made on model (2) leads to the following model:

$$2\theta''=109°\pm3°,\qquad 2\theta'=92°\pm6°,$$
$$s''=1.53\text{A}\pm0.02\text{A},\qquad s'=1.805\text{A}\pm0.05\text{A}.$$

The rotational isotope effect is observed and explained but gives no additional information about the molecular model.

PART I

1. INTRODUCTION

PREVIOUS work[1] on the violet absorption spectrum of ClO_2 has concerned the vibrational structure. Urey and Johnston, and Ku have attempted vibrational analyses which have been modified by the author.[2] Urey and Johnston give an estimate of the relative intensities of the bands of some of the strongest progressions. Ku's measurements of band heads which were made from spectrograms taken with a 21-ft. grating are probably the most accurate published and these spectrograms show evidence of resolvable rotational structure.

The rotational structures of the electronic spectra of only a few non-linear polyatomic molecules have been partially resolved and studied.[3] The violet absorption spectrum of chlorine dioxide offers an opportunity for observing fine structure because an interval of about 250 cm^{-1} in several of the strongest bands is free from overlapping and because one of the moments of inertia differs considerably in the two electronic states. Photographs taken on the University of Chicago 30-foot grating spectrograph in the second order show interesting resolved fine structure in the tails of some bands. It is the purpose of this paper to describe and interpret as much of this rotational structure as seems possible.

2. THE ABSORPTION TUBE

The chlorine dioxide used in the absorption tube was prepared by the reaction of oxalic acid and potassium chlorate as described by Bray.[4] About eight parts of oxalic acid, two parts of potassium chlorate, and one part of water were mixed and sealed into a flask connected to an all

[1] H. C. Urey and H. Johnston, Phys. Rev. **38**, 2131 (1931). Z. W. Ku, Phys. Rev. **44**, 376 (1933).

[2] Jesse B. Coon, Phys. Rev. **58**, 926L (1940). The author plans to publish a detailed account of the vibrational analysis after taking more spectrograms in the vicinity of the origin.

[3] *Formaldehyde*, G. H. Dieke and G. B. Kistiakowsky, Phys. Rev. **45**, 4 (1934). *Nitrogen dioxide*, Louis Harris and G. W. King, J. Chem. Phys. **8**, 775 (1940). *Ammonia*, A. B. F. Duncan and G. R. Harrison, Phys. Rev. **49**, 211 (1936). *Benzene*, Anthony Turkevich and Mark Fred, Rev. Mod. Phys. **14**, 246 (1942). *Sulfur Dioxide*, N. C. Metropolis (cf. R. S. Mulliken), Rev. Mod. Phys. **14**, 204 (1942).

[4] W. Bray, Zeits. f. physik. Chemie **54**, 575 (1906).

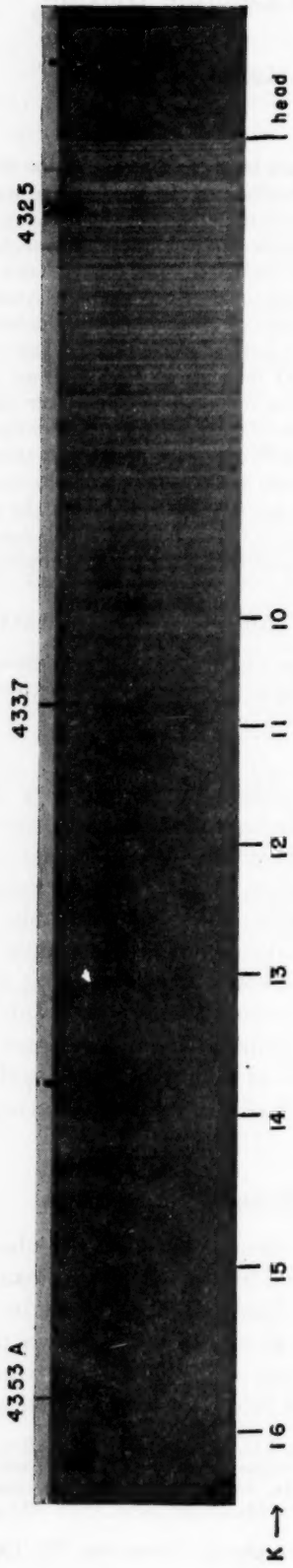

FIG. 1. Band 3. Leaders indicate first line of ν_1 series (persistant component of doublet Q branch) for seven sub-bands.

glass line consisting, in the following order, of a P_2O_5 tube, dry ice trap, 50-cm absorption tube with fused-on Pyrex windows, capillary tube, liquid nitrogen trap, the only stopcock, and an oil pump. The mixture was heated to 60°C under atmospheric pressure and the resulting gaseous mixture (ClO_2, CO_2, H_2O) displaced the air in the system. The ClO_2 was deposited in the dry ice trap in the form of orange red crystals. When the reaction was complete the CO_2 was pumped out, then the reaction flask and P_2O_5 tube were sealed off.

The vapor pressure of ClO_2 at dry ice temperature, less than one mm, was found sufficient to give many of the strong bands. The weaker bands were obtained by replacing the dry ice by a warmer mixture. The weakest band studied, referred to below as band 1, was obtained when the ClO_2 pressure was about 1 cm. Because of the decomposition of ClO_2 upon exposure to light, it was necessary to keep the gas flowing through the absorption tube during an exposure. The rate of flow was limited by the capillary tube at the exit end of the absorption tube. The oil pump was kept running during an exposure. After passing through the capillary, at least four of the constituents of the exposed gas were deposited in the liquid nitrogen trap. These substances were deposited in rings in the trap, the depth of the ring depending on the ease with which the substance condensed. Cl_2 gas penetrated to the bottom of the trap giving a lemon colored condensation. A thin deposit of undecomposed ClO_2 above this was orange in color. A red substance, probably Cl_2O, deposited above the ClO_2. When the liquid nitrogen was removed, the ClO_2 evaporated more quickly than the Cl_2O. Above this was observed, at times, a reddish orange ring which was much slower to evaporate than the other substances when the liquid nitrogen was removed. It is probable that this was Cl_2O_6.[5] The decomposition rate was greatly reduced by using a "noviol *A*" filter which cut out most of the radiation below 4300A.

3. DESCRIPTION OF BANDS MEASURED

Part of the lines of five bands in the region 4000–4700A were measured. These bands corre-

[5] Charles F. Goodeve and Frederick D. Richardson, J. Chem. Soc. 294 (1937, part 1).

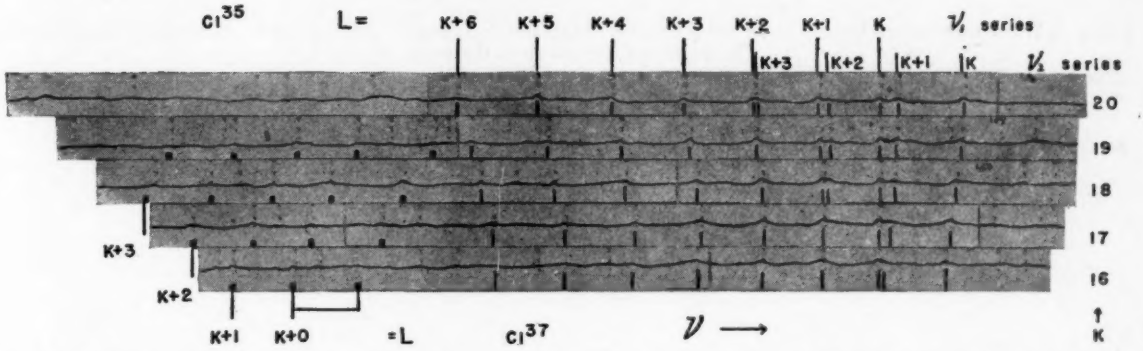

FIG. 2. Microphotometer trace of five sub-bands of band 4 showing isotope effect. The total trace was cut in segments each of which includes a sub-band. The first line of the ν_1 series in each sub-band was arbitrarily set on the same vertical line. Note that the perturbation effect which increases the intervals between the lines is quite marked in sub-band $K=16$. The author is indebted to Professor G. R. Harrison for traces of several bands taken on the Massachusetts Institute of Technology recording microphotometer.

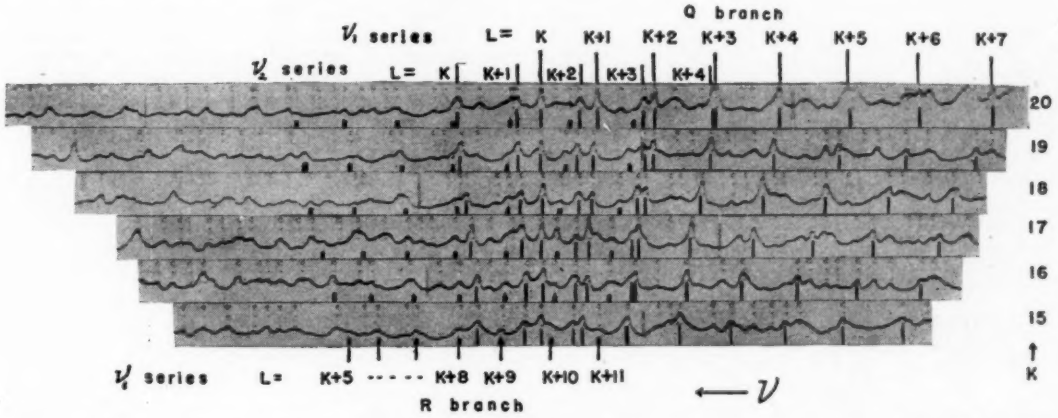

FIG. 3. Microphotometer trace of six sub-bands of band 3 showing identified Q and R branches. The total trace was cut in segments, each of which includes eight members of the Q branch of a sub-band. For all sub-bands the first line of the ν_1 series was arbitrarily set on the same vertical line.

spond to the vibrational transitions (v_1' 0 0) ←(0 0 0) with the breathing vibration quantum numbers $v_1'=1, 2, 3, 4, 5$.[2] These five bands will be designated hereafter by their corresponding values of v_1', band 1 referring to that band for which $v_1'=1$, etc. Predissociation, whose presence in this spectrum has been known for some time, first becomes clearly obvious in band 6, the widths of the lines being of the order of 1 or 2 cm^{-1} in this band. The wave numbers, as given by Ku,[1] of the heads of the bands considered are

v_1'	ν cm^{-1}
0	21016.2
1	21724.2
2	22425.5
3	23119.1
4	23806.9
5	24488.1
6	25164.4

Band 0 was not obtained with the 30-foot grating spectrograph because the spectrograph was not in adjustment for this region. Also, the existence of more overlapping and a greater complexity of fine structure for the bands of lower v_1' did not encourage an attempt to get this band.

Each band has a sharp head and is shaded toward the red (see Fig. 1). The tails of these bands are partially resolved, showing from three to ten sub-bands also shaded toward the red. Each sub-band contains a strong doublet branch which begins with a doublet of high intensity (see lines designated by $L=K$ in Figs. 2 and 3). The series of lines formed by the higher frequency doublet components fades out before that formed by the lower frequency components. The lines of the more persistent series will be designated by ν_1 and those of the shorter

TABLE I. Wave numbers of lines of observed qQ doublet branches (ν_1 components, lower left; ν_2 components, upper right). The band number given is the value of v_1'.

Band 1

K	12	13	14	15	16	17	18	19	$L(\nu_2)$
			607.34	590.19					14
			606.36	589.22	570.90				15
			605.34	588.17		550.36			16
			604.22	587.07		549.22	528.52		17
				585.93		548.07	527.31	505.45	18
						546.82	526.06	504.18	19
$L(\nu_1)$						545.59	524.80	502.88	20
13		623.57					523.45	501.51	21
14	21637.72	622.86	606.73				522.09	500.13	22
15	21636.91	622.05	605.95	588.60					23
16	21636.02	621.21	605.07	587.72	569.15				
17	21635.07	620.20	604.13	586.77	568.25	548.46			
18	21634.09		603.12	585.78	567.24	547.50	526.56		
19				584.72	566.14	546.44	525.49	503.35	
20				583.55	565.06	545.30	524.40	502.23	
21				582.40	563.84	544.12	523.20	501.04	
22				581.10	562.60	542.85	521.92	499.78	
23				579.79	561.27	541.52	520.60	498.49	
24					559.87	540.14	519.17	497.07	
25					558.43	538.68		495.60	
26					556.93	537.19	516.22	494.10	
27						535.59	514.65		
28								490.88	
29								489.17	

Band 2

K	12	13	14	15	16	17	18	19	20	$L(\nu_2)$
	22341.03									12
	22340.20	325.55								13
	22339.26	324.64	308.75							14
		323.66	307.79	290.66						15
			306.68	289.61	271.31					16
			305.65	288.52	270.20	250.74				17
				287.36	269.03	249.55	228.87			18
$L(\nu_1)$					267.82	248.31	227.67	205.75		19
12	22339.78					247.07	226.40	204.45	181.38	20
13	22339.05	324.18				245.68	225.09	203.09	179.98	21
14	22338.27	323.37	307.27					201.66	178.53	22
15	22337.36	322.51	306.42	289.09					177.06	23
16	22336.35	321.49	305.45	288.13	269.59				175.46	24
17	22335.34	320.36	304.44	287.15	268.63	248.91				
18	22334.29	319.43	303.34	286.09	267.55	247.86	226.99			
19	22333.14		302.21	284.88	266.41	246.73	225.89	203.74		
20	22331.86		300.93	283.71	265.19	245.50	224.73	202.53	179.24	
21			299.68	282.41	263.91	244.30	223.48	201.26	177.94	
22			298.33	281.06	262.55	242.88	222.16	199.89	176.62	
23					261.17	241.66		198.49	175.18	
24					259.67	240.04	219.32	196.96	173.47	
25						238.45	217.67		171.80	
26						236.85		193.75		
27						235.15		192.09		
29								190.29		

series by ν_2. In all sub-bands, the doubling is large enough so that the first two lines of the ν_2 series come before the first line of the ν_1 series. However, the interval between successive lines is greater for the ν_2 components and after a few lines the $(n+1)$th ν_2 line blends with the nth ν_1 line. The last line of ν_2 before blending is in most cases weaker or more diffuse than the corresponding line of ν_1. Up to that point ν_1 and ν_2 have approximately equal intensity. In general about two lines of ν_1 are considerably reenforced by this blending. The resulting strong lines have the appearance that would be expected from superimposing a fairly sharp line

TABLE I.—*Continued.*

Band 3

K	11	12	13	14	15	16	17	18	19	20	$L(\nu_2)$
	23048.98										11
		034.80									12
		033.78	019.28								13
			018.25	002.49							14
				001.39	984.34						15
				000.26	983.20	964.93					16
					982.01	963.72	944.23				17
$L(\nu_1)$						962.51	942.99	922.31			18
11	23047.89						941.64	920.98	899.09		19
12	23046.86	033.60				959.77		919.56	897.69	874.62	20
13	23045.86	032.70	017.98				938.79	918.12	896.24	873.18	21
14	23044.74	031.67	017.06	001.07				916.56	894.70	871.62	22
15	23043.56	030.63	016.04	000.09	982.81				893.03	870.03	23
16		029.49	014.93	999.03	981.78	963.29					
17		028.34	013.80	997.87	980.69	962.19	942.49				
18			012.53	996.69	979.47	961.03	941.33	920.44			
19				995.38	978.19	959.77	940.09	919.23	897.13		
20				994.04	976.86	958.40	938.79	917.93	895.83	872.56	
21				992.55	975.44	957.04	937.38	916.56	894.46	871.20	
22					973.97	955.57	935.92	915.07	893.03	869.77	
23					972.40	953.98	934.45	913.53	891.48	868.26	
24					970.76		932.79	911.98	889.89	866.68	
25							931.13	910.37	888.23	864.97	
26							929.35	908.52	886.50	863.28	
27							927.51	906.70	884.64	861.48	
28								904.91	882.76		
29									880.82		
30									878.81		
31									876.70		

Band 4

K	16	17	18	19	20	$L(\nu_2)$
	23652.14					16
		631.42				17
		629.99	609.36			18
			607.87	586.07		19
$L(\nu_1)$			606.31	584.53	561.55	20
16	23650.53			582.92	559.93	21
17	23649.13	629.67			558.29	22
18	23647.70	628.31	607.52			
19	23646.19	626.88	606.16	584.14		
20	23644.65	625.37	604.70	582.70	559.52	
21		623.81	603.17	581.21	558.03	
22		622.13	601.54	579.65	556.50	
23		620.40	599.85	577.95	554.84	
24		618.59	598.06	576.22	553.12	
25			596.22	574.39	551.34	
26			594.26	572.49	549.43	
27				570.50	547.47	
28				568.37	545.51	

Band 5

K	19	20	21	$L(\nu_2)$
	24267.33			19
		242.77		20
$L(\nu_1)$			216.99	21
19	24265.48			
20	24263.70	240.80		
21	24261.88	239.11	214.93	
22	24260.01	237.32	213.17	
23	24258.06	235.46	211.39	
24	24256.09	233.52	209.51	
25	24254.04	231.50		
26		229.41	205.49	
27		227.27	203.39	

and a more diffuse line. Farther along the intensity of the ν_1 lines return to normal, but the ν_2 lines do not reappear on the other side of the ν_1 lines unless perhaps in some cases as very diffuse lines.

The intervals between lines of the ν_1 (and ν_2) series in a sub-band increase with vibrational quantum number, while the doublet widths remain nearly constant. As a result the blending of the ν_1 and ν_2 lines takes place sooner for high than for low vibrational quantum numbers. Nevertheless, the above description of the relationship between ν_1 and ν_2 is true for all bands. Hence, more ν_2 lines are observed in bands corresponding to low vibration. For example, Table I shows that only one ν_2 line is observed in each sub-band of band 5 while five ν_2 lines are observed in each sub-band of band 1. However, it is believed that the coincidence of overlapping with the disappearance of ν_2 may be accidental,

TABLE II. First and second differences of ν_1 series in cm^{-1}. δ_L = best value for interval between first and second lines of a ν_1 series. $\delta\delta_L$ = second difference in a ν_1 series.

	K	δ_L	$\delta\delta_L$	wt.	Av. $\delta\delta_L$
Band 1					
	15	−0.874	−0.0657	1	
	16	−0.931	−0.0647	1	
	17	−0.985	−0.0670	1	
	18	−1.064	−0.0648	1	
	19	−1.125	−0.0652	1	−0.0655
Band 2					
	14	−0.878	−0.0683	1	
	15	−0.941	−0.0686	1	
	16	−0.990	−0.0714	1	
	17	−1.049	−0.0727	½	
	18	−1.097	−0.0731	½	
	19	−1.212	−0.0707	1	−0.0704
Band 3					
	11	−0.998	−0.057	0	
	12	−0.930	−0.061	0	
	13	−0.937	−0.0720	0	
	14	−0.988	−0.0734	½	
	15	−1.038	−0.0753	1	
	16	−1.104	−0.0731	½	
	17	−1.158	−0.0755	1	
	18	−1.238	−0.0668	0	
	19	−1.303	−0.0726	1	
	20	−1.364	−0.0729	1	−0.0739
Band 4					
	16	−1.395	−0.050	0	
	17	−1.356	−0.0757	½	
	18	−1.372	−0.0807	1	
	19	−1.424	−0.0802	1	
	20	−1.476	−0.0818	1	−0.080
Band 5					
	19	−1.77	−0.0537		
	20	−1.71	−0.0754		
	21	−1.74	−0.0749		

since predissociation seems to eliminate more and more lines from observation as the vibrational quantum number v_1' increases. This effect of predissociation also shows up in the fact that for bands 1 and 2 the branches are relatively hard to pick out from the numerous background lines associated with unidentified branches, while bands 4 and 5 appear quite simple, showing relatively few lines in addition to the branches measured.

4. TABLE I

Table I shows the wave numbers of the strong doublet branch for each of thirty-five sub-bands. Most of the lines were measured only once from one plate. However, in the case of band 3, some of the lines were measured on each of two plates. The agreement obtained in that case as well as the agreement when lines of band 4 were measured a second time, indicates that the wave numbers of very few of the lines have an error greater than 0.02 cm^{-1}. Some of the plates were measured by the Massachusetts Institute of Technology recording microphotometer. Because of the large amount of similar data available, it was thought unnecessary to repeat all measurements systematically. A source of error in determining the absolute values of the wave numbers arose from the fact that iron standards on the plates taken were relatively few, so that the correction curve often could not be drawn to a greater accuracy than ± 0.02 cm^{-1}.

Some uncertainty in the measured frequencies is introduced by the frequent blending of lines measured with background fluctuations caused by the great mass of unidentified weak lines. Additional small irregularities in intensities and in line positions apparently exist which may probably be attributed to genuine but minor quantum-mechanical perturbing effects.

It is of interest that the observed resolving power is of the order of 160,000 instead of the theoretical 300,000. This may be caused by broadening of lines because of predissociation.

The arrangement of Table I will now be considered. Two quantum numbers, K and L, are needed (see Eq. (6) below) to describe the rotational component of the wave numbers of the lines of a rigid, symmetrical top, to which the ClO_2 molecule approximates (see below). Providing the spectral positions of the band lines are a good deal more sensitive to one of these quantum numbers than to the other, there occurs for a given value of the sensitive quantum number a more or less isolated group of lines corresponding to various values of the insensitive quantum number. Such a group of lines is referred to as a sub-band. Since no products between quantum numbers occur in the theoretical expression for the spectrum of a rigid, symmetrical top, every sub-band should contain the same wave number intervals except as explained by so-called missing lines. Hence, the lines in one sub-band "corresponding" to the lines in another may be found by comparing the intervals of one sub-band with those of the other.

The molecule under consideration is not quite rigid, symmetrical, or unperturbed; nevertheless, wave number intervals of one sub-band are here found to be almost equal to those of other sub-

bands in the same band. The lower the band number, the better this equality is found to be. Table I gives the wave numbers of the strong doublet branches arranged for each band as follows. Both components of a doublet branch lie in the same column, the ν_1 lines below and the ν_2 lines above. "Corresponding" lines of different sub-bands lie in the same horizontal row. It is to be noted that in passing from any sub-band to the next sub-band toward lower frequencies, one doublet disappears. The quantum number assignment indicated in Table I will be discussed below.

5. FIRST AND SECOND DIFFERENCES WITHIN SUB-BANDS

Table II shows the second difference $\delta\delta_L$ for the ν_1 series of lines of each sub-band; also the best value for the interval δ_L between the first two lines of the ν_1 series of each sub-band is given. In the table each sub-band is characterized by a particular value of K. The best values of $\delta\delta_L$ and δ_L were determined for each sub-band by applying the method of least squares to the series of numbers representing the intervals between the lines assuming a constant second difference. Thus δ_L depends on the trend of these intervals.

Within any given sub-band no systematic variation in the second difference was observed. However, because of fluctuations in the second differences, a third difference as large as 0.001 cm^{-1} could easily exist without being detectable.

It may be noted from Table II that within experimental error the second difference $\delta\delta_L$ is independent of K, that is, it is constant within a given band except for the first one or two sub-bands observed in bands 3, 4, and 5; these sub-bands have an abnormally low second difference. It is interesting that, in the case of these three bands, it is the first sub-bands having recognizable structure that have the low second difference. The irregularity of these first sub-bands must be caused by a perturbing effect which according to the data advances to higher rotational energies as the vibrational energy increases. It is also of interest that although the second difference is small for these irregular sub-bands, the first interval δ_L is larger than would be expected from the trend of the more regular δ_L values. It should further be noted that for a given band the average difference between the first intervals δ_L might be expected to equal, but are smaller than, the average of the second differences $\delta\delta_L$. This anomalous characteristic of the spectrum decreases with decreasing band number becoming fairly small for band 1. This is attributed to a small warping of the spectrum, because of the above-mentioned perturbing effect, which decreases with band number. These irregularities will be disregarded from here on, all considerations below being based on the more regular features of the spectrum.

A second difference has been determined for each band by averaging the values of the second differences obtained from the separate sub-bands. In so doing, the sub-bands were weighted roughly according to the number of observed lines and the smoothness of the observed second differences. From the average second differences for bands 1, 2, and 3, that for band 0 was determined by extrapolation:

$$\delta\delta_L = -0.0615 \text{ cm}^{-1} \quad \text{(band 0)}.$$

There are not enough data to determine accurately the second difference for the ν_2 series of lines in each sub-band. However, the second differences of ν_2 are about the same or possibly smaller than those for ν_1.

TABLE III.

a. Intervals δ_K between sub-bands in cm^{-1}.

K	band 0	band 1	band 2	band 3
12		−14.86*	−14.87	−14.60*
13	(−16.16)	−16.12	−16.08	−15.93*
14	(−17.39)	−17.35	−17.30	−17.23
15	(−18.58)	−18.54	−18.52	−18.45
16	(−19.78)	−19.74	−19.69	−19.68
17	(−20.98)	−20.94	−20.79*	−20.85
18	(−22.18)	−22.14	−22.21*	−22.09
19	(−23.38)		−23.30	−23.25

b. Second differences $\delta\delta_K$ between sub-bands in cm^{-1}.

K	band 1	band 2	band 3	band 4	band 5
12	−1.260*	−1.198	−1.37*		
13	−1.240*	−1.217	−1.33*		
14	−1.185	−1.229	−1.263*		
15	−1.208	−1.163	−1.227		
16	−1.195	−1.112	−1.212	−1.40*	
17	−1.196	−1.421	−1.229	−1.32*	
18		−1.088	−1.180	−1.225	
19					−1.45*
Av $\delta\delta_K$	−1.196 (±0.001)	−1.204 (±0.003)	−1.212 (±0.006)	−1.225	

TABLE IV. Values of the doublings $\Delta\nu(K, L)=\nu_2(K, L)-\nu_1(K, L)$ observed for band 3, and their differences.

L	12		13		14		15		16		17		18		19		20		21		22		23
K																							
12	1.20	.12	1.08																				
			.22																				
13			1.30	.11	1.19																		
					.23																		
14					1.42	.12	1.30	.07	1.23														
							.23		.19														
15							1.53	.11	1.42	.10	1.32												
									.22		.21												
16									1.64	.11	1.53	.05	1.48										
											.21		.18										
17											1.74	.08	1.66	.11	1.55								
													.21		.20								
18													1.87	.12	1.75	.12	1.63	.07	1.56	.07	1.49		
															.21		.23		.22		.18		
19															1.96	.10	1.86	.08	1.78	.11	1.67	.12	1.55
																	.20		.20		.18		.22
20																	2.06	.08	1.98	.13	1.85	.08	1.77

6. FIRST AND SECOND DIFFERENCES BETWEEN SUB-BANDS

Table IIIa shows the best values for the intervals $\delta_K=\nu_1(K+1, L)-\nu_1(K, L)$ between sub-bands. Each number of the table is the average of the intervals between corresponding ν_1 lines of two neighboring sub-bands. The intervals marked by asterisks do not follow the general trend. Values of δ_K for band 0 are determined by extrapolating from observed δ_K values.

The second differences $\delta\delta_K=\delta_{K+1}-\delta_K$ between sub-bands are shown in Table IIIb. Each number of the table is obtained from the three adjacent sub-bands characterized by K, $K+1$, and $K+2$ and is the average of the second difference between corresponding lines of these three bands. No systematic variation with L is observed. The high second differences marked with an asterisk in bands 3, 4, and 5 are apparently caused by the perturbing effect already mentioned. These particular second differences were not included in the determination of the average second difference for each band. From the average $\delta\delta_K$ values for bands 1, 2, and 3, that for band 0 was determined by extrapolation:

$$\delta\delta_K=-1.188\ \text{cm}^{-1}\quad\text{(band 0)}.$$

The ν_2 series furnish relatively few second differences, but the average for all bands is -1.20 cm^{-1}.

It is interesting to note that as the band number increases the second differences $\delta\delta_K$ increase while the first differences δ_K decrease. This will be described by a linear term in K which varies with vibration.

7. OBSERVED DOUBLING

Since ClO_2 has an odd number of electrons, a spin doubling is expected. As was mentioned in Section 3, the strong branch in each sub-band is composed of doublets. Let the doublet widths $\nu_2(K, L)-\nu_1(K, L)$ be designated by $\Delta\nu(K, L)$. It will be shown that the $\Delta\nu(K, L)$ values may be represented reasonably well by

$$\Delta\nu(K, L)=\Delta\gamma(2K-L)-a(v'-1),\qquad(1)$$

with $\Delta\gamma=0.109$ cm^{-1} and $a=0.045$ cm^{-1}. Here the first term describes the major part of the doubling.

The $\Delta\nu(K, L)$ values obtained from the data of band 3 are shown in Table IV. There are three types of differences that can be taken from this table of $\Delta\nu(K, L)$ values: namely, horizontal (h), vertical (v), and diagonal (d). There is no definite indication that any of these differences vary with L or with K. However, a significant variation could be hidden by the fluctuation of the data and the shortness of the series. According to Eq. (1), the horizontal and diagonal differences should be the same, and equal to $\Delta\gamma$, while the vertical differences should be twice this. When the experimental differences are determined, it is found that these simple relations are nearly but not quite true.

A value for the diagonal difference was obtained by applying the method of least squares

to each diagonal. The results for five bands are shown in Table Va. The numbers are underlined according to their weight. The weighted average of these numbers gives a diagonal difference of 0.109. The average of horizontal and vertical differences for the first three bands are shown in Table Vb. The fact that these differences indicate a slightly lower value for $\Delta\gamma$ than the diagonal differences shows that Eq. (1) does not represent the data exactly.

It is observed that for given values of K and L the magnitudes $\Delta\nu(K, L)$ of the doublet widths decrease slightly with increasing vibrational quantum number. To illustrate this variation, smoothed observed values for $\Delta\nu(19, 19)$ and $\Delta\nu(16, 16)$ were estimated to within 0.01 cm^{-1} for each band and compared with values calculated from Eq. (1). The results are given in Table VI. The second term of Eq. (1) is required to describe this variation with band number which appears to be essentially independent of K and L.

8. EVIDENCE FOR "CASE b" COUPLING

A theoretical expression[6] for the rotational term values of a rigid diatomic molecule including doubling due to a resultant electronic spin $S=\frac{1}{2}$ is given by Hill and Van Vleck. In their notation the term values are

$$F_j=B\{(j+\tfrac{1}{2})^2-\sigma_k^2\pm\tfrac{1}{2}[4(j+\tfrac{1}{2})^2+\lambda(\lambda+4)\sigma_k^2]^{\frac{1}{2}}\}.$$

Here j determines the total angular momentum of the molecule including spin, and σ_k the component of the latter along the line joining the atoms. The quantity λB is the coupling constant between σ_k and spin. Interaction between spin and rotation about an axis perpendicular to the symmetry axis is neglected by Hill and Van Vleck. The minus sign corresponds in Hund's "case b" to terms arising from parallel coupling ($j=j_k+\frac{1}{2}$) and the plus sign to antiparallel coupling ($j=j_k-\frac{1}{2}$), where j_k is the total angular momentum excluding spin.

TABLE V.

a. Observed diagonal differences $=\Delta\gamma_d=\Delta\nu(K+1, L+1)-\Delta\nu(K, L)$.

	band 1	band 2	band 3	band 4	band 5
$L=K$	0.123	0.109	0.109	0.102	0.105
$L=K+1$	0.111	0.109	0.1125	0.078	
$L=K+2$	0.104	0.111	0.105		
$L=K+3$	0.104	0.115			
$L=K+4$	0.109				

b. Observed horizontal differences, and vertical differences.

	band 1	band 2	band 3
$\Delta\gamma_h=\Delta\nu(K, L)-\Delta\nu(K, L+1)$	0.105	0.105	0.101
$2\Delta\gamma_v=\Delta\nu(K+1, L)-\Delta\nu(K, L)$	2×0.107	2×0.108	2×0.104

[6] E. L. Hill and J. H. Van Vleck, Phys. Rev. **32**, 261 (1928).

TABLE VI.

Band	Obs. $\Delta\nu(19, 19)$	Calc. $\Delta\nu(19, 19)$	Obs. $\Delta\nu(16, 16)$	Calc. $\Delta\nu(16, 16)$
1	2.07	2.07	1.73	1.74
2	2.02	2.03	1.68	1.70
3	1.97	1.98	1.65	1.65
4	1.93	1.94	1.61	1.61

Apparently this formula should also apply to any rigid symmetrical top molecule with $S=\frac{1}{2}$ if a term AK^2 is added to include the rotational energy about the symmetry axis of the molecule. If the notation is changed to that of the present paper[7] ($j\to J$, $j_k\to L$, $\sigma_k\to K$, $\lambda\to\gamma/\bar{B}$) and if the formula is expressed in terms of L instead of J, it may be written in the form

$$\begin{aligned} F_1&=AK^2+\bar{B}\{(L+1)^2-K^2 \\ &\qquad -\tfrac{1}{2}[4(L+1)^2+\lambda(\lambda-4)K^2]^{\frac{1}{2}}\}, \\ F_2&=AK^2+\bar{B}\{(L)^2-K^2 \\ &\qquad +\tfrac{1}{2}[4L^2+\lambda(\lambda-4)K^2]^{\frac{1}{2}}\}. \end{aligned} \tag{2}$$

For Hund's "case b" a term having given values of K and L is split into two components F_1 and F_2 given by the above formulas. F_1 and F_2 correspond, respectively, to $J_1=L+\frac{1}{2}$ and $J_2=L-\frac{1}{2}$. It is not known whether ν_1 and ν_2, defined empirically in Section 3, correspond to F_1 and F_2, respectively, or *vice versa*.

If it is assumed that the spin coupling in ClO_2 is close to "case b" type (λ small) and if it is noted that L is approximately equal to K for the doublets observed, the F's may be expanded in terms of γ and the following approximate expression for the observed doublet widths

[7] Throughout this paper, L is used as the quantum number of the total angular momentum of molecular rotation excluding electron spin, while J is used for the quantum number of the total angular momentum including the electron spin.

$\Delta\nu=(F_1'-F_1'')-(F_2'-F_2'')$ may be obtained:

$$\Delta\nu=\Delta\gamma K^2/L+\tfrac{1}{2}. \quad (3)$$

It is found that the doubling is approximately symmetrical.

This theoretical expression does not fit the data as well as the empirical relation given by Eq. (1), but a certain qualitative agreement between (1) and (3) indicates that the coupling type is close to "case *b*." For the large K values of the observed doublets, Eq. (3) does not differ greatly from the empirical expression $\Delta\gamma(2K-L)$ which composes the large part of the observed $\Delta\nu$. According to Eq. (3) the diagonal differences should be quite close to $\Delta\gamma$, and the horizontal differences should average about $0.8\Delta\gamma$. This disagreement between diagonal and horizontal differences has the same sign as is observed, but has about four times the observed magnitude. This departure from "case *b*" appears to be a likely explanation for the observed linear terms in L and K. (See Sections 12 and 13.)

PART II

9. ENERGY LEVELS OF AN ASYMMETRICAL TOP[8]

Let $I_A<I_B<I_C$ be the three moments of inertia of a molecule and let A, B, C be the corresponding "reciprocals of inertia" where $A=h/8\pi^2CI_A$, etc. Formulas for calculating the exact energy levels of a rigid asymmetrical top are known[9] for values of the rotational angular momentum[7] up to $L=11$. However, the range of quantum numbers associated with the spectral lines here observed lies above $L=11$, being essentially $L=K$ to $K+8$ with $K=11$ to 20.

For these large values of L an approximate formula given by Witmer[10] is useful. This formula may be written in two forms. One form is

$$F_p=\bar{B}_pL(L+1)+(A-\bar{B}_p)K_p^2$$
$$+\frac{1}{32}\frac{(B-C)^2}{(A-\bar{B}_p)}\left[\frac{L^2(L+1)^2}{K_p^2-1}+2L(L+1)-3K_p^2\right], \quad (4)$$

where $2\bar{B}_p=B+C$, and F_p is the rotational term value in cm^{-1}. The first two terms will be referred to as the "prolate symmetrical top approximation." The last term is the first correction term for asymmetry. Witmer's formula may also be written in the form

$$F_o=\bar{B}_oL(L+1)+(C-\bar{B}_o)K_o^2$$
$$+\frac{1}{32}\frac{(A-B)^2}{(C-\bar{B}_o)}\left[\frac{L^2(L+1)^2}{K_o^2-1}+2L(L+1)-3K_0^2\right], \quad (5)$$

where $2\bar{B}_o=A+B$. Here the first two terms will be referred to as the "oblate symmetrical top approximation." K_p and K_o are approximate quantum numbers.

The range of quantum numbers for which formulas (4) and (5) may be applied will now be considered. The energy levels of a rigid asymmetrical top model may be calculated for say $L=8$ using the exact formulas of Nielsen. The levels obtained are doublets. If the average be taken for each doublet, a set of levels are obtained which may be compared to the two sets of levels obtained by using Eqs. (4) and (5) and if this comparison is made for several models of different asymmetry, the following relationships may be noted. For a given value of L, the high energy levels (average of doublets) may be approximately calculated using Eq. (4) ($K_p=L$ giving the highest level) while the low energy levels may be calculated using Eq. (5) ($K_o=L$ giving the lowest level). Only a few intermediate levels cannot be approximated in this way. Hence, the approximate quantum number K_p may be associated with the high doublet levels and K_o may be associated with the low doublet levels. The doublet separation for a given L is small when $K=L$ and increases as $(L-K)$ increases, remaining small compared to the asymmetry correction except for the few intermediate levels. If the top is more nearly prolate than oblate, Eq. (4) holds through a greater range than Eq. (5), and *vice versa*. If the top is only slightly asymmetric being nearly prolate for example, Eq. (4) holds except for the lowest values of K.

In the next section it will be shown, on the basis of what is already known about ClO_2, that it is closer to a prolate symmetrical top than to an oblate top. Hence, in the following sections the prolate symmetrical top approximation is

[8] A theoretical discussion of rotational energy levels of non-linear triatomic molecules is given by R. S. Mulliken, Phys. Rev. **59**, 873 (1941).

[9] H. H. Nielsen, Phys. Rev. **38**, 1432 (1931). For corrections and extension to $L=11$, see H. M. Randall, D. M. Dennison, N. Ginsberg, and L. R. Weber, Phys. Rev. **52**, 160 (1937). See also G. W. King, R. M. Hainer, and P. C. Cross, J. Chem. Phys. **11**, 27 (1943).

[10] E. E. Witmer, Proc. Nat. Acad. **13**, 60 (1927).

assumed. The energy levels will be designated by the quantum numbers of the corresponding prolate symmetrical top. In a closing section it will be shown that the asymmetry correction is of the order of experimental error.

10. TENTATIVE MODEL OF ClO_2 MOLECULE AND IDENTIFICATION OF K AND L STRUCTURES

Tentative moments of inertia were calculated for the lower electronic state using the Cl−O distance of 1.53A found from electron diffraction experiments[11] and the approximate O−Cl−O angle of 122° 50′ determined from the three vibrational frequencies established for the lower state.[2] It is recognized that the angle determined on the basis of the valence force approximation may have a considerable error. However, that the angle is fairly large in the ground state is supported by the electron diffraction result for this angle, 137°±15°. Thus, tentatively,

$$I_A'' = 14.77\times10^{-40}\ \text{g-cm}^2.$$
$$I_B'' = 95.2\times10^{-40}\ \text{g-cm}^2.$$
$$I_C'' = 110.0\times10^{-40}\ \text{g-cm}^2.$$

Since I_B and I_C are roughly equal, the molecule in the normal state approximates a prolate symmetrical top with the symmetry axis (A axis) parallel to the line joining the oxygen atoms. The same is assumed to be true for the excited state since, according to vibrational analysis, the angle diminishes only about 11 degrees in this state.

In order to make some preliminary calculations, it will be assumed that the rotational energy levels of ClO_2 are given by the "prolate top approximation" formula

$$F(K,L) = \bar{B}L(L+1) + (A-\bar{B})K^2. \qquad (6)$$

Here K must not be too small. This approximation neglects the asymmetry term which is quite small for the above-mentioned model. Even for a 109° model the coefficient of the asymmetry term of Eq. (4) is less than 0.0002 while $\bar{B}$ is of the order of 0.3. The effect of asymmetry will be discussed in detail in a later section. This expression also neglects terms such as might arise from rotational stretching, interactions between rotation and vibration, and perturbations.

[11] L. Pauling and L. O. Brockway, J. Am. Chem. Soc. 57, 2684 (1935).

The wave number ν of a line of an electronic band is usually expressed as the sum of three terms, namely, electronic, vibrational, and rotational. That is,

$$\nu = \nu^e + \nu^v + \nu^r.$$

For a symmetrical top molecule the rotational part is given by

$$\nu^r(K'', L'') = F'(K', L') - F''(K'', L''). \qquad (7)$$

According to customary symmetrical top notation, $\Delta K \equiv K' - K'' = -1,\ 0,\ +1$ correspond, respectively, to p, q, and r branches, while $\Delta L \equiv L' - L'' = -1,\ 0,\ +1$ correspond, respectively, to P, Q, and R branches.

Whether we are dealing with perpendicular-type bands ($\Delta K = \pm 1$) or with parallel-type bands ($\Delta K = 0$), and regardless of what branches in these bands we are dealing with, the second differences in the L structure (K' and K'' constant) and in the K structure (L' and L'' constant) should, on the basis of Eqs. (6) and (7), be equal to $2\Delta\bar{B}$ and $2(\Delta A - \Delta\bar{B})$, respectively, where

$$\left.\begin{aligned} \Delta\bar{B} &= \frac{h}{8\pi^2 c}\left(\frac{1}{I_{\bar{B}}'} - \frac{1}{I_{\bar{B}}''}\right) \\ \text{and} \\ \Delta A &= \frac{h}{8\pi^2 c}\left(\frac{1}{I_A'} - \frac{1}{I_A''}\right) \\ \text{in which} \\ \frac{1}{I_{\bar{B}}} &= \frac{1}{2}\left(\frac{1}{I_B} + \frac{1}{I_C}\right). \end{aligned}\right\} \qquad (8)$$

It is necessary to determine which of the second differences called $\delta\delta_L$ and $\delta\delta_K$ in Sections 5 and 6 is to be identified as essentially $2\Delta\bar{B}$ and which as $2(\Delta A - \Delta\bar{B})$. Both the intervals between the sub-bands and the intervals between the lines of a sub-band increase toward the red end of the spectrum. Hence, both of the observed second differences are negative; therefore, both $\Delta\bar{B}$ and $(\Delta A - \Delta\bar{B})$ are negative. It then follows from (8) that both $I_{\bar{B}}$ and I_A become larger in the excited state. The observed second differences divided by two are approximately -0.03 and -0.6. Considering the value of $I_B'' \approx I_C''$ calculated above, it is impossible to identify -0.6

with $\Delta\bar{B}$ since $h/8\pi^2cI_B''$ is considerably less than 0.6. Therefore, -0.03 is identified with $\Delta\bar{B}$ and -0.6 with $(\Delta A-\Delta\bar{B})$. Hence,

$$\delta\delta_L\approx 2\Delta\bar{B}, \quad \delta\delta_K\approx 2(\Delta A-\Delta\bar{B}). \tag{9}$$

These relations are not necessarily exact because Eq. (6) is not the exact expression for the actual term values. Equation (9) means that K quantum numbers are associated with the sub-bands and L quantum numbers are associated with the lines of the sub-bands and explains the notation already used for the observed differences. Whether this or the reverse assignment is correct may also be determined on the basis of the rule $L\geqq K$.

The values of $\Delta\bar{B}$ and $(\Delta A-\Delta\bar{B})$ from the observed second differences determine the changes in the moments of inertia at excitation. Using the tentative moments of inertia calculated above for the lower state, and the second differences $-0.0739\approx 2\Delta\bar{B}$ and $-1.212\approx 2(\Delta A-\Delta\bar{B})$ that were found from band 3, tentative moments of inertia for the excited state may be calculated. These are

$$I_A' = 22.50\times 10^{-40}\ \text{g-cm}^2,$$
$$I_B' = 118.2\times 10^{-40}\ \text{g-cm}^2.$$

These moments of inertia correspond to a Cl$-$O distance of 1.69A and an angle of 115°. This angle is qualitatively consistent with the result of 112° determined from the three vibrational frequencies established for the upper state.[2] The above considerations give tentative models for both states.

11. PROOF THAT THE OBSERVED BANDS ARE PARALLEL BANDS

Evidence will now be given to show that the electric moment associated with the electronic transition is parallel to the quasi-symmetry axis (A axis). On the basis of the above-mentioned tentative model, diagrams of sub-bands for both parallel- and perpendicular-type bands were constructed,[12] showing the distribution of the separate lines as well as their relative intensities. The relative intensities of the lines are given by the Hönl-London formulae.[13] It was found that, for sub-bands with K values greater than 10, there are certain similarities between perpendicular-type sub-bands with $\Delta K=-1$ and parallel-type sub-bands. Figure 4 shows an example of each type of sub-band. In both types each sub-band has a strong branch consisting of a group of lines in which the spacing increases and the intensity decreases toward the red, and a weaker branch which starts on the violet side of the first line of the strong branch and extends into the strong branch. In the case of the perpendicular-type sub-band the two branches mentioned are P (strong) and Q (weak), while in the case of the parallel-type sub-band the two branches are Q (strong) and R (weak). The third branch which is weak in both types of sub-bands will be mentioned below.

In the spectrum under consideration, it is observed that there is one strong branch (doublet) in each sub-band. A weak branch which follows the above description is also found in eight of the sub-bands (see Fig. 3). It is observed that at a given point in the spectrum the interval between two lines of the strong branch is smaller than the interval between two lines of the weak branch. This means that the strong branch must be a Q branch and, hence, that the weak branch is an R branch. *Therefore, the observed bands must be of the parallel type.*

Further evidence supporting this conclusion is the fact that a weak third branch (P) has been observed in two sub-bands. These P branches are qualitatively in the same position as in the constructed diagram of a parallel sub-band. The reality of the above-mentioned P branches was proven by obtaining the same Δ_1F' and Δ_1F'' values (see Eq. (18) below) from these P and the Q branches as are obtained from the R and Q branches.

Additional evidence that the bands are of the parallel type is given by the fact that the r branch of sub-bands ($\Delta K=+1$) expected for perpendicular-type bands does not appear. Using the observed second differences in the K structure one can compute that, if the bands were perpendicular, the r branch of sub-bands would come to a head very quickly and degrade to the red only about three sub-bands behind the p branch of sub-bands ($\Delta K=-1$).

A qualitative consideration of the observed

[12] Some examples of such a construction for SO_2 are discussed by N. Metropolis, Phys. Rev. 60, 283 (1941).

[13] G. Herzberg, *Infra-Red and Raman Spectra* (D. Van Nostrand Company, New York, 1945), pp. 421 and 426.

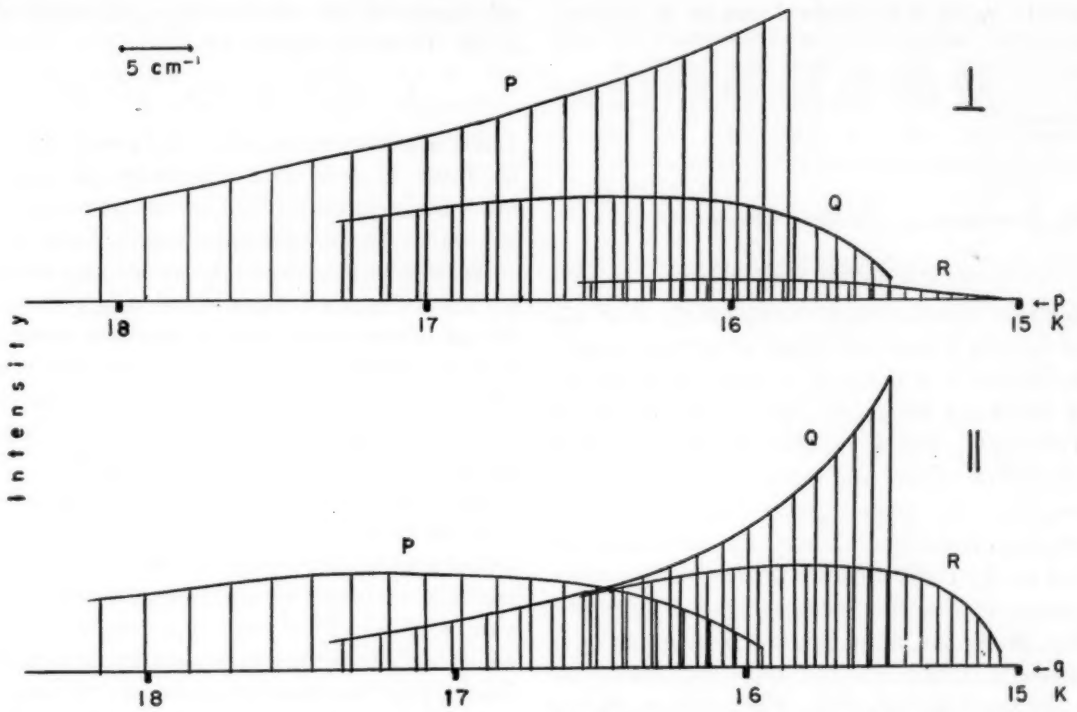

FIG. 4. Computed sub-band $K''=15$ constructed for both perpendicular and parallel type bands on the basis of the symmetrical top approximation and the tentative model. (See Section 10 for the moments of inertia of this model.) The heavy leaders show the relative positions of the origins of other sub-bands, p branch of origins above and q branch below. Wave numbers increase toward the right.

distribution of intensity within the sub-bands also indicates parallel type bands. The Q branch of a sub-band of a parallel type band diminishes in intensity faster than the P branch of a sub-band of a perpendicular type band. The author noticed this indication of parallel bands before any of the above arguments were considered.

12. ASSIGNMENT OF THE QUANTUM NUMBERING AND DESCRIPTION OF THE K STRUCTURE

The large second difference in the K structure must, of course, be attributed primarily to the coefficient of the K^2 term in the prolate symmetrical top approximation, see Eq. (6). Because of the large magnitude of this second difference, which is attributed to the fact that I_A approximately doubles in the excited state, it is considered probable that terms such as might arise from stretching, asymmetry, perturbations, and interactions would be small in comparison to the K^2 term. Therefore, the quantum numbering determined in this section on the basis of the K structure is considered more reliable than that determined from any other feature of the spectrum. For the first line of a Q branch of a given sub-band $L=K$. Hence, if the K numbering is determined, the L numbering is known.

On the basis of the prolate symmetrical top approximation to the energy levels, the qQ branch ($\Delta L=\Delta K=0$) for a given band should be given by

$$\nu_{1,2}{}^r=(\Delta\bar{B})L(L+1)+(\Delta A-\Delta\bar{B})K^2 \mp\tfrac{1}{2}[\Delta\gamma(2K-L)-a(v'-1)], \quad (10)$$

where the quantity in square brackets is added to describe the doubling attributed to spin. Since ν_1 has been chosen to designate the doubling component toward the red, it corresponds to the minus sign in the doubling term. It is not known whether $\nu_1{}^r$, defined here empirically, corresponds to $F_1'-F_1''$ or to $F_2'-F_2''$, see Eq. (2).

On the basis of (9) and (10) it might be expected that the K structure would be fairly well described by

$$\nu_{1,2}{}^r=f(L,v')+\tfrac{1}{2}\delta\delta_K K^2\mp\tfrac{1}{2}\Delta\gamma(2K). \quad (11)$$

Substituting Eq. (11) into the expression $\delta_K=\nu_1{}^r(K+1,L)-\nu_1{}^r(K,L)$ giving the first difference

TABLE VII. Values of K calculated from the K structure.

Band 1	11.83	12.89	13.91	14.91	15.91	16.92	17.92	
Band 2	11.76	12.76	13.78	14.79	15.76	16.68	17.88	18.76
Band 3	11.46	12.55	13.63	14.63	15.65	16.61	17.64	18.59
K numbering indicated	12	13	14	15	16	17	18	19

in the K structure, one may obtain

$$\delta_K=\tfrac{1}{2}\delta\delta_K(2K+1)-\Delta\gamma. \quad (12)$$

Using the experimental values of δ_K and $\delta\delta_K$ from Section 6 and the value of $\Delta\gamma=0.11$ cm^{-1} from Section 7, a value of K was calculated for each sub-band interval. The results are given in Table VII. The K numbering indicated here is adopted as correct and is the same as that used throughout the paper. Since this integral K numbering is assumed correct, a term must be added to the right member of Eq. (12) in order to make it describe accurately the observed values of δ_K given in Section 6. This term is empirically found to be $\Delta b(v'-d)$ where $\Delta b=0.174$ cm^{-1} and $d=0.41$. The addition of this term to the right member of Eq. (12) requires that the term $\Delta b(v'-d)K$ be added to the right member of Eqs. (10) and (11). Hence, the K structure of the qQ branch is accurately described by

$$\nu_{1,2}{}^r=f(L,v')+\tfrac{1}{2}\delta\delta_K K^2 +\Delta b(v'-d)K\mp\tfrac{1}{2}\Delta\gamma(2K). \quad (13)$$

Because of the experimental error in $\delta\delta_K$, the values of Δb and d may be in considerable error. For example, the variation in $\delta\delta_K$ with band number could be adjusted within experimental error so as to reduce d to zero. On the other hand, it is certain that the term $\Delta bv'K$ describes a real characteristic of the observed K structure.

13. QUANTUM NUMBERING INDICATED BY L STRUCTURE AND DESCRIPTION OF THE L STRUCTURE

The quantum number assignment may be determined on the basis of the L structure in a manner analogous to the determination on the basis of the K structure. On the basis of Eq. (10), it might be expected that the L structure would be fairly well described by

$$\nu_{1,2}{}^r=F(K,v')+\tfrac{1}{2}\delta\delta_L L(L+1)\pm\tfrac{1}{2}\Delta\gamma L. \quad (14)$$

Now the first interval of the ν_1 series for a given sub-band is $\delta_L=\nu_1{}^r(L+1,K)-\nu_1{}^r(L,K)$ in which $L=K$. Hence by using (14),

$$\delta_L=\delta\delta_L(L+1)+\tfrac{1}{2}\Delta\gamma, \quad (L=K). \quad (15)$$

Using experimental values of δ_L and $\delta\delta_L$ given in Table II and using the value of $\Delta\gamma=0.11$ cm^{-1} from Section 7, K was calculated for each sub-band. The results are given in Table VIII.

As shown in the table, the numbering indicated by the L structure is two less than that indicated by the K structure. The L structure determination is, however, considered less reliable because the second differences $\delta\delta_L$ are relatively small and any terms that have been neglected would be likely to produce a significant effect.

Substituting the adopted quantum numbering and the observed constants into Eq. (15), it is found that a term must be added to the right member in order to describe the experimental values of δ_L. This term is constant ($\Delta c=0.13$ cm^{-1}) within a band, especially for band 1. There may be some increase of this constant with v', but this increase is of the order of experimental error. The addition of a constant Δc to the right member of Eq. (15) requires the addition of a term ΔcL to the right member of Eq. (14). Hence, the L structure of the qQ branch is accurately described by

$$\nu_{1,2}{}^r=F(K,v')+\tfrac{1}{2}\delta\delta_L L(L+1)+\Delta cL\pm\tfrac{1}{2}\Delta\gamma L. \quad (16)$$

14. FINAL DESCRIPTION OF qQ BRANCHES AND POSITION OF BAND HEADS

It has been shown that the qQ branches of bands 1, 2, and 3 can be described by

$$\nu_{1,2}{}^r=\tfrac{1}{2}\delta\delta_L L(L+1)+\tfrac{1}{2}\delta\delta_K K^2+\Delta cL +\Delta b(v'-d)K\mp\tfrac{1}{2}[\Delta\gamma(2K-L)-a(v'-1)]. \quad (17)$$

It should be emphasized that this formula does not necessarily hold outside of the range of observations, $K=11$ to 20 and $L=K$ to $K+8$.

TABLE VIII. Values of K calculated from L structure.

Band 1		13.2	14.0	14.9	16.1	17.0	
Band 2	12.2	13.1	13.8	14.7	15.4	17.0	18.3
Band 3				15.4	16.5	17.4	18.2
Band 4						17.5	18.1
Numbering indicated here	12	13	14	15	16	17	18
Numbering used throughout paper	14	15	16	17	18	19	20

It is also to be noted that all the constants except $\Delta\gamma$ and a were obtained from the ν_1 series, which corresponds to the minus sign in the doubling term. The first two terms are identified with the prolate symmetrical top approximation. The constants of these terms, given in Tables II and IIIb, vary with band number v'. In Section 18 it will be shown that asymmetry may contribute as much as 30 percent to $\delta\delta_L$. However, up to that Section it is considered that, except for the linear terms, the spectrum is that of a symmetrical top. The doubling term is attributed to spin. The constants of this term are given in Section 7. The third and fourth terms, see Sections 12 and 13, are empirical terms which, except for $\Delta bKv'$, may possibly be associated with the spin doubling. This term in Kv' is not interpreted. There is no empirical evidence of the existence of fourth power terms in L and K.

The observed interval between a line $K=L=19$ and the head of the corresponding band may be determined from the wave number of the line given in Table I and the wave number of the band head given in Section 3. This interval for five bands is given in the right hand column of Table IX. It is interesting to compare this interval with the value of $\nu_1{}^r$ calculated for bands 1, 2, and 3 from Eq. (17). The results of this calculation are given in the left-hand column. It is to be noted that Eq. (17) was obtained without reference to the band heads. The position of the band origin with respect to the observed lines $K=L$ is, of course, not appreciably affected by asymmetry if, as is the case, the energy levels for high $K=L$ values are not appreciably affected by asymmetry.

In order to compare $\nu_1{}^r$ with $\nu_1-\nu_{\text{head}}$, the interval between the band origin and the band head, which should be caused by the R branch of the first sub-band, must be added to the magnitude of $\nu_1{}^r$. If the effect of asymmetry is taken into account, the calculated interval is about 1.3 cm^{-1}. Hence, for band 1 the disagreement between calculated and observed $\nu_1-\nu_{\text{head}}$ is about 5.4 cm^{-1}. It seems possible that this disagreement is caused by the observed perturbation. For example, for band 3, see Table III, the first few intervals δ_K between sub-bands are smaller than would be expected on the basis of a constant second difference of about 1.20. If it be supposed that the intervals between several of the unobserved sub-bands in all bands are smaller than would be expected on the basis of a constant second difference, the actual distance to the head would be less than the theoretical distance, as is found to be the case.

TABLE IX.

	$\nu_1{}^r(19, 19)$ calc.	$\nu_1(19, 19)-\nu_{\text{head}}$
Band 1	-224.9 cm^{-1}	-220.8 cm^{-1}
Band 2	-224.0	-221.8
Band 3	-222.8	-222.0
Band 4		-222.8
Band 5		-222.6

PART III

15. Δ_1F VALUES

It has been pointed out that each sub-band contains a strong doublet Q branch which was easily identified. However, it was also necessary to locate the weaker P and R branches (see Fig. 4) in order to determine the moments of inertia for the upper and lower states without having to assume for the lower state a model based partly on vibration analysis as is done in Section 10. Since both components of the doublets are observed for only the first few members of each Q branch, it is not to be expected that the doubling would be observed in the P and R branches, where the first few members are so weak that they are not observed at all. Since in the Q branches the ν_1 series is more persistent, it is assumed that the P and R lines observed are all ν_1 lines. Hence these branches will be designated by P_1 and R_1, and the corresponding term values by F_1. This F_1 is not to be necessarily identified with F_1 of Eq. (2). With the aid of the constructed band diagram given in Fig. 4 and after considerable searching, the branches given in Table X were picked out. Figure. 3 shows some of the R branches. The wave numbers were determined by interpolation between lines of Q branches which had previously been measured. The L assignments were obtained as described below.

If it be assumed that any K doubling, caused by asymmetry or by interactions analogous to those which give rise to Λ-doubling for diatomic

TABLE X. Observed P_1 and R_1 branches.

	Band 2		Band 3						Band 4	
K	15 $R_1(L)$	17 $R_1(L)$	15 $R_1(L)$	16 $R_1(L)$	17 $R_1(L)$	18 $R_1(L)$	19 $R_1(L)$	19 $P_1(L)$	18 $P_1(L)$	19 $R_1(L)$
L										
19	22295.32									
20	294.62									
21	293.91		22986.82							
22	293.06	22254.86	985.86	22967.50						
23	292.22	254.04	984.83	966.52				22879.57		23590.30
24	291.21	253.08	983.77	965.38	22945.80			877.41	23585.76	589.14
25		252.06		964.23	944.64	22923.66		875.24	583.44	587.82
26		251.06		963.02	943.35	922.56	22900.53	872.91	580.93	586.42
27		249.91			942.12	921.31	899.32	870.63	578.39	584.89
28		248.68			940.74	920.04	897.97		575.79	583.44
29		247.42				918.59	896.54		573.06	581.88
30		246.10					895.00			580.19
31		244.64								

molecules, is of negligible magnitude, a simple energy level diagram may be used to verify the following combination relations:

$$\Delta_1F'(L)\equiv F'(L+1)-F'(L)=Q(L+1)-P(L+1)=R(L)-Q(L),$$
$$\Delta_1F''(L)\equiv F''(L+1)-F''(L)=Q(L)-P(L+1)=R(L)-Q(L+1); \quad (18)$$

K is constant for a given relation.

To find the Δ_1F_1' values for a given band the wave numbers of the lines of a P branch were subtracted from those of the Q branch of the same sub-band, shifting one branch with respect to the other until the numbers obtained agreed with those obtained from another sub-band by similarly subtracting the lines of the Q branch from those of the R branch. That the above $Q-P$ combination does not belong to the same sub-band as the $R-Q$ combination is permissible since the Δ_1F values are found to be independent of K within experimental error. In accordance with Eq. (18), when the same Δ_1F_1' value is obtained from a $Q-P$ combination and an $R-Q$ combination, the L number of the Q line of the first combination must be one greater than the L number of the Q line of the second combination. This limitation was an aid in finding the desired agreement. Having found an agreement and having numbered the lines of the P and R branches on the basis of the known numbering of the Q branches, a check was obtained by finding agreement between the Δ_1F_1'' values obtained from both pairs of branches. The results are shown in Table XI. The subscript e means that the value was obtained using a Q branch line whose wave number was obtained by extrapolating beyond observed lines. The fact that the same Δ_1F_1'' values are obtained from three different bands is further proof that the Δ_1F_1 values are correct since the three bands are known to have a common lower vibrational state. It is to be noted that no systematic variation of the Δ_1F_1 values with K is evident.

Although the Δ_1F_1' values are different for different bands as would be expected, they are the same for different sub-bands within a given band except in band 4. In this band it seems that the perturbation effect, which is greater the higher the band number, causes the Δ_1F_1' values to vary from sub-band to sub-band.

Within each band a weighted mean value of Δ_1F_1' for each value of L was chosen and recorded in Table XII. Also a weighted mean value of Δ_1F_1'' for each value of L was determined using data from all bands. The first differences between the Δ_1F_1 values are constant within experimental error except for a possible slight alternation in magnitude. This can be attributed to a very small K doubling with one component of each doublet missing because of the zero spin of oxygen nuclei. ΔF values with a subscript e were obtained essentially from ΔF values in Table XI having a subscript e.

16. DETERMINATION OF CONSTANTS FROM ΔF VALUES

On the basis of Eq. (9) and the empirical expression for the qQ branches given by Eq.

(16), the rotational term values are assumed to have the form

$$F_{1,2}=f(K,v')+\bar{B}L(L+1)+cL\pm\tfrac{1}{2}\gamma L, \quad (19)$$

where the plus sign corresponds to the subscript one. Accordingly,

$$\Delta_1F_1(L)=F_1(L+1)-F_1(L)$$
$$=2\bar{B}(L+1)+c+\tfrac{1}{2}\gamma, \quad (20)$$

and the first differences between these Δ_1F_1 values should be given by

$$\delta(\Delta_1F_1)=2\bar{B}. \quad (21)$$

The value of $\delta(\Delta_1F_1)$ was determined for each column in Table XII by the method of least squares. Numbers in this table having a subscript e were not used. The results are given in Table XIII. The last column of this table gives the values of $2\bar{B}'$ as calculated from $2\bar{B}''=0.612$ cm^{-1} and the second differences $2\Delta\bar{B}=\delta\delta_L$ given in Table II. The values for $2\bar{B}'$ in the last column are considered the more accurate. Extrapolation gives the value of $2\bar{B}'$ for band 0 as 0.550 cm^{-1}. Since theoretically, $\delta\delta_L\equiv\delta(\Delta F')-\delta(\Delta F'')$ regardless of the interpretation of these constants and regardless of the choice of the quantum numbering, the experimental agreement between the two members of this equation is considered as support for the identification of the ΔF values.

The constant $(c+\frac{1}{2}\gamma)$ may now be determined from Eq. (20). A value for this constant was determined from each Δ_1F_1' value of band 2 in Table XII, as well as from each Δ_1F_1'' in this table. The value of $(c+\frac{1}{2}\gamma)$ was found to be constant with respect to L. Averaging for all values of L

$$(c+\tfrac{1}{2}\gamma)'=-0.45, \quad (c+\tfrac{1}{2}\gamma)''=-0.62.$$

Hence,

$$\Delta(c+\tfrac{1}{2}\gamma)=0.17.$$

TABLE XI.

a. Δ_1F_1' values.

	Band 2		Band 3						Band 4	
K	15 $R(L)$ $-Q(L)$	17 $R(L)$ $-Q(L)$	15 $R(L)$ $-Q(L)$	16 $R(L)$ $-Q(L)$	17 $R(L)$ $-Q(L)$	18 $R(L)$ $-Q(L)$	19 $R(L)$ $-Q(L)$	19 $Q(L+1)$ $-P(L+1)$	18 $Q(L+1)$ $-P(L+1)$	19 $R(L)$ $-Q(L)$
L										
19	10.44									
20	10.91									
21	11.50		11.38							
22	12.00	11.98	11.89	11.93				11.91		
23	12.59$_e$	12.38	12.43	12.50				12.48	12.30	12.35
24	13.08$_e$	13.04	13.01	12.99$_e$	13.01			12.99	12.78	12.92
25		13.61		13.54$_e$	13.51	13.29		13.59	13.33	13.43
26		14.21		14.11$_e$	14.00	14.04	14.03	14.01	13.85$_e$	13.93
27		14.76			14.61	14.61	14.68		14.35$_e$	14.39
28		15.30$_e$			15.14$_e$	15.23	15.21		14.90$_e$	15.07
29		15.88$_e$				15.75$_e$	15.72			15.60$_e$
30		16.46$_e$					16.19			16.14$_e$

b. Δ_1F_1'' values.

	Band 2		Band 3						Band 4	
K	15 $R(L)$ $-Q(L+1)$	17 $R(L)$ $-Q(L+1)$	15 $R(L)$ $-Q(L+1)$	16 $R(L)$ $-Q(L+1)$	17 $R(L)$ $-Q(L+1)$	18 $R(L)$ $-Q(L+1)$	19 $R(L)$ $-Q(L+1)$	19 $Q(L)$ $-P(L+1)$	18 $Q(L)$ $-P(L+1)$	19 $R(L)$ $-Q(L+1)$
L										
19	11.61									
20	12.21									
21	12.85		12.85							
22	13.43$_e$	13.20	13.46	13.48				13.46		
23	14.09$_e$	14.00	14.07	14.13$_e$				14.07	14.09	14.08
24	14.65$_e$	14.63	14.73$_e$	14.69$_e$	14.67			14.65	14.62	14.75
25		15.21		15.32$_e$	15.29	15.14		15.32	15.29	15.33
26		15.91			15.84	15.86	15.89	15.87	15.87	15.92
27		16.53$_e$			16.52$_e$	16.50	16.56		16.45$_e$	16.52
28		17.14$_e$			17.13$_e$	17.20$_e$	17.15		17.08$_e$	17.16$_e$
29		17.78$_e$					17.73			17.83$_e$
30										18.45$_e$

TABLE XII.

L	Δ_1F_1' band 2	band 3	band 4	Δ_1F_1'' all bands
19	10.44			11.61
20	10.91			12.21
21	11.50	11.38		12.85
22	11.99	11.91		13.46
23	12.59	12.47	12.33	14.09
24	13.06	13.00	12.85	14.67
25	13.61	13.54	13.38	15.30
26	14.21	14.02	13.89	15.88
27	14.76	14.63	14.37	16.52
28	15.30$_e$	15.20	14.99	17.15$_e$
29	15.88$_e$	15.73	15.55$_e$	17.78$_e$
30	16.46$_e$	16.19	16.09$_e$	

From the values of $\Delta\gamma=0.11$ (Section 7) and $\Delta c=0.13$ (Section 13)

$$\Delta(c+\tfrac{1}{2}\gamma)=0.185,$$

which agrees with 0.17.

It may be instructive, in connection with the constant $(c+\frac{1}{2}\gamma)$, to note the identity $\delta_L\equiv\Delta_1F_1'-\Delta_1F_1''$ which holds regardless of the interpretation of the constants of the identity. In Section 13 it was shown that a constant $(\Delta c+\frac{1}{2}\Delta\gamma)$ was needed to describe the observed δ_L values of the ν_1 series. According to the above identity, this requires a constant $(c+\frac{1}{2}\gamma)$ in the expression for Δ_1F_1 as has already been shown (see Eq. (20)). These constants depend on the choice of the quantum numbering.

If any numbering is indicated by the ΔF values, it is that given by $\Delta F/\delta(\Delta F)\approx L+1$ which may be obtained from Eqs. (20) and (21). This expression would be sufficiently accurate to determine the numbering if $(c+\frac{1}{2}\gamma)$ were fairly small compared to $\delta(\Delta F)$, as is entirely possible. The numbering calculated on the basis of this expression is nearly integral and almost the same, whether using $\Delta F'$ or $\Delta F''$ values. The indicated quantum numbering, which is one less than that used throughout the paper, is therefore considered plausible. However, the fact that the unknown constant $(c+\frac{1}{2}\gamma)$ is present in the expression for ΔF makes this numering uncertain. In any case, the quantum numbering does not affect the $\bar{B}$ values.

17. MOLECULAR MODEL

The following is a list of constants available for calculating a molecular model for both electronic states. These constants correspond to the vibrational transition (0 0 0)←(0 0 0). s designates the Cl−O distance and 2θ, the O−Cl−O angle.

$s''=1.53\pm.02$A	from electron diffraction.[11]
$2\theta''=122°\ 50'$ $2\theta'=112°\ 10'$	from vibrational frequencies[2] using valence force approximation.
$2\Delta\bar{B}=-0.0615\pm0.001$ cm^{-1}	from second differences in L structure, Section 5; and Eq. (9).
$2(\Delta A-\Delta\bar{B})=-1.188\pm0.005$ cm^{-1}	from second differences in K structure, Section 6; and Eq. (9).
$2\bar{B}''=0.612\pm0.003$ cm^{-1}	from Δ_1F_1'' values, Section 16.
$2\bar{B}'=0.550\pm0.003$ cm^{-1}	from $2\bar{B}''$ and $2\Delta\bar{B}$; also from Δ_1F_1' values, Section 16.

The last four constants are obtained in the present paper and are based on the prolate symmetrical top approximation. They, therefore, contain small errors because of the asymmetry of the actual molecule. The effect of asymmetry is neglected for the present but will be discussed in the next section.

For a bent triatomic molecule only two constants are required to determine the geometrical configuration of a given electronic state, while three constants s'', $2\theta''$, $2\bar{B}''$ are here available for calculating a model for the lower state. That these constants are definitely inconsistent is illustrated in Table XIVa, where, for a given model, the constant in parenthesis is calculated from the other two. Physical constants used in the calculation are:

physical mass unit = 1.6599×10^{-24} g,
mass of $O^{16}=16.00$ mass units,
mass of $Cl^{35}=34.98$ mass units,
$h/8\pi^2c=27.98\times10^{-40}$ g cm.

For a given lower state model, the upper state constants may be determined using the sec-

TABLE XIII. $\bar{B}'$ and $\bar{B}''$ from ΔF values.

Band	$2\bar{B}''=\delta(\Delta_1F_1'')$	$2\bar{B}'=\delta(\Delta_1F_1')$	$2\bar{B}'=\delta(\Delta_1F_1'')+\delta\delta_L$
0			(0.550)
1			0.546
2	0.612	0.543	0.542
3		0.536	0.538
4		0.525	0.532

TABLE XIV.

Model	a			b		
	s''	$2\theta''$	$2\bar{B}''$	s'	$2\theta'$	$2\bar{B}'$
(1)	1.53A	122° 50′	(0.5445) cm^{-1}	1.671A	115° 10′	0.483 cm^{-1}
(2)	1.53	(108° 10′)	0.612	1.785	89° 40′	0.550
(3)	(1.443)	122° 50′	0.612	1.559	116° 20′	0.550

ond differences $2\Delta\bar{B}=-0.0615$ and $2(\Delta A-\Delta\bar{B})=-1.188$. A model for the upper electronic state was calculated for each lower state model and the results are given in Table XIVb. Fairly accurate intermediate models may be determined from Table XIV by interpolation.

According to experience with other molecules, it is entirely possible that $2\theta''=122°\ 50'$ calculated from the vibrational analysis on the basis of the valence force approximation is considerably in error. For this reason the author considers that *model (2) is probably the most nearly correct.* The greatest source of error is considered to be the uncertainty in the electron diffraction value of s''. From Table XIV it may be seen that an experimental error of 0.02A in s'' corresponds to an error of 3° in $2\theta''$ and to errors of 0.05A and 6° in s' and $2\theta'$, respectively.

Figure 5 shows both states of model (2) corrected for asymmetry, see Section 18. It is interesting to note that as the molecule goes into the upper state, the distance between the oxygen atoms changes only very slightly. It is also of interest that the vibrational structure of the absorption spectrum shows that only the breathing vibration is appreciably excited in the upper state and that this mode of vibration is excited considerably. On the basis of these facts the Franck-Condon principle requires that the motion of the oxygen atoms in this mode in the upper state is roughly perpendicular to the line joining the oxygen atoms. In such a case the valence force approximation would not be expected to give very good values for the angles.

A more complete vibrational analysis[2] of this electronic band system which would include isotope frequencies would allow a fairly accurate calculation of the angles for both states giving an interesting check on the correctness of this model. Also a quantitative application of the Franck-Condon principle would give a check on the change of the Cl—O distance at excitation.

18. CONSIDERATION OF ASYMMETRY

Model (2) was determined using constants of the spectrum which were interpreted as if the spectrum were that of a symmetrical top. Hence, model (2) differs from the actual molecule because the effect of asymmetry on the constants of the spectrum has not been allowed for. It will be seen that this difference, because of asymmetry, between model (2) and the actual molecule is small. Hence, the contribution of the asymmetry term of Eq. (4) to the constants of the spectrum is about the same for molecule and model and may be approximately computed using model (2). If these contributions are subtracted from the observed constants of the spectrum, an approximate value of the constants corrected for the effect of asymmetry may be obtained. A corrected model may then be calculated from the corrected constants.

The lower state of model (2) was determined using s'' from electron diffraction experiments, and the value of $\delta(\Delta_1F'')$ which is interpreted as $2\bar{B}''$. In the range of observation the average contribution of the asymmetry term of Eq. (4) to the value of $\delta(\Delta_1F'')$ is positive and about 0.8 percent. Hence, the value of $2\bar{B}''$ given in Section 17 is 0.8 percent too large. Therefore,

$$2\bar{B}''=0.607\ cm^{-1}\ \text{(corrected)}.$$

The upper state was determined from the experimental constants $\delta(\Delta_1F')$ and $\delta\delta_K$ which were interpreted as $2\bar{B}'$ and $2(\Delta A-\Delta\bar{B})$, respectively. In the range of observation the average contribution of the asymmetry term of Eq. (4) to $\delta(\Delta_1F')$ is a positive and about 5 percent. Hence, the correct value of $2\bar{B}'$ is about 5 percent smaller than the value given in Section 17, so that

$$2\bar{B}'=0.522\ cm^{-1}\ \text{(corrected)}.$$

The effect of the asymmetry term is to reduce the magnitude of $\delta\delta_K$ by about 0.7 percent.

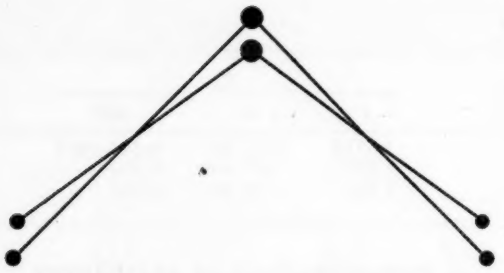

FIG. 5. Probable model for both states. The model with the larger angle represents the normal state, O−Cl−O angle = 109°, Cl−O distance = 1.53A. The model with the smaller angle represents the excited state, O−Cl−O angle = 92°, Cl−O distance = 1.805A. The models are drawn so that their centers of gravity coincide.

Hence, the correct magnitude of $2(\Delta A - \Delta \bar{B})$ is about 0.7 percent greater than the value given in Section 17,

$$2(\Delta A - \Delta \bar{B}) = -1.196 \text{ cm}^{-1} \text{ (corrected)}.$$

The above three corrected constants with the electron diffraction value of s'' determine model (2) corrected for the effect of asymmetry. The resulting model is

$$2\theta'' = 109° \qquad 2\theta' = 92°$$
$$s'' = 1.53\text{A} \qquad s' = 1.805\text{A}$$

This is considered as the probable model for both states. It is of interest that for the range of quantum numbers observed the error caused by neglecting the effect of asymmetry (see model (2), Table XIV) is small even though the upper state model has an angle of 92°.

A formula for the magnitude of the splitting of the rotational levels due to asymmetry is given by Wang.[14] For levels which are expressed in terms of prolate symmetrical top quantum numbers (see Eq. (4)), this formula, written in the notation of this paper, is

$$\Delta\nu = \left[\frac{C-B}{2(A-\bar{B})}\right]^K \frac{8(A-\bar{B})}{2^{3K}} \frac{(L+K)!}{(L-K)!(K-1)!^2} \quad (22)$$

where $\Delta\nu$ is in cm^{-1}. This formula is obtained on the basis of the assumption that the asymmetry factor b in square brackets is limited by $|b| \ll 1$. For the 92° model b is about 0.1. This splitting is much too small to be observed for the range of quantum numbers involved in this paper, being, for example, 3×10^{-7} cm^{-1} for the level $K=15$, $L=25$ of the 92° model. For a given K, the splitting decreases as L decreases.

The quantum numbering was determined on the basis of the K structure using the constants δ_K and $\delta\delta_K$, see Eq. (12). The effect of asymmetry is to reduce the magnitude of both of these constants by a little less than 1 percent. Hence, the K value calculated essentially from their ratio is affected very little by asymmetry.

The effect of asymmetry on the observed L structure is fairly large for model (2). Calculation shows that the effect of asymmetry is to reduce the first interval in the L structure by about 10 percent, while the magnitudes of the second difference in the L structure would be reduced by 30 percent on the average. This would cause the value of the K numbering, calculated from the ratio of the first interval to the second difference in the L structure, to be too large by about 3. But Table VII shows that the K numbering calculated by this method is too small by about 2. Hence, if model (2) is correct, there is apparently some term which more than balances this effect of asymmetry on the L structure.

19. ISOTOPE EFFECT

Absorption lines arising from molecules containing the less plentiful of the two isotopes of chlorine, Cl^{37}, are to be expected, and some of the stronger lines of the qQ doublet branches of $Cl^{37}O_2$ are observed in bands 3 and 4 (see Table XV). Though the isotope lines of band 4 were easily found, those of band 3 were located with considerable difficulty because of the jumble of background lines.

In general, no systematic variation of the total isotope shift $\nu_{37} - \nu_{35} = P(v, K)$ was observed within a sub-band. A weighted average value for this shift for each sub-band is given in Table XVI. These values are probably correct to within 0.02 cm^{-1}. Although the total isotope shift is quite different for bands 3 and 4, the differences $P(v, K+1) - P(v, K)$, also shown in Table XVI, are essentially the same for both bands.

The approximate theoretical magnitude of the rotational isotope shift will now be determined. The rotational component P_r of the isotope

[14] S. C. Wang, Phys. Rev. **34**, 249 (1929).

TABLE XV.

Isotope lines of qQ doublet branch of band 3

K	15	16	17	18	19	20	$L(\nu_2)$
	22975.30						15
	974.10	22956.34					16
$L(\nu_1)$		955.15	22936.24				17
15	973.79		934.92	22914.78			18
16	972.77	954.72		913.42	22892.04		19
17	971.63	953.68	934.53		890.76	22868.28	20
18	970.41	952.50	933.35	912.96		866.98	21
19		951.19	932.13	911.70	890.21		
20		949.95	930.72	910.42	888.90	866.22	
21			929.35	909.00	887.58	864.92	
22				907.56	886.10	863.48	

Isotope lines of qQ doublet branch of band 4

K	16	17	18	19	$L(\nu_2)$
	23636.97				16
$L(\nu_1)$		23617.74			17
16	636.43		23596.22		18
17	634.93	616.06		23573.53	19
18		614.68	594.50		
19		613.20	593.10	571.67	
20		611.64	591.60	570.22	
21			590.05	568.71	
22				567.18	
				565.48	

shift is given by

$$P_r = \nu_{37}{}^r - \nu_{35}{}^r = (F_{37}' - F_{37}'') - (F_{35}' - F_{35}''). \quad (23)$$

The prolate symmetrical top approximation to the energy levels is

$$F = \frac{h}{8\pi^2 c}\frac{1}{I_{\bar{B}}}[L(L+1) - K^2] + \frac{h}{8\pi^2 c}\frac{K^2}{I_A}. \quad (24)$$

Since the chlorine atom contributes relatively little to $I_{\bar{B}}$ and since $I_{\bar{B}}$ is nearly the same in both electronic states, the coefficient of the $[L(L+1)-K^2]$ term in P_r is expected to be small. Calculation shows that for model (2) this coefficient is about 1 percent of the coefficient K^2. The fact that L does not differ greatly from K gives further reason for neglecting this term. Hence,

$$P_r = (\Delta A_{37} - \Delta A_{35})K^2. \quad (25)$$

Now $\Delta A = (\Delta A - \Delta\bar{B}) + \Delta\bar{B}$, so that for band 3 $\Delta A_{35} = (-1.212/2) - (0.0739/2) = -0.643$ cm^{-1}. It may be shown that

$$\Delta A_{37} = [(35\times 69)/(37\times 67)]\Delta A_{35}.$$

Hence,

$$P_r = 0.0166K^2 \text{ (theoretical)}.$$

Correcting ΔA for asymmetry increases the coefficient of K^2 to about 0.0170 cm^{-1}.

The coefficient of K^2 may also be determined empirically from the observed isotope shift. The total isotope shift of the $Cl^{37}O_2$ spectrum with respect to the $Cl^{35}O_2$ spectrum is described by

$$\nu_{37} - \nu_{35} = P(v, K) = P_v(v) + P_r(K), \quad (26)$$

where P_v is the vibrational component and $P_r = \alpha K^2$ is the rotational component of the isotope shift. Both P_v and P are observed to be negative, that is, both the band heads and the lines observed in the tail of the bands have an isotope shift toward the red. However, the fact that the magnitude of the total shift decreases as K increases shows that the rotational component P_r is positive. For a given band P_v is

TABLE XVI. Observed isotope effect $P(v, K)$ and differences.

K	*band 3*	*band 4*
15	−9.04	
	0.47	
16	−8.57	−14.10
	0.50	0.49
17	−8.07?	−13.61
	0.55	0.55
18	−7.52	−13.06
	0.59	0.58
19	−6.93	−12.48
	0.62	
20	−6.31	

constant so that

$$P(v, K+1)-P(v, K)=P_r(K+1) \\ -P_r(K)=\alpha(2K+1).$$

Hence,

$$\alpha=\frac{P(v, K+1)-P(v, K)}{2K+1}. \quad (27)$$

By use of the data of Table XVI for band 3, this formula gives an average value of $\alpha=0.0156 \pm 0.0003$. Hence,

$$P_r=0.0156K^2 \text{ (empirical)}.$$

It may be significant that if the numbering were reduced by one, as is suggested by the ΔF values, this empirical coefficient of K^2 becomes 0.0165 which is in better agreement with the theoretical coefficient of K^2. However, the linear term in K, which varies with v', may contribute to the isotope effect.

ACKNOWLEDGMENT

I am grateful to Professor R. S. Mulliken for suggesting this interesting problem and for guidance and continued interest during the work.

THE JOURNAL OF CHEMICAL PHYSICS VOLUME 14, NUMBER 11 NOVEMBER, 1946

Erratum: "Note on the Conditions of Equilibrium for Systems of Many Constituents"

[J. Chem. Phys. 14, 563 (1946)]

STUART R. BRINKLEY, JR.
Research and Development Division, Department of the Interior, Bureau of Mines, Pittsburgh, Pennsylvania

THE paragraphs given below should be inserted following the paragraph containing Eq. (8) in the second column of page 564. The author did not receive proof and was, therefore, unable to supply this correction before publication of the article.

The derivation by means of the method employed by Gibbs,[4] subject to the constraints of Eqs. (8), of the conditions for equilibrium is straight forward, and it is unnecessary to reproduce it here. The usual conditions for thermal and mechanical equilibrium are obtained, and the conditions for chemical equilibrium take the form,

$$\mu_j^{(k)}=\lambda_j, \quad (9)$$

$$\mu_j^{(k)}=\sum_{j=1}^{c} \nu_{ij}\lambda_j, \quad (10)$$

$k=1, 2, \cdots p; j=1, 2, \cdots c; i=c+1, c+2, \cdots s,$

where $\mu_i^{(k)}$ and $\mu_j^{(k)}$ are the chemical potentials in the kth phase of the ith and jth substances, respectively, the λ_j are constants which may be eliminated from Eqs. (9), and where it has been assumed for simplicity that each substance of the system is included in every phase.[8]

[8] If a particular component, say the j'th, is a possible but not an actual constituent of a particular phase, say the k'th, then the determination of the conditions for equilibrium is subject to the additional constraint, $\delta n_{j'}^{(k')} \geqslant 0$, and the corresponding number of Eqs. (7) becomes $\mu_{j'}^{(k')} \geqslant \lambda_j$. A similar additional constraint must be applied if a particular dependent constituent, say the i'th, is a possible but not an actual constituent of the k'th phase, the corresponding member of Eqs. (9) becoming $\mu_{i'}^{(k')} \geqslant \sum_{j=1}^{c} \nu_{i'j}\lambda_j$. If the j'th component is excluded *a priori* from the k'th phase, the corresponding member of Eqs. (9) disappears as being without meaning, and similar considerations obtain if the i'th dependent constituent is excluded *a priori* from the k'th phase. The number of relations in Eqs. (9) and (10) is reduced by the number of such additional constraints, and the number of variables upon which the chemical potentials depend is reduced by the same number, thereby producing no effect upon the phase rule, Eq. (11). See Gibbs, reference 3, pp. 66, 67.

THE JOURNAL OF CHEMICAL PHYSICS VOLUME 14, NUMBER 11 NOVEMBER, 1946

The Determination of Polymeric Molecular Weights by Light Scattering in Solvent-Precipitant Systems

R. H. EWART AND C. P. ROE
General Laboratories, United States Rubber Company, Passaic, New Jersey

AND

P. DEBYE AND J. R. MCCARTNEY
*Department of Chemistry, Cornell University, Ithaca, New York**

(Received July 12, 1946)

The theory of scattering by an inhomogeneous dielectric medium has been extended so as to account for the turbidimetric behavior of polymer solutions in solvent-precipitant mixtures. It is predicted by this theory and verified by experiment that correct values of molecular weight are obtained by the usual interpretation of turbidity measurements if and only if the solvent and precipitant have the same refractive index. The practical utility of turbidimetry in high polymer solutions is shown to be greatly increased by the proper use of solvent-precipitant mixtures. If the solvent and precipitant have different refractive indices, scattering measurements give information about the extent of selective absorption of solvent by the polymer.

INTRODUCTION

WHEN the reciprocal of the specific turbidity, namely, c/τ, of a dilute high polymer solution in a pure solvent is multiplied by a constant H, characteristic of the scattering system, and the product $H(c/\tau)$ is plotted against the polymer concentration, c, in the solution, a linear relationship is obtained. The slope of this line varies with the solvent for a given polymer, and is in general greater for the so-called "good" solvents than for "poor" solvents. However, the intercept with the axis of $H(c/\tau)$ at $c=0$ is independent of the solvent in pure solvents. These results are in harmony with the currently accepted theory[1–6] of the scattering of monochromatic light by solutions. This theory gives a simple relation between the intercept and the molecular weight of the solute, and thus yields a means of estimating polymer molecular weights.

It has been observed by previous investigators[7] that, as one adds a precipitant to a high polymer solution, the turbidity progressively increases at concentrations of precipitant well below the threshold necessary to produce macroscopic separation into two phases. This fact suggests the possibility that scattering data capable of yielding accurate molecular weights may be obtained more easily from solutions in solvent-precipitant mixtures than in pure solvents, especially in cases where the turbidities in pure solvents are so small that they can be measured accurately only with very sensitive apparatus, and also only by taking extreme care to clarify the solutions.

Experiments have shown that in some solvent-precipitant systems correct values of molecular weight are obtained, whereas in others considerable departures from the correct values are found. Thus, the data shown in Fig. 2, on polystyrene in benzene-methanol mixtures, are the results of a careful investigation at concentrations as low as 0.000225 gram of polymer per milliliter of solution. The extrapolation of these results at very low concentrations proves definitely that the value of the intercept at infinite dilution is not constant for this system and depends on the concentration of methanol used. All of the known facts can be correlated by a proper consideration of the refractive indices of

* The portion of the work here reported which was done at Cornell University was carried out in connection with the Government Research Program on Synthetic Rubber under contract with the Office of Rubber Reserve, Reconstruction Finance Corporation.

[1] S. Bhagavantam, *Scattering of Light* (Chemical Publishing Company, Brooklyn, New York, 1942).
[2] J. Cabannes, *La Diffusion Moleculaire de la Lumiere* (University of France Press, Paris, 1929).
[3] M. Born, *Optik* (Julius Springer, Berlin, 1933).
[4] P. Debye, J. App. Phys. **15**, 338 (1944).
[5] B. Zimm, R. S. Stein, and P. Doty, Polymer Bull. **1**, 90 (1945).
[6] P. Doty, B. Zimm, and H. Mark, J. Chem. Phys. **13**, 159 (1945).
[7] Gehman and Field, Ind. and Eng. Chem. **30**, 1031 (1938).

the solvent and precipitant, coupled with the assumption that the solute selectively absorbs solvent from the solvent-precipitant mixture.

THEORETICAL

It was shown in 1897 by H. Kneebone Tompkins[8] that when rubber is soaked in a mixture of carbon disulfide and acetone, the solvent medium becomes poorer in carbon disulfide. A closely related phenomenon is observed in the precipitation of a polymeric solute from homogeneous solution by the addition of a precipitant. The addition of precipitant beyond a certain threshold causes the separation of two phases, one of which is richer than the other in polymer. In general the polymer-rich phase contains both solvent and precipitant, but the ratio of solvent to precipitant is higher than in the other phase. Prior to reaching the threshold necessary to cause incipient precipitation the progressive addition of precipitant causes steadily increasing turbidity. It is assumed for this discussion that this increase in turbidity is caused by two factors, namely, (1) shrinkage of the swollen polymer molecules in solution, and (2) selective absorption of solvent by the polymer. If we confine our attention to the problem of determining molecular weights by means of scattering, then it is necessary to consider only the effects of these two factors on the quantity $(1/H)(\tau/c)$ at infinite dilution, or at $c=0$. In order to do this, it is helpful to discuss the behavior of solutions in which the solute concentration is small but finite and subsequently to pass to the limit. Thus we shall show that shrinkage alone should produce augmented turbidity at finite concentrations, but should not affect the limiting value of $(1/H)(\tau/c)$. Also we shall show that both at finite concentrations and at infinite dilution selective absorption should produce changes in $(1/H)(\tau/c)$, and that in this case the changes may be either positive or negative. In terms of the properties of the conventional scattering curves, the characteristic effect of shrinkage is to decrease the slope but not to alter the intercept, whereas the effect of selective absorption is to change both the intercept and slope.

[8] H. Kneebone Tompkins, *The Physics and Chemistry of Colloids* (H. M. Stationery Office, London, 1921), p. 163.

Consider the properties of a suspension of spheres, the linear dimensions of which are small by comparison with the wave-length of light. Let us define the following symbols:

τ = excess turbidity of the suspension over that of the suspending medium in absence of any spheres.
v = volume of a sphere in the suspension.
c = weight concentration of solute per unit volume.
λ = wave-length of the exciting radiation.
n = refractive index.
N = number of spheres per unit volume.
N_0 = Avogadro's number.
M = molecular weight.
ϵ = homogeneous dielectric constant of the suspension.
ϵ_0 = dielectric constant of the suspending medium in absence of any spheres.
ϵ_1 = dielectric constant of the medium surrounding the spheres.
ϵ_2 = dielectric constant of a sphere.
ψ = volume fraction of solvent in a solvent-precipitant mixture, exclusive of the volume occupied by the solute.
ψ_0 = original value of ψ in absence of any spheres.
ψ_1 = value of ψ in the medium surrounding the spheres.
ψ_2 = value of ψ within a sphere.

If the suspension is very dilute, then from electromagnetic theory, values of the turbidity and dielectric constant may be calculated. The resulting expressions are

$$\tau=\frac{24\pi^3Nv^2}{\lambda^4}\epsilon_1^2\left(\frac{\epsilon_2-\epsilon_1}{\epsilon_2+2\epsilon_1}\right)^2, \tag{1}$$

$$\epsilon-\epsilon_1=3Nv\epsilon_1\left(\frac{\epsilon_2-\epsilon_1}{\epsilon_2+2\epsilon_1}\right). \tag{2}$$

Now the quantity $v\epsilon_1[(\epsilon_2-\epsilon_1)/(\epsilon_2+2\epsilon_1)]$ may be eliminated between (1) and (2) to yield

$$\tau=\frac{8\pi^3}{3N\lambda^4}(\epsilon-\epsilon_1)^2. \tag{3}$$

But since $N/N_0=c/M$,

$$\tau=M\frac{8\pi^3c}{3\lambda^4N_0}\left(\frac{\epsilon-\epsilon_1}{c}\right)^2. \tag{3a}$$

The usual discussion of this equation for the case in which the solvent medium is a pure compound assumes that ϵ_1 may be identified with ϵ_0, the dielectric constant for the solvent in absence of any dispersed material. This assumption is well justified by experiment, and we find that in the

limit as $c \to 0$

$$\lim_{c\to 0}\left(\frac{\tau}{c}\right) = M\frac{8\pi^3}{3\lambda^4 N_0}\left(\frac{\partial\epsilon}{\partial c}\right)^2 = M\frac{32\pi^3 n^2}{3\lambda^4 N_0}\left(\frac{\partial n}{\partial c}\right)^2. \quad (3b)$$

However, if we are dealing with a solvent medium having two components, one of which may be selectively absorbed by the solute, then it is no longer justifiable to set $\epsilon_1 = \epsilon_0$, and Eq. (3a) must be rewritten as follows:

$$\tau = M\frac{8\pi^3}{3\lambda^4 N_0}c\left[\frac{\epsilon-\epsilon_0}{c}+\frac{\epsilon_0-\epsilon_1}{c}\right]^2. \quad (4)$$

The term $(\epsilon_0-\epsilon_1)/c$ alone requires discussion. Let us consider the behavior of ϵ in the neighborhood of a given value of ψ, namely ψ_0, corresponding to ϵ_0.

$$\epsilon = \epsilon_0 + (\psi-\psi_0)(\partial\epsilon/\partial\psi). \quad (5)$$

If we assume that the factor $(\psi-\psi_0)$ owes its existence to selective absorption, we may, for sufficiently small values of c, rewrite Eq. (5)

$$\epsilon_1 = \epsilon_0 + \frac{\partial\epsilon_0}{\partial\psi}\frac{\partial\psi_1}{\partial c}c. \quad (5a)$$

Then we get at once

$$\frac{\epsilon-\epsilon_1}{c} = \frac{\epsilon-\epsilon_0}{c} - \frac{\partial\epsilon_0}{\partial\psi}\frac{\partial\psi_1}{\partial c} \quad (5b)$$

and

$$\lim_{c\to 0}\left(\frac{\epsilon-\epsilon_1}{c}\right) = \frac{\partial\epsilon}{\partial c} - \frac{\partial\epsilon_0}{\partial\psi}\frac{\partial\psi_1}{\partial c}. \quad (5c)$$

If we now set $\partial\psi_1/\partial c = -\alpha$,

$$\tau = M\frac{8\pi^3 c}{3\lambda^4 N_0}\left(\frac{\partial\epsilon}{\partial c}+\alpha\frac{\partial\epsilon}{\partial\psi}\right)^2. \quad (6)$$

Or if we assume $\epsilon = n^2$ (n = refractive index),

$$\lim_{c\to 0}\left(\frac{\tau}{c}\right) = \left(\frac{\tau}{c}\right)_0 = M\frac{32\pi^3 n^2}{3\lambda^4 N_0}\left(\frac{\partial n}{\partial c}+\alpha\frac{\partial n}{\partial\psi}\right)^2. \quad (6a)$$

Equation (6a) contains all that is needed in order to give a satisfactory semiquantitative interpretation of the observed facts. If the solvent is a pure compound, $\alpha = 0$, and Eq. (6a) reduces to (3b), i.e., to the conventional form of the molecular weight equation in turbidimetry. If we are dealing with a solvent-precipitant mixture in which the two components have the same refractive index, $\partial n/\partial\psi = 0$, and again we arrive at Eq. (3b). If the two components have different refractive indices, then in general at values of $\psi < 1$, the term $\alpha(\partial n/\partial\psi) \neq 0$, but may have either positive or negative values. If α is assumed to be positive, if $\partial n/\partial c > 0$ and $\partial n/\partial\psi > 0$, $(\tau/c)_0$ will be greater than in the pure solvent and the value of M obtained from Eq. (3b) will be higher than the true molecular weight. If $\alpha\partial n/\partial\psi > 0$ and $\partial n/\partial c < 0$, the value of M may be too small or too large, depending on the numerical magnitudes of these terms. If $\alpha\partial n/\partial\psi < 0$ and $\partial n/\partial c > 0$, the value of M in (3b) may again deviate either positively or negatively from the true molecular weight. If $\partial n/\partial c = 0$ in a system such that $\alpha\partial n/\partial\psi \neq 0$, the theory predicts a finite value of $(\tau/c)_0$ which is traceable solely to selective absorption.

The unpredictable feature of the theory is the presence of the factor α introduced in Eq. (6). This factor is not a constant for any one system, nor does it appear to behave in the same way for different systems. It seems reasonable to suppose on general grounds that it may have positive values less than or of the order of unity in solvent-precipitant mixtures, and that it vanishes in pure solvents. It appears from experiment that it may sometimes have negative values for very small precipitant concentrations. Fortunately there has appeared to be no need to make more precise assumptions about this factor, since those mentioned above have enabled us to discuss the equations of the theory in all interesting cases.

The experiments presented here may be considered as a method for the determination of α or $(\partial\psi_1/\partial c)$. The experimental significance of this factor α is clear and unambiguous. It measures the change in composition of the solvent-precipitant mixture surrounding the particles due to selective absorption. A complete theoretical account of the factor α will have to await future developments.

The preceding paragraphs deal exclusively with very dilute solutions. It therefore seems appropriate to include a few remarks about the slopes of scattering curves at finite concentrations. The slope of the light scattering curve for a given system is predicted by the usual theory to be twice the slope of the corresponding osmotic

pressure curve. Now it is well known that the introduction of a precipitant has the effect of reducing the slope of the osmotic pressure curve, and that this reduction in slope may be traced to the heat of mixing of the polymer and solvent medium. Since as c approaches zero, the ratio of the partial molal heat of mixing to the concentration also approaches zero, the lowering of osmotic pressure at finite concentrations does not lead to any change in the intercept at infinite dilution. Hence the use of solvent-precipitant mixtures, regardless of selective absorption, has no effect on the apparent molecular weight as derived from osmotic measurements. On the other hand, selective absorption produces a purely optical effect on the turbidity—an effect which is additive and proportional to the polymer concentration, and which therefore persists in the limiting value, $(c/\tau)_0$.

EXPERIMENTAL PART

Turbidity Measurements

All turbidities were measured by 90° scattering of monochromatic light. Absolute values were obtained by comparison with primary standards whose turbidities had been determined by transmission measurements, upon the assumption that Beer's law is valid. Correction for the turbidity of the solvent was made in all cases. No corrections for dissymmetry were introduced. Recent measurements have shown that although the dissymmetry of scattering by the polymers here studied was sufficient to necessitate an appreciable correction (about 12 percent) to the calculated molecular weights, there is very little variation of this correction with the composition of a solvent-precipitant mixture. Hence, the omission of such corrections does not affect the comparison of molecular weight values obtained on any one polymer sample in different mixtures.

Refractive Index

Refractive index measurements were made with an Abbe refractometer which was equipped with compensating Amici prisms adjusted so as to yield correct values of refractive index for $\lambda = 5890$A when dispersion was eliminated. Refractive indices at other wave-lengths were calculated with the aid of a dispersion chart furnished with the instrument.

Refractive Index Gradient with Polymer Concentration

All measurements of this quantity reported here have been made by means of an instrument built substantially according to a design obtained from Dr. P. P. Debye.[9] This is a differential instrument and has a sensitivity of approximately 5×10^{-6}. The instrument enables one to measure the angular deviation of light which passes through a hollow prism immersed in solvent, when the prism is first filled with the solvent and then with a dilute solution in the same solvent.

Materials

Most of the measurements on polystyrene were made with a fractionated sample which was derived from a thermally polymerized material. A few measurements were also made with a commercial unfractionated polystyrene. The polymethylmethacrylate used was also a fractionated material polymerized with the aid of benzoyl peroxide.

Solvents and precipitants were usually of c.p. grade. Where it was necessary to use commercial materials, these were suitably purified.

RESULTS AND DISCUSSION

This research was initiated in an attempt to extend the turbidimetric method of determining polymeric molecular weights to systems in which the dispersion medium, instead of being a pure solvent, is a mixture of a solvent and a precipitant. The experimental results will be presented by means of the conventional type of scattering curves, in conformity with the equation of Debye

$$\frac{Hc}{\tau} = \frac{1}{M} + 2Bc, \tag{7}$$

where

c = concentration of polymer in grams per ml of solution.
τ = turbidity.
M = molecular weight.
B = a constant characteristic of the solvent-solute system.
$H = \dfrac{32\pi^3}{3\lambda^4 N_0} n^2 \left(\dfrac{\partial n}{\partial c}\right)^2$.
N_0 = Avogadro's number.
λ = wave-length of exciting radiation.
n = refractive index of the solvent.
$\dfrac{\partial n}{\partial c}$ = refractive index gradient with respect to polymer concentration.

[9] P. P. Debye, Bull. Am. Phys. Soc. 21, 16 (1946).

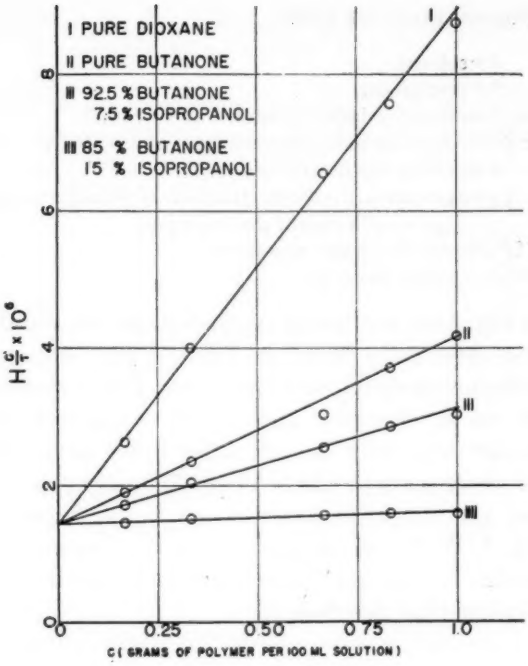

FIG. 1. Scattering curves: fractionated polystyrene.

If the linear relationship (7) be extrapolated to $c=0$, the result may be expressed

$$H(c/\tau)_0=1/M. \tag{7a}$$

This is equivalent to Eq. (3b), which was shown in a previous section to be valid for pure solvents.

If the solvent is not a pure compound, but is instead a mixture of a solvent and a precipitant, then the quantity M is in general not the true molecular weight but differs from the true value by an amount which depends on the composition of the entire system. The discrepancy occurs because of failure in the calculation of H to take account of selective absorption of solvent by the polymer. It is, nevertheless, convenient to represent the results of experiments with solvent-precipitant systems in terms of the Debye equation, retaining the definition of H which was given following Eq. (7). If this is done, then visual inspection of the scattering curves shows immediately which mixtures give polymeric molecular weights in agreement with those found in pure solvents.

Much of the experimental work was done prior to development of the theory. However the results will be considered under three cases, each of which is regarded as a test of the validity of Eq. (6a).

Case (1) $\alpha\partial n/\partial\psi$ Is Negligible with Respect to $\partial n/\partial c$

This condition is fulfilled if either α or $\partial n/\partial\psi$ is sufficiently small. Presumably α vanishes in a pure solvent but assumes appreciable values in solvent-precipitant mixtures. Hence all pure solvents fall under this case. α is probably very small for mixtures which are sufficiently poor in precipitant, but these are of slight practical interest and have not been studied. $\partial n/\partial\psi$ may be made small by the choice of a solvent and precipitant which have nearly equal refractive indices and a sufficiently small volume change on mixing.

Preliminary turbidimetric data are presented in Fig. 1. The polymer used was a polystyrene fraction having an intrinsic viscosity of 2.06 and an osmotic molecular weight of 0.8×10^6. Inspection of curves I and II in Fig. 1 makes it clear that the data in pure solvents may be represented by straight lines having the same intercept at $c=0$. The light scattering molecular weight is 0.69×10^6, from Eq. (7a). The discrepancy between this and the osmotic value is probably because of the inaccuracy of the latter at high values of M.

Choice of the solvent-precipitant pair, butanone-isopropanol, is a very fortunate one, since $\partial n/\partial\psi=0.0004$, whereas $\partial n/\partial c=0.219$ according to our measurements. Inspection of curves III and IV in Fig. 1 shows at once that extrapolation to $c=0$ leads to precisely the same intercept as that found with pure solvents. Thus all the data of Fig. 1 are in accord with theory.

Case (2) $\alpha\partial n/\partial\psi$ and $\partial n/\partial c$ Both Finite and of the Same Order

The solvent-precipitant pair, benzene-methanol, is used for the discussion of this case. The polymer was an unfractionated polystyrene. In mixtures of benzene and methanol it is found that

$$\frac{\partial n}{\partial c}=0.108+0.1447(1-\psi),$$

$$\frac{\partial n}{\partial\psi}=0.16, \text{ and is practically independent of } \psi.$$

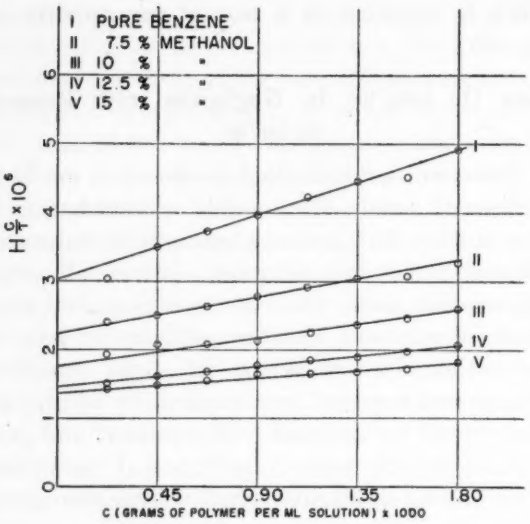

FIG. 2. Unfractionated polystyrene in $C_6H_6-CH_3OH$ mixtures.

Data on scattering are presented in Fig. 2. In order to explain these curves in terms of Eq. (6a), we must assume that α is positive and of the order of unity for $\psi<1$, also that α increases with increasing methanol concentration. Each of these assumptions appears physically reasonable. If they are granted, then theory predicts that the term $\alpha\partial n/\partial\psi$ will make a finite contribution to $(\tau/c)_0$ and that this contribution will increase as the methanol concentration increases. The steady decrease of $H(c/\tau)_0$ with increasing methanol content bears this out.

Further Examples Illustrating Cases (1) and (2)

A somewhat broader study of solvent-precipitant mixtures matched with respect to refractive index was suggested by the data presented in Figs. 1 and 2. Hence the turbidities of polystyrene solutions in the mixtures listed in Table I have been investigated. In this table, the following abbreviations are used:

S = solvent.
P = precipitant.
$n(S)$ = refractive index of solvent at $\lambda=5461$A.
$n(P)$ = refractive index of precipitant at $\lambda=5461$A.
ψ = volume fraction of solvent.
ψ_P = approximate volume fraction of solvent at the point of incipient precipitation.
$n(SP)$ = refractive index of mixture.
DEF = diethyl fumarate.

In Fig. 3 the scattering curves for solutions in the first three pairs listed in Table I are compared with the curve for pure butanone. These systems are to be classified under case (1) as may be readily seen from the refractive index data. The last three pairs should be classified under case (2), and the scattering curves are to be found in Fig. 4. With one exception these data require no further discussion, since they yield the results predicted by the theory.

Exceptional interest attaches to the mixture of butanone and 1,3 dichloro-isopropanol, since in this case $\partial n/\partial\psi<0$ and $\partial n/\partial c>0$. Thus application of the simple theory should lead to a value of M less than the true molecular weight. Inspection of curve II in Fig. 4 shows this to be the case, since the extrapolated curve has too high an intercept.

Case (3) $\partial n/\partial c$ Is Negligible with Respect to $\alpha\partial n/\partial\psi$

The system selected for study of this case consisted of a fractionated polymethylmethacrylate dissolved in mixtures of bromobenzene and methanol. It has been found that

$$\frac{\partial n}{\partial c}=-0.054+(1.568-n_0)\times1.06,$$

$$\frac{\partial n}{\partial\psi}=0.232,$$

TABLE I.

S	P	ψ	ψ_P	$n(S)$	$n(P)$	$n(SP)$	$\frac{\partial n}{\partial c}$	$\frac{\partial n}{\partial\psi}$
$C_2H_5COCH_3$	$(CH_3)_2CHOH$	0.85	0.80	1.3740	1.3736	1.3732	0.219	0.0004
DEF	CH_2ClCH_2OH	0.80	0.74	1.4372	1.4385	1.436	0.152	−0.0013
C_6H_6	$(CH_2Cl)_2CHOH$	0.33	0.28	1.495	1.476	1.483	0.112	0.019
$C_2H_5COCH_3$	$(CH_2Cl)_2CHOH$	0.46	0.33	1.3740	1.476	1.433	0.165	−0.102
C_6H_6	$(CH_3)_2CHOH$	0.65	0.59	1.4954	1.3736	1.450	0.154	0.122
C_6H_6	CH_3OH	0.80	0.75	1.4954	1.33	1.460	0.137	0.16

where n_0 = refractive index of mixture in question at $\lambda = 4358$A.

Data of the usual sort were obtained in several mixtures near the point where $\partial n/\partial c$ vanishes. Values of $(\tau/c)_0$ were obtained by extrapolation and were compared with the corresponding values of $\partial n/\partial c$ by referring both to n_0 as a parameter. This is shown graphically in Fig. 5. It is of interest to note that at the point where $\partial n/\partial c = 0$, $(\tau/c)_0$ has a finite value which is solely caused by selective absorption of solvent by dissolved polymer. This is, of course, in accord with our present theory.

The Magnitude of Selective Absorption

We have already noted the experimental significance of the factor α. It gives us at once the magnitude of the change in composition of the solvent-precipitant mixture surrounding the particles due to removal of solvent by selective absorption. If we now wish to calculate the composition of the solvent-precipitant mixture within the particles, we must introduce an assumption concerning the physical size of the particles in the solution. A reasonable and convenient assumption for this purpose is furnished

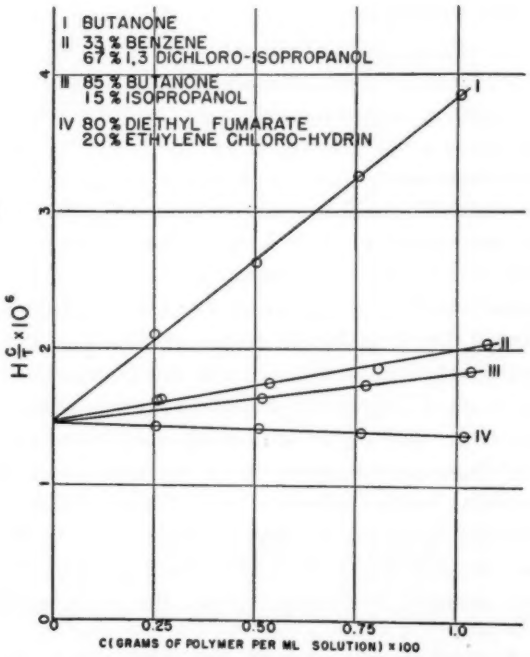

FIG. 3. Fractionated polystyrene in solvent-precipitant pairs matched with respect to refractive index.

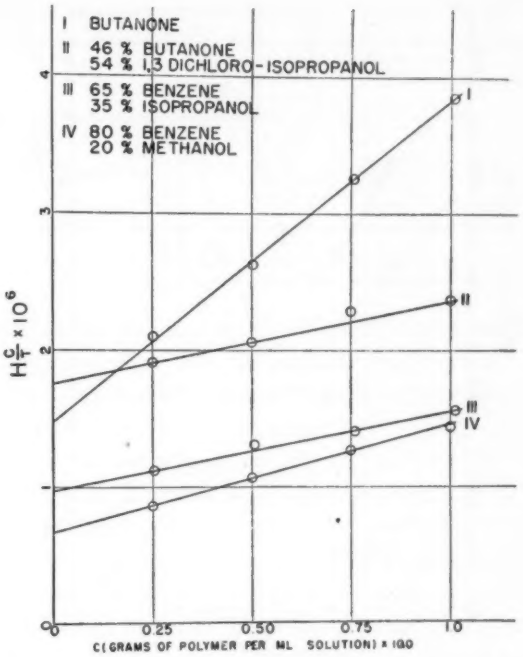

FIG. 4. Fractionated polystyrene in solvent-precipitant pairs unmatched with respect to refractive index.

by consideration of the intrinsic viscosity of the solution.

If we give the correct dimensions to the absolute intrinsic viscosity, $\{\eta\}$, (with concentration measured in grams per ml.) then $\{\eta\}$ is expressed in ml per gram, and Einstein's theory of viscosity leads to

$$\{\eta\} = 2.50\frac{v}{m}$$

in which v is the volume of the particle and m is its mass. In these units the absolute intrinsic viscosity $\{\eta\}$ is 100 times the conventional intrinsic viscosity, usually denoted by $[\eta]$. If, for instance, $[\eta] = 1.5$, this means that $\{\eta\} = 150$ ml per gram, and the polymer behaves in solution as if it possessed a specific volume of 60 ml per gram.

Now if we adopt this picture, it follows that

$$\alpha = -\frac{\partial\psi}{\partial c} = \left(\frac{v}{m} - \bar{v}\right)(\psi_2 - \psi_1),$$

where $\bar{v}$ is the partial specific volume of the solute ($\bar{v} = 0.92$ for polystyrene in benzene). If we calculate $\partial\psi/\partial c$ from light scattering and v/m from viscosity data, we can obtain $(\psi_2 - \psi_1)$ at once. $(\psi_2 - \psi_1)$ is, of course, the difference in the concen-

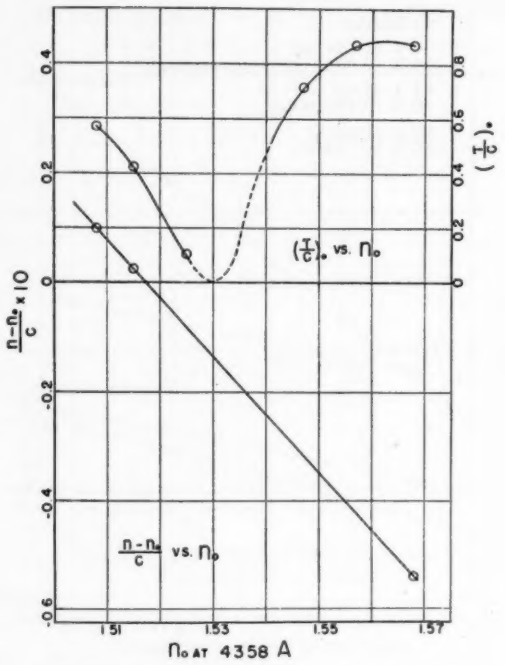

FIG. 5. Polymethylmethacrylate in mixtures of $C_6H_5Br-CH_3OH$.

trations of solvent in the solvent-precipitant mixture inside and outside the particles. The most convenient means of calculating α is to note that

$$\left(1+\alpha\frac{\partial n/\partial\psi}{\partial n/\partial c}\right)^2 = \frac{\left[H\left(\frac{c}{\tau}\right)_0\right]\text{ pure solvent,}}{\left[H\left(\frac{c}{\tau}\right)_0\right]\text{ solvent-precipitant mixture.}}$$

The results shown in the last two columns of Table II are derived from these considerations, on the basis of the data represented in Fig. 2. A similar calculation at $\psi=0.80$ from the data of Fig. 4 shows (since in this case $\{\eta\}=110$ and $v/m=44$) that $\alpha=0.42$, and $\psi_2-\psi_1=0.97\times10^{-2}$. This appears to be a remarkably good fit, since the two items of data were obtained by independent experimenters on different polymer samples in different laboratories.

GENERAL DISCUSSION

It might be thought that the phenomenon of increased turbidity with the addition of a precipitant to a polymer solution is caused by preflocculation or Van der Waals association of the solute. However, such an assumption is not only unnecessary to account for the observed results presented in this paper, but is indeed incompatible with these results. Thus, for example, the association hypothesis would require that the scattering curves bend upward to the correct value of $1/M$ at $c=0$, since at infinite dilution, association should vanish. This was not found to be the case from the data plotted in Fig. 2. Also in the cases of curves III and IV in Fig. 1, curve II in Fig. 4, and the picture presented by Fig. 5, the association hypothesis fails completely. It is shown furthermore to be untenable from consideration of the data on ψ_P in Table I, since the curves of Fig. 3, all of which lead to correct molecular weight values, represent systems in which the solvent compositions are much closer to the precipitation points than those of the curves in Fig. 2, all of which lead to values of M higher than the true molecular weight.

Measurements of molecular weight in mixed solvents by osmotic pressure also indicate that the displacement of the intercepts of the conventional $H(c/\tau)$ curves is an optical phenomenon and not caused by association. A. Dobry[10] studied the osmotic pressures of cellulose acetate in chloroform-alcohol mixtures and found that the conventional curves (pressure/c *versus* c) exhibited decreasing slopes as the precipitant concentration was increased. However, all the curves had the same intercept, regardless of the composition solvent-precipitant mixture. It is well known, of course, that the slope of the osmotic pressure curve should be one-half that of the conventional light scattering curve, also that the intercept at $c=0$ is a direct measure of molecular weight. Geoffrey Gee[11] has obtained similar results and has pointed out the usefulness of small slopes. It should be noted, however, that osmotic pressure measurements will be less sensitive to small degrees of polymer-polymer association than will light scattering measurements, since osmometry leads to a number average molecular weight whereas turbidimetry leads to a weight average. It thus appears that in the cases studied light scattering data present the most decisive evidence against the association

[10] A. Dobry, J. chim. phys. **36**, 102 (1939).
[11] Geoffrey Gee, Trans. Faraday Soc. **36**, 1171–8 (1940); **40**, 463–8 (1944).

hypothesis and in favor of selective absorption. This does not excluse the possibility that in some systems polymer-polymer association may occur prior to incipient precipitation. However, light scattering data should be interpreted as indicating polymer-polymer association in a solvent-precipitant mixture only after a suitable correction for the effect of selective absorption of the solvent has been made.

The increase of turbidity with added precipitant in high polymer solutions is a very great advantage in the determination of molecular weights by turbidimetry. It not only raises the relative accuracy obtainable in the measurement of absolute turbidity, but at the same time greatly reduces the slope of the conventional scattering curves. The latter circumstance enables one safely to make the linear extrapolation to infinite dilution from a smaller amount of data than would be necessary in case the data had to be relied on to determine both a high slope and the intercept. It is probable that in most cases conditions can be found which reduce the slope practically to zero, so that τ/c may be set equal to $(\tau/c)_0$. The sole condition which must be satisfied is that $\partial n/\partial\psi$ is negligible with respect to $\partial n/\partial c$ in the system considered.

TABLE II.

ψ	$[\eta]$	$\frac{\bar{\nu}}{m}$	α	$(\psi_2-\psi_1)\times 100$
1	131.5	52.6	0	0
0.925	122.0	48.8	0.12	0.25
0.90	118.7	47.5	0.24	0.51
0.875	110.6	44.2	0.34	0.79
0.85	102.6	41.0	0.40	1.00

The theory presented by the writers gives a satisfactory correlation of all the observed facts. In particular it accounts for the apparently anomolous molecular weights of high polymers as obtained by the application of simple scattering theory to measurements in solvent-precipitant systems. This theory also enables us to estimate the magnitude of selective absorption in these systems.

THE JOURNAL OF CHEMICAL PHYSICS VOLUME 14, NUMBER 11 NOVEMBER, 1946

A Simple Method of Obtaining a Particle Mass Distribution by Inverting the X-Ray Intensity Scattered at Small Angles

L. C. ROESS
Beacon Research Laboratory of The Texas Company, Beacon, New York
(Received June 28, 1946)

THE purpose of this note is to describe a simple and practical method of obtaining a particle mass distribution by inverting the x-ray intensity scattered at small angles by a collection of spherical particles. The method is much simpler than that published by Bauer,[1] whose procedure is complex analytically and appears to be impractical numerically.

The exact equation for the intensity scattered by a randomly-spaced distribution of spherical particles is[2]

$$I(\xi)=B\int_0^\infty M(R)R^3S(R\xi)dR, \qquad (1)$$

where B is a constant containing as factors the incident intensity, the Thomson scattering term for a single electron, including the polarization factor, and the ratio of the square of the electron density to the mass density, $M(R)dR$ is the mass contained in a group of particles having radii between R and $R+dR$, $S(x)$ is the "form factor" for one particle, and $\xi=(4\pi/\lambda)\cdot\sin\theta$ (λ = wavelength, θ = Bragg angle). The scattered intensity $I(\xi)$ is that produced by a monochromatic[3] and parallel beam defined by a pinhole having a very small cross section. If a beam defined by slits is used, suitable corrections[4] must be made.

[1] S. H. Bauer, J. Chem. Phys. **13**, 450 (1945).
[2] For example, A. Guinier, Ann. de Physique **13**, 161 (1939); R. Hosemann, Zeits. f. Physik **113**, 751 (1939).
[3] Experiments performed in this laboratory show that large errors may be introduced by the use of heterochromatic filtered radiation.
[4] A simple analytical method of making this correction has been devised by C. G. Shull, and will be published elsewhere.

The mathematical problem is: given $f(x)$ and $k(x)$ such that

$$f(x)=\int_0^\infty k(xy)g(y)dy, \tag{2}$$

determine $g(y)$. A solution can be obtained if $h(x)$ can be found such that

$$g(y)=\int_0^\infty h(xy)f(x)dx. \tag{3}$$

Titchmarsh[5] discusses this problem and shows how its solution can be obtained. Formally, the Mellin transforms of Eqs. (2) and (3) are

$$F(s)=K(s)G(1-s),$$

and

$$G(s)=H(s)F(1-s).$$

Eliminating F and G, we obtain

$$K(s)H(1-s)=1. \tag{4}$$

$h(x)$ can then be found by inverting the Mellin transform $H(s)$ given by Eq. (4), $K(s)$ being known.

Titchmarsh proves that the pair of equations

$$f(x)=\frac{d}{dx}\int_0^\infty \frac{k_1(xy)}{y}g(y)dy \tag{5}$$

and

$$g(y)=\frac{d}{dy}\int_0^\infty \frac{h_1(xy)}{x}f(x)dx \tag{6}$$

hold under quite general conditions on $f(x)$ and $g(x)$. k_1 and h_1 are such that Eqs. (5) and (6) are equivalent to Eqs. (2) and (3) if differentiation under the integral sign is permitted. The conditions for validity of Eqs. (5) and (6) given by Titchmarsh, page 226, are that $H(\frac{1}{2}+it)$ and $K(\frac{1}{2}+it)$ are both bounded, that $h_1(x)/x$ and $k_1(x)/x$ are Mellin transforms of $H(\frac{1}{2}+it)/(\frac{1}{2}-it)$ and $K(\frac{1}{2}+it)/(\frac{1}{2}-it)$, and that $f(x)$ belongs to $L^2(0,\infty)$, i.e.,

$$\int_0^\infty |f(x)|^2dx<\infty.$$

Then $g(y)$ also belongs to $L^2(0,\infty)$, and the reciprocal formulas (5) and (6) hold.

[5] E. C. Titchmarsh, *Introduction to the Theory of Fourier Integrals* (Oxford University Press, New York, 1937), Chapter VIII.

The function $S(x)$ in Eq. (1) may be written[6]

$$S(x)=\frac{9}{x^6}(\sin x-x\cos x)^2=\frac{9\pi}{2}\frac{J_{3/2}^2(x)}{x^3}$$

$$={}_1F_2(2;4,5/2;-x^2). \tag{7}*$$

In order to have $K(\frac{1}{2}+it)$ and $H(\frac{1}{2}+it)$ bounded, considerations similar to those given under part (3) on page 215 of reference 5 show that we must take[7]

$$k(x)=x^4\,{}_1F_2(2;4,5/2;-x^2)-(9/2). \tag{8}$$

We next calculate the Mellin transform $K(s)$, and determine $H(s)$ by use of Eq. (4). $h_1(x)$ is then calculated as the Mellin transform of $H(s)/(1-s)$, giving

$$h_1(x)=\frac{-8x}{27\pi}\,{}_1F_2\left(\frac{1}{2};-\frac{1}{2},\frac{5}{2};-x^2\right), \tag{9}$$

and

$$h(x)=\frac{d}{dx}h_1(x)=\frac{-8}{27\pi}\,{}_1F_2\left(\frac{3}{2};-\frac{1}{2},\frac{5}{2};-x^2\right). \tag{10}$$

Identifying ξ with x, R with y, $M(R)/R$ with $g(y)$, putting

$$f(x)=\xi^4I(\xi)/B-\frac{9}{2}\int_0^\infty \frac{M(R)}{R}dR,$$

and using Eqs. (8) and (9), the Eqs. (5)[7] and (6) can be written

$$I(\xi)=B\int_0^\infty M(R)R^3 \times{}_1F_2(2;4,5/2;-R^2\xi^2)dR \tag{11}$$

and

$$M(R)=-\frac{8R}{27\pi B}\frac{d}{dR}\int_0^\infty R\xi^4I(\xi) \times{}_1F_2\left(\frac{1}{2};-\frac{1}{2},\frac{5}{2};-R^2\xi^2\right)d\xi. \tag{12}$$

Equation (12) gives the desired inversion.

[6] G. N. Watson, *Theory of Bessel Functions* (Cambridge University Press, Cambridge, 1922), pages 54, 147, and 100.

* The use of generalized hypergeometric functions in the following is unnecessary for the case of spherical particles, but permits a direct generalization to the case of spheroidal particles.

[7] The last formula for $k(x)$ given on page 215 of reference 5 is valid only when $\alpha_1+\phi/2>0$; when $\alpha_1+\phi/2=0$ an additional term, of which the $-9/2$ in Eq. (8) is an example, must be added because of the pole of $K(s)$ at the origin. For the functions involved in the present problem, it is permissible to substitute (2) for (5), but not (3) for (6).

It can be shown[8] that

$$ {}_1F_2\left(\frac{1}{2};\ -\frac{1}{2},\frac{5}{2};\ -x^2\right)=-\frac{3\pi}{2}J_{3/2}(x)J_{-3/2}(x)$$

$$=-\frac{3}{2x}\left[\left(1-\frac{1}{x^2}\right)\sin 2x+\frac{2\cos 2x}{x}\right]. \quad (13)$$

Also, it follows from Eq. (11) that for large ξ

$$\xi^4 I(\xi)\sim B\int_0^\infty \frac{M(R)}{R}dR+O(\xi^{-\mu})+O(\xi^{-2}), \quad (14)$$

if

$$M(R)=O(R^\mu) \quad \mu>0^9$$

for small R. Therefore, Eq. (12) can be written, differentiating under the integral sign in the finite integral,

$$M(R)=\frac{4R}{9\pi B}\frac{d}{dR}\int_0^\infty \xi^3 I(\xi)\left[\left(1-\frac{1}{R^2\xi^2}\right)\sin 2R\xi+\frac{2\cos 2R\xi}{R\xi}\right]d\xi, \quad (15)$$

$$=\frac{8R}{9\pi B}\int_0^{\xi_0}\xi^4 I(\xi)\left[\left(1-\frac{2}{R^2\xi^2}\right)\cos 2R\xi-\frac{2}{R\xi}\left(1-\frac{1}{2R^2\xi^2}\right)\sin 2R\xi\right]d\xi$$

$$+\frac{4R}{9\pi B}\frac{d}{dR}\int_{\xi_0}^\infty \xi^3 I(\xi)\left[\left(1-\frac{1}{R^2\xi^2}\right)\sin 2R\xi+\frac{2\cos 2R\xi}{R\xi}\right]d\xi. \quad (16)$$

If ξ_0 is large enough the asymptotic expansion of $\xi^3 I(\xi)$ can be used in the last integral, which then can be evaluated analytically. In many cases, ξ_0 can even be chosen to make this integral vanish. The asymptotic expansion of $\xi^4 I(\xi)$ must be obtained from the measured data, and is subject to error. In a practical application, the treatment of the second term in Eq. (16) will depend upon the nature of the asymptotic behavior of $\xi^4 I(\xi)$. The mathematical situation and procedure are analogous to those encountered in inverting liquid scattering data.[10]

The general procedure described above can be applied whenever the "form factor" of the scattering particle is known and is characterized by a single size parameter. In particular, it has been applied to the calculation of the mass distribution of randomly oriented and spaced spheroidal particles having a fixed but arbitrary shape parameter v (major axes R, R, vR).

[8] Reference 6, pages 147 and 54.

[9] Actually, in order for the L^2 theory underlying (11) and (12) to be valid, we must have $\mu>\frac{1}{2}$.

[10] N. S. Gingrich, Rev. Mod. Phys. **15**, 90 (1943).

Letters to the Editor

THIS section will accept reports of new work, provided these are terse and contain few figures, and especially few halftone cuts. The Editorial Board will not hold itself responsible for opinions expressed by the correspondents. Contributions to this section should not exceed 600 words in length and must reach the office of the Managing Editor not later than the 15th of the month preceding that of the issue in which the letter is to appear. No proof will be sent to the authors. The usual publication charge ($3.00 per page) will not be made and no reprints will be furnished free.

Geometry of the Molecules CH_3Cl and CH_3Br

BÖRGE BAK
University of Copenhagen, Copenhagen, Denmark
October 7, 1946

IN organic-chemical problems one often meets with the question to what extent the substitution of one or more hydrogen atoms by so-called "electronegative" groups alters the original stereochemistry of the compound. The simplest case which can be studied in this respect is the substitution of one of the hydrogen atoms of methane by a halogen atom. Among the methyl halides conditions for studying the geometry are most favorable in the case of CH_3Cl and CH_3Br. Here, comparatively exact spectroscopic and interferometric data are available, which, in connection with thermodynamic data, give the best possible information on intramolecular distances and angles.

Penney[1] has given an approximative quantum-mechanical treatment of the bond energies and the valency angles of the methyl halides. To quote Penney, the result is that "if some or all of the hydrogen atoms in methane are replaced by other monovalent groups, the resulting deviations from the tetrahedral angle are remarkably small and can hardly exceed a few degrees."

If the greatest moment of inertia of a methyl halide is denoted by I_A, the small one by I_C, the C–X distance by a (X being a halogen atom), the C–H distance by d, the valency angle H–C–X by α and the mass of the atom or molecule Y by m_Y, we have:

$$I_C = 3m_H d^2 \sin^2\alpha \qquad \text{(I)}$$

$$(I_A - \tfrac{1}{2}y_C)m_{CH_3X} = a^2 m_X m_C + 3(a - d\cos\alpha)^2 m_X m_H + 3d^2\cos^2\alpha\, m_C m_H. \qquad \text{(II)}$$

The quantities to be determined are a, d, and α. Sutherland[2] has discussed the matter from the point of view that the methyl group of the methyl halides has the same shape as in methane, e.g., that $d=1.09$A and $\alpha=110°$. In the case of CH_3Cl, I_A and I_C were known from spectroscopic work. Thus, Sutherland could calculate a, the C–Cl distance. He found $a=1.66$A with a maximum possible error of 0.05A. However, from electronic diffraction experiments[3] a had been found to be $1.77\text{A}\pm0.02$A. A serious discrepancy seemed to exist. As is easily seen this discrepancy will vanish if we assume that the methyl group of the methyl halides and of methane may have a different shape. Indeed, new experimental data, published since the paper of Sutherland, seem to support this point of view.

In the case of CH_3Cl we can take $I_A = 57.9\cdot10^{-40}$ gcm² from the paper by Nielsen.[4] The value is good to 1–2 percent. $I_C = 5.44\cdot10^{-40}$ gcm² is good to about 5 percent.[5,6] Setting $a=1.77\pm0.02$A we get:

$I_A\cdot10^{40}$	$I_C\cdot10^{40}$	a A	$\alpha°$	d A	<HCH°
57.9	5.44	1.77	93	1.05	118
59.0	5.17	1.75	102	1.04	114
Val. for CH_3 group in CH_4:			110	1.09	110

$\alpha=93°$ is the value obtained by using middle numbers of all experimental data. $\alpha=102°$ is the maximum possible value. To some extent a similar result can be established in the case of CH_3Br. Taking $I_C = 5.37\cdot10^{-40}$ gcm² ±5 percent[5,6] and $a=1.91\pm0.06$A[7] we only miss a value for I_A to be able to calculate α and d. Egan and Kemp[8] have determined the standard entropy of CH_3Br at 276.66°K. Besides being a function of a number of quantities, such as the vibrational frequencies of the molecule, which are all known practically exact, the entropy is a function of $I_A^2\cdot I_C$. We get:

$$I_A^2 I_C = 33{,}400\cdot10^{-120}\ \text{g}^3\ \text{cm}^6 \pm 10\ \text{percent}.$$

Substituting $I_C = 5.37\cdot10^{-40}$ we get $I_A = 78\cdot10^{-40}\pm8$ percent. Another estimate of I_A can be obtained from the doublet separation, $\delta\nu$, of the ∥ bands in infra-red. Taking the average value of the $\delta\nu$'s which have been determined by several authors,[5,9–11] as 25.0 cm^{-1} ±1 cm^{-1} we get: $I_A = 82\cdot10^{-40}\pm10$ percent.

In a paper to be published the author[12] has studied the equilibrium $CH_3Br + HCl \lesssim CH_3Cl + HBr$ in a temperature interval from 70°C to 335°C. The exact knowledge of the equilibrium constant at different temperatures permits of calculating the ratio $I_A(CH_3Br):I_A(CH_3Cl)$, as $I_C(CH_3Br)$ to a good approximation is equal to $I_C(CH_3Cl)$. The result is that $I_A = 76.0\cdot10^{-40}\pm4$ percent. From these three determinations we conclude that $I_A = 77.5\cdot10^{-40}$ gcm² ±4 percent. The corresponding values of α and d are given below.

$I_A\cdot10^{40}$	$I_C\cdot10^{40}$	a A	$\alpha°$	d A	<HCH°
77.5	5.37	1.91	90	1.04	120
80.5	5.11	1.85	111	1.08	110
Val. for CH_3 group in			110	1.09	110

$\alpha=90°$ is the value obtained using middle numbers of all experimental data. $\alpha=111°$ is the maximum possible value.

For CH_3Cl it thus seems firmly established that α deviates considerably from the tetrahedral angle. For CH_3Br the same is very probably the case. The methyl group in CH_3Cl and CH_3Br thus seems to be considerably more 'flat' than in CH_4.

[1] Penney, Trans. Faraday Soc. **31**, 734 (1935).
[2] Sutherland, Trans. Faraday Soc. **34**, 325 (1938).
[3] Sutton and Brockway, J. Am. Chem. Soc. **57**, 473 (1935).
[4] Nielsen, Phys. Rev. **56**, 847 (1939).
[5] Bennett and Mayer, Phys. Rev. **32**, 888 (1928).
[6] Johnston and Dennison, Phys. Rev. **48**, 868 (1935).
[7] Levy and Brockway, J. Am. Chem. Soc. **59**, 1662 (1937)
[8] Egan and Kemp, J. Am. Chem. Soc. **60**, 2097 (1938).
[9] Moorhead, Phys. Rev. **39**, 788 (1932).
[10] Sleator, Phys. Rev. **38**, 147 (1932).
[11] Barker and Nielsen, Phys. Rev. **46**, 970 (1934).
[12] Bak, Dansk. Vidensk. Selsk. math.-fys. Medd. (1947).

The Adiabatic Compressibility of Liquids

M. Rama Rao
Indian Meteorological Service, Madras, India
September 26, 1946

IN recent years a number of investigators have determined the adiabatic compressibility of liquids. Tyrer[1,2] has determined the adiabatic compressibility of a few liquids in the range 0 deg. to 80 deg. C, while Shiba has found the adiabatic compressibility of liquids at two temperatures, namely 30 deg. and 35 deg. C. Measurements on the velocity of sound in liquids also yield values of adiabatic compressibility. In general, these values compare well with those determined by direct methods with the piezometer.

A simple relation[3] between the velocity of sound v in liquids and its volecular volume V exists, viz.

$$v^{\frac{1}{7}}V=R, \tag{1}$$

where R is a constant independent of temperature. It has also been shown[4] that the constant R is an additive function of the chemical composition as in the case of the parachor. R is further related[5] to the molecular critical volume V_c and critical temperature θ_c and molecular weight M by the relation $R=\alpha(\theta_c/M)^{1/6}V_c$ where α is a constant with a mean value of 2.68. The velocity of sound in a liquid is related to the adiabatic compressibility β_ϕ and density ρ of the liquid by the relation

$$v=1/(\beta_\phi\rho)^{\frac{1}{2}}. \tag{2}$$

Combining relation (1) with (2) it follows that

$$\beta_\phi^{1/7}\rho=\text{constant} \tag{3}$$

independent of temperature for each liquid. In Table I values of β_ϕ and ρ are given at various temperatures and the last column gives the values of $\beta_\phi^{1/7}\rho$ computed in the case of benzene. The same result is found to hold good for other liquids like carbontetrachloride ether, toluene, chlorobenzene, chloroform, cyclohexane, bromobenzene, *o*-nitrotoluene, *M*-nitrotoluene, actophenone, carbondisulphide, cyclohexanone, and acetic acid.

As regards the temperature variation of the adiabatic compressibility, it is generally found that the value of β_ϕ increases with temperature, the increase becoming more rapid as the temperature increases. With many liquids the adiabatic compressibility increases by about 60 percent for a rise of temperature 0 to 60 deg. C. A large part of the high initial compressibility of ordinary liquids is connected with the nearness of the critical point liquid-gas for compressibility in the gas phase which is high and which at the critical point itself, β_ϕ, is infinite. Hence the absolute value of the compressibility depends on how far the temperature is from the critical point.

TABLE I

Liquid	Temp.	$\beta_\phi 10^6$	ρ density	$\beta_\phi^{1/7}\rho$
Benzene	0	56	0.9001	1.599
	10	61	0.8896	1.601
	20	66.32	0.8790	1.601
	30	72	0.8684	1.601
	40	78.26	0.8576	1.599
	50	85.12	0.8467	1.597
	60	92.99	0.8351	1.595
	70	101.91	0.8262	1.600
	80	111.50	0.8145	1.597

For temperatures at which the saturation vapor density can be neglected in comparison with the liquid density the variation of liquid[6] density with temperature is represented by the relation

$$\rho=\rho_0\{1-\theta/\theta_c\}^{3/10}. \tag{4}$$

Combining (3) with (4) it follows that

$$\beta_\phi=\beta_{\phi 0}\{1-\theta/\theta_c\}^{-2.1} \tag{5}$$

where $\beta_{\phi 0}$ is independent of the temperature, θ is any temperature on the absolute scale. The critical temperatures calculated from the above relation are in good agreement with observed values of θ_c.

By starting from the general equation of state for the liquid and using Maxwell's thermodynamic relations, it can be shown that the compressibility in the case of liquids should be a function of the density only. Details about these will be published elsewhere.

[1] Tyrer, J. Chem. Soc. **105**, 2334 (1914).
[2] For a review see Bridgman, Rev. Mod. Phys. **7** (1935).
[3] M. Rama Rao, Cur. Sci. **8**, 510 (1939) and Ind. J. Phys. **14**, 109 (1940).
[4] M. Rama Rao, J. Chem. Phys. **9**, 682 (1941).
[5] M. Rama Rao, J. Mys. Uni. **12**, 896 (1942).
[6] Sugden, J. Chem. Soc. 1700–1786 (1927); J. Chem. Soc. 1055 (1929).